1962
BNWL-1540
UC-25

MASTER

Battelle
Pacific Northwest Laboratories
Richland, Washington 99352

AEC Research and Development Report

HIGH-TEMPERATURE IRRADIATIONS (1000-1300°C) ON A VARIETY OF GRAPHITES TO EXPOSURES > 10^{22} n/cm^2

July 1971

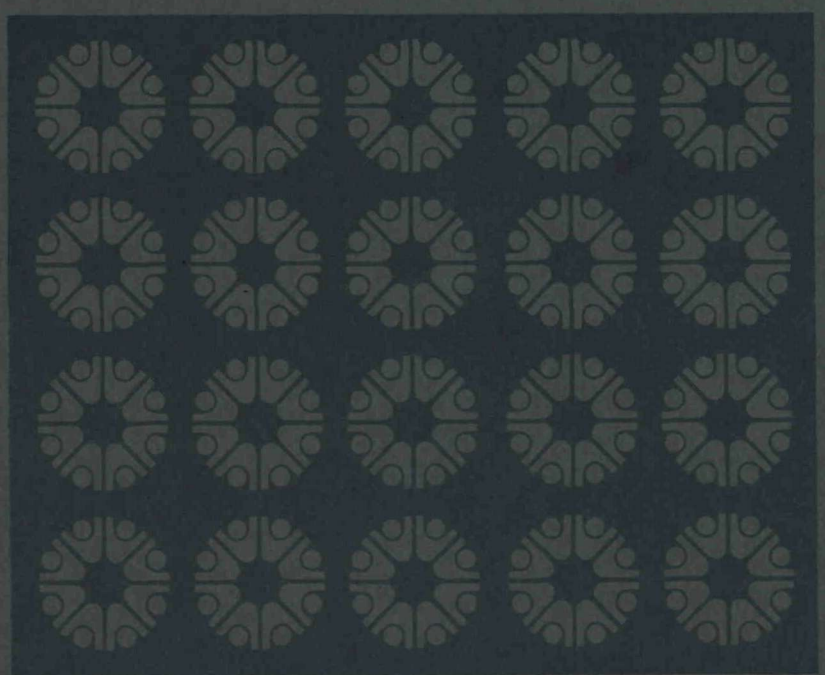

BNWL-1540

PACIFIC NORTHWEST LABORATORY
operated by
BATTELLE
for the
U.S. ATOMIC ENERGY COMMISSION
Under Contract AT(45-1)-1830

Printed in the United States of America
Available from
National Technical Information Service
U.S. Department of Commerce
5285 Port Royal Road
Springfield, Virginia 22151
Price: Printed Copy $3.00; Microfiche $0.95

AEC-RL RICHLAND, WASH

UNCLASSIFIED

BNWL-1540
UC-25, Metals,
Ceramics, & Materials

HIGH-TEMPERATURE IRRADIATIONS (1000-1300°C) ON A VARIETY OF GRAPHITES TO EXPOSURES > 10^{22} n/cm^2

By

A. L. Pitner*

Ceramics and Graphite Section
Fuels and Materials Department

July 1971

*Now employed by WADCO Corporation, Richland, Washington.

BATTELLE
PACIFIC NORTHWEST LABORATORIES
RICHLAND, WASHINGTON 99352

DISCLAIMER

TABLE OF CONTENTS

LIST OF FIGURES

LIST OF FIGURES (Cont'd)

LIST OF FIGURES (Cont'd)

LIST OF FIGURES (Cont'd)

HIGH TEMPERATURE IRRADIATIONS (1000-1300°C) ON A VARIETY OF GRAPHITES TO EXPOSURES > 10^{22} n/cm^2

A. L. Pitner

INTRODUCTION

The trend in future power reactors is toward higher operating temperatures to increase thermal-to-electrical conversion efficiencies. Present High-Temperature Gas Reactor (HTGR) designs prescribe operating temperatures to 1100°C, and future designs will likely specify even higher temperatures. Utilization of graphite as the moderator and basic structural material in these reactors requires that the irradiation behavior of graphite at these high temperatures be well characterized to insure preservation of integrity and attainment of maximum lifetimes. Previous data[1] indicated that irradiation of graphite above 800°C resulted in accelerated damage accumulation and earlier turnaround and expansion after initial irradiation induced contraction. More recent data[2] at higher temperatures, however, suggested that post-turnaround expansion rates were lower in some graphites when irradiation temperatures exceeded 1200°C. Certainly, this behavior would have a direct influence on reactor lifetime. A variety of graphites has consequently been irradiated to high exposures to accurately characterize their high-temperature performance and allow the selection of the best material for specific high-temperature applications. This report presents the irradiation data concerning the dimensional change, thermal expansivity, electrical resistivity, and Young's modulus for 21 types of graphite irradiated at temperatures of 1000-1300°C to exposures approaching 15 x 10^{21} n/cm^2 (E > 0.18 MeV).

SUMMARY

Twenty-one grades of graphite were irradiated in instrumented capsules at temperatures of 1000-1300°C to exposures approaching 15×10^{21} n/cm (E > 0.18 MeV). At 1000-1200°C, dimensional distortions were similar to those observed in lower-temperature irradiations but occurred at an accelerated rate. Above 1200°C, however, the expansion rate after turnaround in the transverse orientation was considerably reduced from that seen at 1000-1200°C, thereby increasing the useful lifetime of the graphite. Near-isotropic graphites displayed improved dimensional behavior over conventional graphites in that distortions were more isotropic and generally less severe, and turnaround was slower. Isotropic graphites with a high coefficient of thermal expansion ($\sim 7 \times 10^{-6}$ in./in./°C) showed quite rapid expansion at the onset of irradiation, but after about 2×10^{21} n/cm^2, the expansion rate decreased to nearly zero for the high-density materials and actually became negative for the low density graphites. Expansion again became prevalent after about 10^{22} n/cm^2, but the expansion rates were considerably less than observed in conventional graphites at high fluences. Above 1200°C, the isotropic graphites contracted slightly with irradiation. Dimensional changes in these materials were generally quite small (< 1%). In the conventional, anisotropic graphites the coefficient of thermal expansion (CTE) generally decreased about 25% with irradiation, but then increased after an exposure corresponding to dimensional turnaround. The high CTE isotropic graphites showed a reduction from approximately 7×10^{-6} in./in./°C to 1-2 in./in./°C with irradiation. Electrical resistivity increased by a factor of approximately 2-1/2 when the irradiation temperature was below 1200°C but only doubled at temperatures of 1200-1300°C. Young's modulus generally increased with irradiation exposure, with a smaller increase at 1200-1300°C than at 1000-1200°C.

EXPERIMENTAL

Capsule Design

Recent graphite irradiations conducted by Battelle-Northwest have utilized a capsule design considerably modified from that reported in earlier work.[3] Therefore, a complete description of experimental techniques is presented here to give an updated account of methods currently in practice.

The irradiation samples were in the form of cylinders with nominal dimensions of 0.25 in. dia. x 1.75 in. long. Samples were cut parallel and perpendicular to the extrusion axis or molding direction of the manufactured blocks. The ends of the samples were rounded and polished to facilitate length measurements. All samples were annealed at > 1600°C for one hour at a pressure of 3×10^{-4} Torr to remove any strains that may have been introduced in machining the samples.

Samples were contained in the irradiation capsule in graphite holders as shown in Figure 1. Holes drilled in the holder to accommodate the samples were tapered at the bottom to prevent wear against the measuring surface of the sample. The sample holders were centered within the capsule by alumina rods imbedded in their sides. The gas gap between the holder and the capsule wall was selected to provide the desired heat-transfer characteristics at any specific location but was generally on the order of 0.060 inch. Usually, 15 holders were joined in a train to form the capsule assembly as illustrated in Figure 2. The holders were connected to and spaced from their neighbors by alumina struts. Adjacent holders were separated by a nominal 0.25 inch gap. Thermocouple leads and gas tubes traversed the capsule in slots machined in the sides of the holders. The capsule body was normally two-inch diameter 304 stainless steel tubing with an overall in-core length of approximately 36 inches. The irradiations were primarily conducted in the Engineering Test Reactor (ETR), although several of the samples received an early portion of their exposure in irradiation tests conducted in the General Electric Test Reactor (GETR).

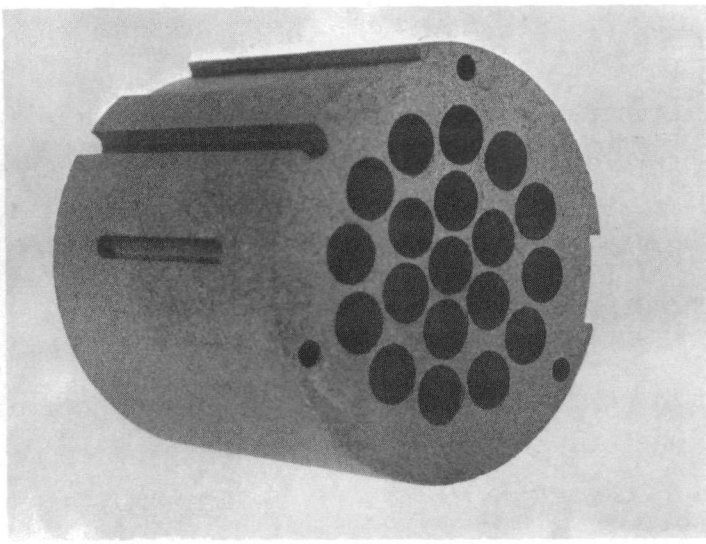

FIGURE 1. Graphite Sample Holder.

Temperature Determinations

Temperatures of the sample holders were monitored by Geminol (N,P) or W 5% Re/W 26% Re thermocouples. The tungsten-rhenium wires were each composed of seven strands of 0.003 in. dia. wire and were very flexible. The W/Re thermocouples exhibited a considerably higher survival rate under service conditions than did the Geminol thermocouples. Temperatures were controlled by manually adjusting the composition of the binary gas (helium and argon) that continually purged the capsule. The control gases were purified by passing them through copper turnings heated to 500°C and also through a desicant. Gas flow through the capsule was approximately 100 cc/minute.

The temperatures reported for the samples are the time-averaged values of the holders in which they were located. There are three conditions in the irradiation test, however, that affect the reported temperatures. First, there is a temperature gradient through the sample holder. Thermocouples were located near the outer edge of the holders, and calculations have shown

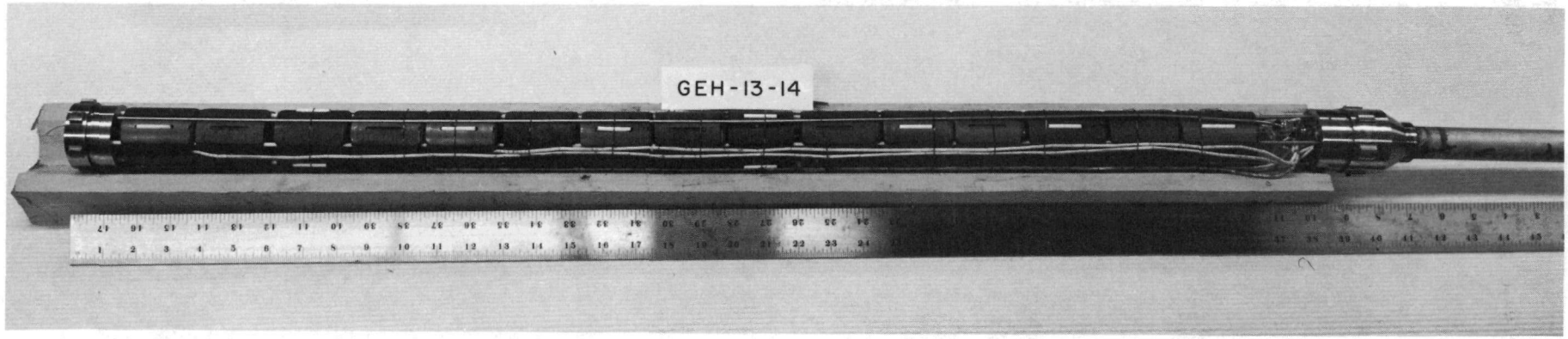

FIGURE 2. Typical Capsule Assembly.

that temperatures in the center of the holders can be about 65°C higher than at the surface when the nuclear heating is 15 watts/gram. However, most samples were located closer to the circumference of the holder and also at positions of lower heating, so that the deviation from the reported temperature would be considerably less than indicated in this extreme condition. The average underestimate of the sample temperature is closer to 20-30°C.

It is known that the effect of irradiation on thermocouples is to reduce their emf output, i.e., cause them to indicate a lower temperature than they are actually experiencing. Previous post-irradiation calibrations of Geminol (N,P) thermocouples[4] indicated that a correction factor of 1.044 was necessary to obtain the correct temperature. Consequently, if an irradiated Geminol thermocouple indicated a temperature of 1000°C, the true temperature would be 1044°C. Correction factors for W/Re thermocouples are not well known, but appear to be greater than for Geminol thermocouples. Values ranging from 1.05 to 1.10 have been used, depending upon which factor gave the best agreement with the few surviving Geminol thermocouples. Temperatures assigned to the irradiated samples in this report have been corrected for the thermocouple calibration errors.

The third effect that influences capsule temperatures is shifting of the heating profile in the reactor. This results when control rods are withdrawn during the course of the irradiation to compensate for reactivity losses. This effect is most severe at the ends of the capsule where temperature variations may reach 150°C. Consequently, temperature deviations from the time-averaged values reported in this document can be as high as 75°C. Therefore, if a temperature range for a particular group of samples is given as 1000-1100°C, it must be realized the temperatures of these samples averaged between 1000 and 1100°C. A given sample, whose average temperatures was 1000°C, may have experienced a temperature of 925°C for a short period, while another sample, whose average temperature was 1100°C, may have reached 1175°C briefly.

Fluence Determinations

Exposures were determined by analysis of the activation of flux wires of iron, nickel, and cobalt included in the capsule. A description of the analytical techniques involved has been given previously.[3] Different effective cross sections for the flux monitors were, of course, used depending on the reactor position. All fluences reported here are for neutrons with energy greater than 0.18 MeV.

Property Measurements

Length measurements on the samples were made with a Bausch and Lomb DR-25 Optical Comparator accurate to 5×10^{-5} inch. The average coefficient of thermal expansion was measured from 25-425°C. Electrical resistivity was determined by measuring the voltage drop between two accurately-spaced knife edges while passing a known current through a sample. Elastic modulus was measured using a sonic resonance technique.[5]

MATERIALS

Manufacturing variables and properties of the 21 grades of graphites are summarized in Table I.

RESULTS

Length Change

The dimensional behavior of the 21 graphites irradiated is shown in Figures 3 through 23. In some of the figures, the behavior of the graphite at lower temperatures is shown as a dashed curve to provide a comparison to the high temperature results. These lower-temperature reference curves were taken from Ref. (1). In several recent capsule irradiations, one of the sample holders was insulated with carbon felt to increase the irradiation temperature. Although the felt deteriorated and the temperature gradually decreased with time, the temperature nevertheless averaged approximately 1400°C. These low exposure points are also included on the curves.

TABLE I. Graphite Description

Graphite	Manufacturer	Coke	Forming Method	Graphitization Temperature, °C	Remarks	Density g/cm³	CTE(25-425°C) 10^{-6} in/in/°C ⊥	CTE(25-425°C) 10^{-6} in/in/°C ∥	Resistivity 10^{4} ohm-cm ⊥	Resistivity 10^{4} ohm-cm ∥	Young's Modulus 10^{6} psi ⊥	Young's Modulus 10^{6} psi ∥
EGCR*	UCC	Needle	Extruded	2800	Reactor Grade, Anisotropic	1.72	3.3	1.4	11.0	6.7	0.8	1.5
CSF*	UCC	Conventional	Extruded	2800	Reactor Grade, Anisotropic	1.66	3.8	1.8	13.3	7.7	0.7	1.6
TSX*	UCC	Needle	Extruded	3000	Reactor Grade, Anisotropic	1.71	4.0	0.9	12.6	6.0	0.9	2.0
TSGBF	UCC	Conventional	Extruded	2450	Reactor Grade, Poorly Graphitized	1.65	4.5	2.1	19.5	13.8	0.9	1.6
RP4	SCC	Composite	Extruded	2800	Near-isotropic	1.82	4.9	3.6	11.0	9.1	1.3	1.6
RC5	SCC	Non-Needle	Extruded	2800	Near-isotropic	1.73	5.4	4.7	9.9	9.9	1.4	1.3
JOZ*	GLCC	Raw	Molded	2800	Experimental Raw-Coke Graphite	1.72	6.4	5.8	14.8	12.9	1.3	1.4
H327*	GLCC	Needle	Extruded	2800	Commercially Available in Large Sizes	1.78	3.3	1.0	11.3	5.6	1.2	2.2
H328*	GLCC	Gilsonite	Molded	2800	Isotropic	1.72	5.6	5.6	12.0	11.8	1.5	1.6
9567*	SCC	Needle	Extruded	2800	Commercially Available in Large Sizes	1.71	4.4	2.0	9.6	5.8	0.9	1.7
9640	SCC	Needle	Molded	2800	Isotropic Needle-Coke	1.58	3.1	3.1	15.7	15.3	1.1	1.3
9650	SCC	Raw	Molded	2800	Isotropic, High Density	1.92	6.7	6.7	24.7	23.1	0.8	0.8
9751	SCC		Molded	2800	Near-Isotropic	1.73	5.9	5.9	10.5	11.9	1.3	1.4
GN*	BCC	Non-Needle	Extruded	2650	Pre-graphitized Coke	1.87	1.4	2.2	13.7	10.8	1.3	1.7
AXF-Q1	POCO	Proprietary	Isostatically Molded	2300	Fine-Grained, Isotropic High Strength	1.83	7.2	7.2				

TABLE I. (Cont'd)

Graphite	Manufacturer	Coke	Forming Method	Graphitization Temperature, °C	Remarks	Density g/cm³	CTE(25-425°C) 10^{-6} in/in/°C ⊥	CTE(25-425°C) 10^{-6} in/in/°C ∥	Resistivity 10^{4} ohm-cm ⊥	Resistivity 10^{4} ohm-cm ∥	Young's Modulus 10^{6} psi ⊥	Young's Modulus 10^{6} psi ∥
AXF-5Q1	POCO	Proprietary	Isostatically Molded	2500	Fine-Grained Isotropic, High Strength	1.81	7.2	7.2	14.6	14.6	2.0	2.0
AXF-8Q1	POCO	Proprietary	Isostatically Molded	2800	Fine-Grained Isotropic, High Strength	1.80	7.1	7.1	15.8	15.8	1.7	1.7
AXZ-5Q1	POCO	Proprietary	Isostatically Molded	2500	Fine-Grained Isotropic, High Strength	1.51	6.7	6.7	16.7	16.7	1.1	1.1
AXZ-8Q1	POCO	Proprietary	Isostatically Molded	2800	Fine-Grained Isotropic, High Strength	1.53	6.2	6.2	16.0	16.0		
AXF-5QBG1*	POCO	Proprietary	Isostatically Molded	2500	Fine-Grained Isotropic, High Strength	1.89	7.2	7.2	16.3	16.3	2.0	2.0
AXF-8QBG1*	POCO	Proprietary	Isostatically Molded	2800	Fine-Grained Isotropic, High Strength	1.89	6.5	6.5	10.0	10.0	2.0	2.0

* *Impregnated.*

UCC = Union Carbide Corporation.

SCC = Speer Carbon Company.

GLCC = Great Lake Carbon Corporation.

BCC = Basic Carbon Corporation.

The dimensional behavior of EGCR graphite is shown in Figure 3. This is a needle-coke, anisotropic grade of nuclear graphite. At temperatures of 1000-1200°C, the initial contraction rate in the transverse direction is considerably higher and the point where contraction ceases and expansion begins (turnaround) occurs considerably sooner than at 700°C. However, above 1200°C, the expansion following turnaround is much slower than observed at temperatures of 1000-1200°C. In fact, the post-turnaround expansion rate above 1200°C very nearly coincides with that of samples irradiated at 700°C. In the parallel direction, the contraction rate is greatly increased at all temperatures above 1000°C. There is considerable scatter in the 1200-1300°C data, and several of the points representing data on the same samples have been numbered so that the contraction trend at high exposures can be recognized. The samples are still contracting at 14×10^{21} n/cm^2.

The irradiation behavior of CSF, a conventional-coke nuclear graphite, is shown in Figure 4 and is very similar to that of EGCR. Again the expansion rate after turnaround in the transverse orientation is relatively slow at temperatures above 1200°C.

Figure 5 presents the length change behavior of TSX graphite, another commercial needle-coke graphite. Here it appears that turnaround and expansion occur earlier at 1200-1300°C in the transverse direction than at lower temperatures. However, there are very few data points to support this behavior. At 1400°C, contraction in the perpendicular direction is very much increased over that at 1200-1300°C, whereas in the other conventional nuclear graphites this was not true. Therefore, the behavior at 1200-1300°C appears very suspicious. If additional samples were irradiated at 1200-1300°C, they might be expected to show better agreement with the trends seen in the other graphites (slow expansion after turnaround). In the parallel direction, the data are again badly scattered. However, it is apparent that the contraction rate above 1000°C is greatly increased over that at 700°C. There appears to be no indication of turnaround yet in the parallel data at an exposure of 12×10^{21} n/cm^2.

The radiation-induced dimensional distortion in TSGBF, a poorly graphitized nuclear graphite, is shown in Figure 6. Here, even though turnaround and expansion occur relatively early in both directions at 1200-1300°C, the improvement over the behavior at 1000°C is apparent. The one transverse sample irradiated at 1400°C shows a much higher contraction than samples irradiated at lower temperatures.

RP4 is a near-isotopic composite of several non-needle cokes. In this material (Figure 7), the post-turnaround behavior is improved at 1100-1200°C over that at 1000°C. At 1200-1300°C, even better performance is again evidenced. The more-isotopic behavior under irradiation compared to other anisotropic graphites is also obvious.

The dimensional behavior of another near-isotropic graphite, RC5, is shown in Figure 8. The trends noted in RP4 graphite are also true for RC5. Expansion after saturation of the contraction is extremely slow at 1200-1300°C.

The data for JOZ graphite, manufactured with uncalcined coke, are quite brief (Figure 9). The slow expansion in the transverse direction after turnaround is again very apparent at 1200-1300°C.

H327 graphite is another needle-coke material commercially available in large block sizes. This graphite is being used as the moderator and structural material in the Fort St. Vrain HTGR. Turnaround and expansion occur early in the transverse direction in this graphite even when irradiated at temperatures above 1200°C (Figure 10). However, it should be pointed out that the transverse samples irradiated above 1200°C were badly warped after turnaround, making length measurements difficult and questionable. Contraction in the parallel direction is very rapid at temperatures above 1000°C.

The behavior of a Gilsonite coke graphite, H328, is shown in Figure 11. Dimensional changes are very isotropic, and greater stability over conventional graphites is exhibited at 1000-1200°C. Data at temperatures

above 1200°C are limited, but do indicate isotropic behavior and increased contraction rate at low exposures.

Figure 12 displays the dimensional behavior of 9567, another needle-coke graphite available in large sizes. Trends are similar to those of other needle-coke graphites with quite anisotropic behavior and slow turnaround with irradiation at temperatures above 1200°C.

Grade 9640 is an unusual material in that it is a needle-coke graphite with quite isotropic properties. Its dimensional behavior under irradiation is also considerably less anisotropic than other needle-coke graphites (Figure 13). The expansion rate after turnaround is very slow in both orientations at temperatures above 1200°C. Irradiation behavior above 1200°C even appears to be more isotropic than at lower temperatures.

Quite good dimensional stability is displayed by 9650, an isotropic, raw-coke graphite (Figure 14). At temperatures of 1000-1100°C, there is a slight expansion in both directions during initial irradiation, but it saturates early and does not become prevalent again until an exposure of approximately 10^{22} n/cm^2 is reached. The expansion rate even at high exposures, however, is slow. At 1100-1200°C, the graphite contracts slightly with irradiation before returning to its original length at approximately 8×10^{21} n/cm^2. Above 1200°C, the graphite shows almost no dimensional change after early saturation of contraction at approximately 1/2%, even to exposures of 13×10^{21} n/cm^2.

Grade 9751 is a molded graphite with near-isotropic properties, but its dimensional behavior under irradiation deviates from this isotropic nature (Figure 15). At 1000-1100°C, the material expands continuously with exposure in the transverse direction. In the parallel direction, however, there is only slight expansion followed by a small contraction to less than its original length, and then expansion again after approximately 7×10^{21} n/cm^2. At 1200-1300°C, the expansion in the transverse orientation is reduced, while in the parallel direction the graphite contracts from the

beginning of irradiation. Contraction is observed in both directions when irradiated at 1400°C.

Irradiation data was obtained only at 1200-1300°C for GN, a graphite manufactured from a pregraphitized, non-needle coke (Figure 16). It is seen that expansion is less after turnaround in the transverse direction than shown in the 1000°C reference curve. Also, contraction in the parallel direction is increased at 1200-1300°C over that at 1000°C, while turnaround appears to occur at approximately the same exposure ($\sim 6 \times 10^{21}$ n/cm^2) for both temperature ranges.

The dimensional change data for seven grades of POCO graphite are shown in Figures 17 through 23. Actually, the seven grades are derived from variations in graphitization temperature and impregnation of two basic grades, AXF and AXZ, with densities of 1.8 and 1.5 g/cc, respectively. All the POCO graphites behave isotropically and show generally similar dimensional behavior under irradiation. At temperatures of 1000-1200°C, the graphites expand with initial irradiation, but the expansion saturates by 3×10^{21} n/cm^2 and is often followed by contraction. The AXZ (low density) grades, in particular, contract to less than their original length after the initial expansion. In any case, expansion does not again become prominent until the exposure approaches 10^{22} n/cm2. Above 1200°C, the graphites contract from the onset of irradiation to a nominal shrinkage of approximately 1%. In almost every grade, the graphite has not yet returned to its original length by an exposure of 14×10^{22} n/cm^2. The behavior of the POCO graphites very much resembles that of Grade 9650, described previously. A detailed study of the irradiation behavior of POCO graphites is presented in Ref. (6).

Coefficient of Thermal Expansion

The data showing the effect of irradiation on the coefficients of thermal expansion (CTE) of the graphites are presented in Figures 24 through 44. Curves have been drawn as a visual best-fit to the data, even though in some instances there is considerable scatter in the results.

The behavior of the CTE of EGCR, CSF, and TSX graphites under irradiation is generally similar, as shown in Figures 24, 25, and 26, respectively. At 1000-1200°C, in the transverse direction, the CTE decreases about 25% from its unirradiated value of 3-4 x 10^{-6} in./in./°C by an exposure of 4-5 x 10^{21} n/cm^2, and then begins to increase again. At 1200-1300°C, the decrease is slower, but it appears that final saturation is at about the same level as for 1000-1200°C. There is no indication of increase in the CTE again by an exposure of 14 x 10^{21} n/cm^2. In the parallel direction, the CTE decreases slightly with irradiation at 1000-1200°C, but begins increasing again after an exposure of approximately 5 x 10^{21}n/cm^2. The decrease in CTE at 1200-1300°C is slower, and the CTE usually remains below its unirradiated value to exposures beyond 10^{22} n/cm^2.

The data for TSGBF graphite are presented in Figure 27. In the transverse direction, the CTE decreases slightly with irradiation at 1200-1300°C, but then apparently begins to increase again after approximately 5 x 10^{21} n/cm^2. The behavior of the CTE in the parallel direction is quite unexpected, showing a continued increase from the beginning of irradiation at 1200-1300°C.

The CTE of RP4, RC5, and JOZ as a function of irradiation exposure is shown in Figures 28, 29, and 30, respectively. These graphites are near isotropic, with an unirradiated CTE of about 5-6 x 10^{-6} in./in./°C. After irradiation to approximately 4 x 10^{21} n/cm^2, there is a fairly rapid drop in CTE to a value of about 1-2 x 10^{-6} in./in./°C in both orientations. There appears to be little change in the CTE with irradiation once it has saturated at this new level.

The CTE behavior of H327 is similar to that of other needle-coke graphites with a decrease followed by an increase after approximately 4 x 10^{21} n/cm^2 in the transverse orientation (Figure 31). In H327, however, the CTE also increases after the initial decrease even at irradiation temperatures of 1200-1300°C. In the parallel direction, there is very little change in thermal expansivity with irradiation.

H328, a Gilsonite-coke isotropic graphite, shows CTE behavior similar to that of other near isotropics (Figure 32). After an exposure of $\sim 2 \times 10^{21}$ n/cm^2, the CTE drops from $\sim 6 \times 10^{-6}$ in./in./°C to $\sim 1 \times 10^{-6}$ in./in./°C quite rapidly, and then shows little change with exposure.

9567 is a needle-coke graphite whose CTE in the transverse direction decreases continuously with irradiation at 1000-1200°C, at least up to 6×10^{21} n/cm^2 (Figure 33). In the parallel direction, the CTE is reduced very early to about half of its unirradiated value of 2×10^{-6} in./in./°C, and then shows little change with additional irradiation.

The CTE of 9640, an isotropic needle-coke graphite, decreases from 3×10^{-6} in./in./°C to $\sim 2 \times 10^{-6}$ in./in./°C fairly early with irradiation at 1000-1300°C, and then stays fairly constant with exposure (Figure 34).

The behavior of the CTE of 9650 (Figure 35) is similar to that of other isotropic graphites. The CTE decreases rapidly after some early exposure from $\sim 7 \times 10^{-6}$ in./in./°C to $\sim 1 \times 10^{-6}$ in./in./°C. The decrease to saturation seems to occur faster at irradiation temperatures of 1000-1200°C than at 1200-1300°C.

The effect of irradiation on the CTE of 9751, a near-isotropic graphite, is shown in Figure 36. The CTE again decreases rapidly with irradiation from 6×10^{-6} in./in./°C to $\sim 1 \times 10^{-6}$ in./in./°C at 1000-1200°C. Limited data at 1400°C, however, indicate the decrease in CTE to be much slower at this temperature. In other graphites, there is generally far less dissimilarity in the behavior at 1200-1300°C and 1400°C.

The CTE of GN graphite shows little change with irradiation at 1200-1300°C (Figure 37), even to high exposures ($\sim 14 \times 10^{21}$ n/cm^2).

The behavior of CTE with irradiation for the POCO graphites is shown in Figures 38 through 44. All grades, in general, behave the same. After some initial exposure, usually about 2 x 10^{21} n/cm^2, there is a rapid decrease in CTE from $\sim$ 7 x 10^{-6} in./in./^{o}C to about 1-2 x 10^{-6} in./in./^{o}C. Once saturation of the CTE at the lower value has been achieved, there is very little change with additional irradiation. If there is a detectable difference in the rate of decrease in CTE, it is always slower above 1200^{o}C than below 1200^{o}C.

Electrical Resistivity

The effect of irradiation on the electrical resistivity of the graphites is presented in Figures 45 through 65. Generally, the same trends are evident in all the graphites. The resistivity increases rapidly with irradiation, but saturates at a relatively low exposure. In some of the conventional anisotropic materials, it appears that the resistivity begins to increase again after $\sim$ 6 x 10^{21} n/cm^2 when the irradiation temperature is below 1200^{o}C. This exposure approximately corresponds to the point where rapid dimensional expansion becomes prominent in these graphites. The level of saturation of the resistivity appears to be independent of irradiation temperature below 1200^{o}C but demonstrates a definite dependency on temperature above 1200^{o}C. At temperatures below 1200^{o}C, the resistivity normally increases to at least 2-1/2 times its unirradiated value, while above 1200^{o}C the resistivity usually only doubles. Where data are available at 1400^{o}C, the resistivity increase is without exception significantly less than observed at 1200-1300^{o}C at an equal exposure. Another observation that can be made concerning the electrical resistivity data is that while the unirradiated resistivity of isotropic graphites is generally higher than that of conventional anisotropic materials, the fractional increase with irradiation is usually less.

Young's Modulus

The effect of irradiation on Young's modulus of the graphitesis shown in Figures 66 through 86. The data are badly scattered and no attempt was made to fit curves to them. In conventional, anisotropic graphites, there appears to be a small increase in Young's modulus with irradiation. The increase at 1200-1300°C is generally less than at 1000-1200°C. In the isotropic and near isotropic graphites (RP4, RC5, H328, 9650, 9751, and POCO), the increase in Young's modulus is more apparent and seems to increase continuously with exposure. Again the increase at 1200-1300°C is generally less than at 1000-1200°C. Where low exposure 1400°C data are available for some graphites, the increase in Young's modulus is nearly always less than at lower temperatures.

DISCUSSION AND CONCLUSIONS

The dimensional behavior of conventional- and needle-coke graphites (EGCR, CSF, TSX, H327, and 9567) under irradiation at 1000-1200°C follows the same anisotropic trends observed in earlier irradiations at lower temperatures, but the distortions occur at an accelerated rate. Contraction in the transverse direction is faster and turnaround occurs earlier, usually around 3-4 x 10^{21} n/cm^2. Also, the expansion rate after turnaround is greatly increased at 1000-1200°C over that at 700°C. In the parallel orientation, contraction again is faster at 1000-1200°C, and it does not appear that the contraction has ceased by an exposure of 14 x 10^{21} n/cm^2. At irradiation temperatures above 1200°C, however, a markedly different behavior is observed. While the initial contraction rate in the transverse direction is increased over that at 1000-1200°C, turnaround is slower and the subsequent expansion rate is considerably reduced. Although there are a few exceptions where turnaround appears to occur faster above 1200°C, there is reason to suspect the validity of the data in these cases. In the parallel direction, the behavior at 1200-1300°C is generally the same as seen at 1000-1200°C. Since lifetimes of reactor graphites are usually limited by high exposure expansion, the effect of the slower

turnaround and reduced expansion rate at temperatures above 1200°C on reactor lifetime is apparent. Designing graphite reactors to operate at temperatures above 1200°C would not only achieve better thermal-to-electrical conversion efficiencies, but would also result in extended reactor lifetimes. However, it is recognized that fuel-melting problems in HTGRs may preclude reactor operation at these high temperatures. The reason for the slow turnaround and reduced expansion rate at temperatures above 1200°C is believed to be due to the increased irradiation-creep constant at these higher temperatures. Expansions of the crystallites are thought to be accommodated by creep rather than resulting in intercrystalline fracture and the accompanying crack generation and expansion in the bulk graphite. A more complete discussion concerning this behavior is presented in Ref. (7).

The behavior of the isotropic and near isotropic graphites with an intermediate coefficient of thermal expansion (RP4, RC5, H328, and 9640) is considerably improved over that of the conventional nuclear graphites. While the same trends are evident, i.e., contraction, turnaround, and expansion, there is much less anisotropy in the behavior. Also, the point of turnaround is usually delayed and the rate of subsequent expansion at 1000-1200°C is reduced from that of conventional graphites. Again, at temperatures above 1200°C, the rate of expansion after turnaround is very slow in these graphites.

The isotropic graphites (9650 and POCO) that have a high coefficient of thermal expansion (6-7 x 10^{-6} in./in./°C) behave much differently than the other materials when irradiated at 1000-1200°C. There is immediate expansion with irradiation, but the expansion peaks out at approximately 1% after $\sim$ 3 x 10^{21} n/cm^2 and does not become prominent again until the exposure approaches 10^{22} n/cm^2. The expansion rate even at these high exposures is considerably less than observed in conventional graphites at high fluences. When irradiated at 1200-1300°C, these graphites gradually contract about 1% with irradiation and do not return to their original length before an exposure of $\sim$ 15 x 10^{21} n/cm^2. In general, these graphites show very good dimensional stability after the initial expansion at 1000-1200°C,

and behavior is quite isotropic. The fact that these graphites expand immediately with irradiation at temperatures below 1200°C is really not surprising, in view of the large coefficient of thermal expansion of these materials. Whereas in convention graphites, there is some accommodation of crystallite expansion (as evidenced by the low CTE's), the crystallite growths in these isotropic graphites are apparently transmitted more directly to the bulk material.

The CTE in the conventional- and needle-coke graphites in the transverse direction generally decreases about 25% with irradiation at 1000-1200°C, and then begins to increase again at an exposure where post-turnaround dimensional expansion becomes prominent ($\sim 4 \times 10^{21}$ n/cm^2). Above 1200°C, there is a gradual decrease of about 25%, and the CTE remains below its unirradiated value to an exposure of at least 14×10^{21} n/cm^2. The behavior of the CTE in the parallel orientation is similar to that of the transverse orientation, although absolute changes are smaller.

The CTE of the isotropic graphites drops rapidly after an exposure of 2-4 $\times 10^{21}$ n/cm^2 from a value of $\sim 7 \times 10^{-6}$ in./in./°C to a value of 1-2 $\times 10^{-6}$ in./in./°C. The exposure where the CTE begins to drop in the high CTE isotropics coincides with the exposure where dimensional growth at 1000-1200°C saturates in these graphites. The reduction in CTE is usually more gradual at temperatures above 1200°C.

The effect of irradiation on electrical resistivity is about the same for all graphites. Below a temperature of 1200°C, the resistivity increases rapidly and saturates at a level > 2-1/2 times that of the unirradiated value. At 1200-1300°C, the increase in resistivity is about double. The limited data at 1400°C show a lesser increase yet. It appears that the dependence of resistivity on the irradiation temperature agrees with the dependence on annealing temperature seen in previous studies with irradiated graphite.[8,9] Here, there was no decrease in resistivity until the annealing temperature approached 1200°C. Higher temperature anneals

reduced the resistivity further, until all of the resistivity increase was annealed out at a temperature of approximately 1800°C.

Several conclusions can be drawn from the results of these high-temperature irradiations:

- Dimensional changes in graphites irradiated at 1000-1200°C follow the trends observed in irradiations at lower temperatures, but the distortions occur at an accelerated rate.
- At irradiation temperatures above 1200°C, initial contraction is faster than at 1000-1200°C, but turnaround is slower and subsequent expansion occurs at a considerably-reduced rate, thereby increasing the useful lifetime of the graphite.
- Graphites with near-isotropic properties and intermediate CTE's ($3\text{-}6 \times 10^{-6}$ in./in./°C) show improved dimensional behavior over conventional graphites. Length changes are less anisotropic and generally smaller, and turnaround is slower.
- Isotropic graphites with a CTE of $\sim 7 \times 10^{-6}$ in./in./°C show immediate expansion with irradiation at 1000-1200°C. The expansion peaks at ~1% after an exposure of $\sim 3 \times 10^{21}$ n/cm^2, however, and does not become prominent again until an exposure of 10^{22} n/cm^2 is approached. Above 1200°C, these graphites contract (~ 1%) and do not return to their original length before an exposure of $\sim 15 \times 10^{21}$ n/cm^2. Dimensional stability of these graphites is considered very good.
- Limited data at 1400°C shows increased contraction rate at low exposures for all graphites.
- The effect of irradiation on the coefficient of thermal expansion of conventional graphites is a small reduction (~ 25%) followed by an increase again at an exposure where post-turnaround dimensional expansion becomes prominent at 1000-1200°C. Above 1200°C, the CTE decreases gradually about 25% and does not increase again before an exposure of $\sim 15 \times 10^{21}$ n/cm^2.

- The CTE of the isotropic graphites decreases rapidly after an exposure of $\sim 2 \times 10^{21}$ n/cm^2 from $\sim 7 \times 10^{-6}$ in./in./^{o}C to 1-2 x 10^{-6} in./in./^{o}C. The rate of decrease is generally slower at irradiation temperatures above 1200^{o}C.
- Electrical resistivity of all graphites increases rapidly with irradiation and saturates early. The level of saturation appears to be temperature-independent below 1200^{o}C, but shows a definite temperature dependency above 1200^{o}C. The resistivity increases $\sim$ 250% at irradiation temperatures below 1200^{o}C, but only double when the temperature is 1200-1300^{o}C. The increase at an irradiation temperature of 1400^{o}C is considerably less than it is at 1200-1300^{o}C.
- Results of Young's modulus measurements on irradiated graphite are scattered, but it appears that the general trend is an increase in Young's modulus with exposure. The increase at 1200-1300^{o}C is generally less than at 1000-1200^{o}C.

ACKNOWLEDGEMENTS

The comments and suggestions of W. J. Gray were very helpful in preparing this report. Also appreciated were the determined efforts of R. G. Henderson and F. D. Hobbs in capsule assembly, sample measurements, and data handling.

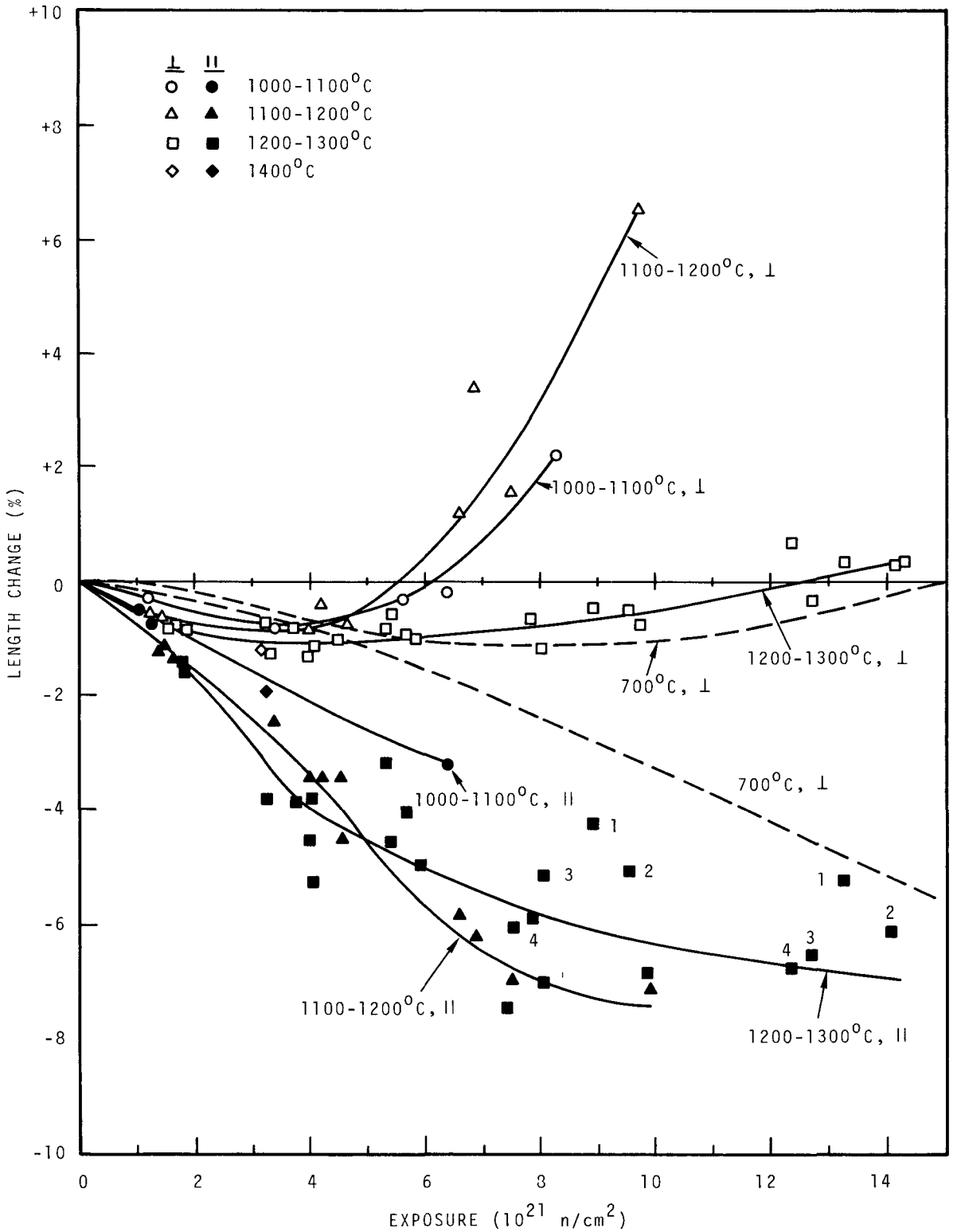

FIGURE 3. Length Change of EGCR.

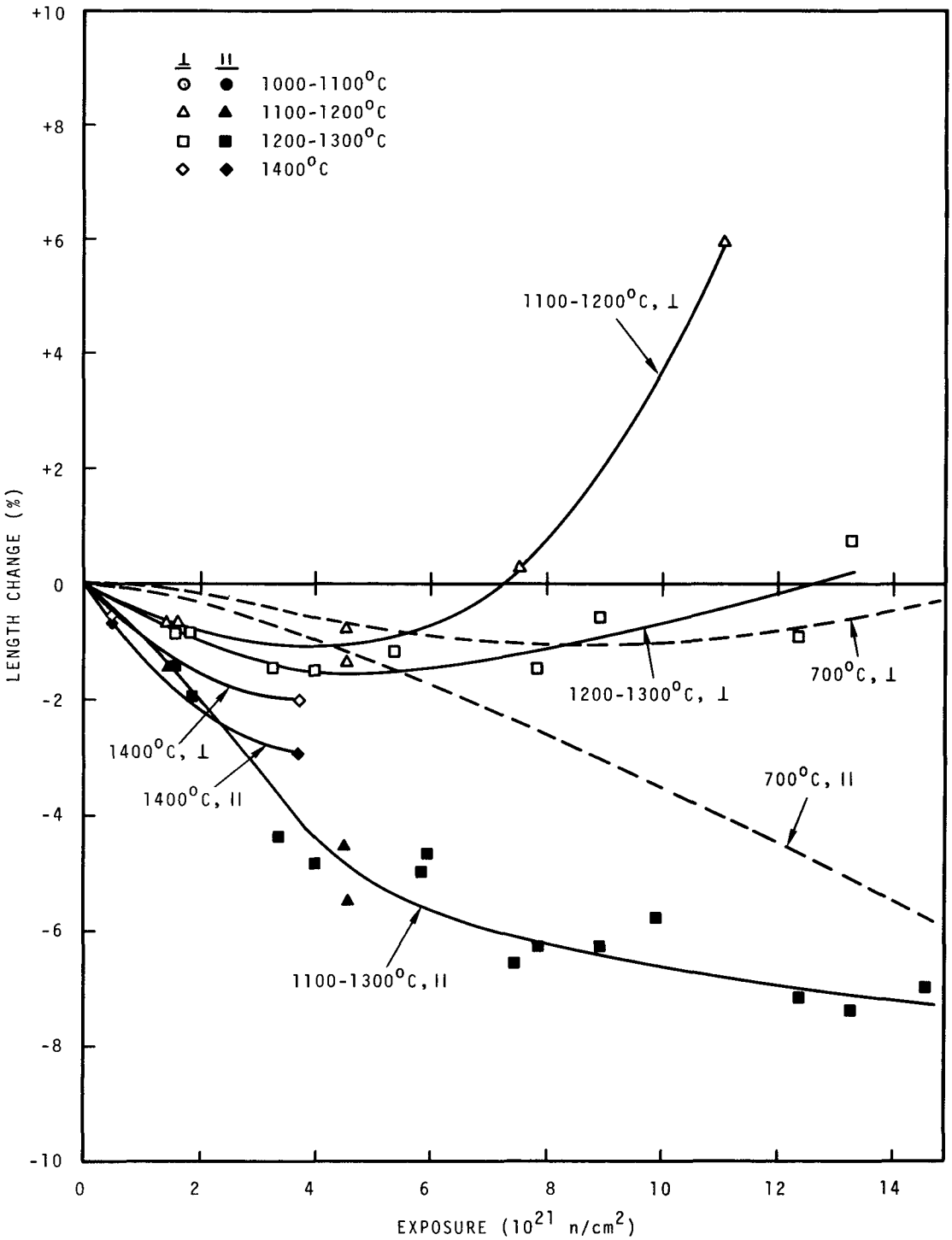

FIGURE 4. Length Change of CSF.

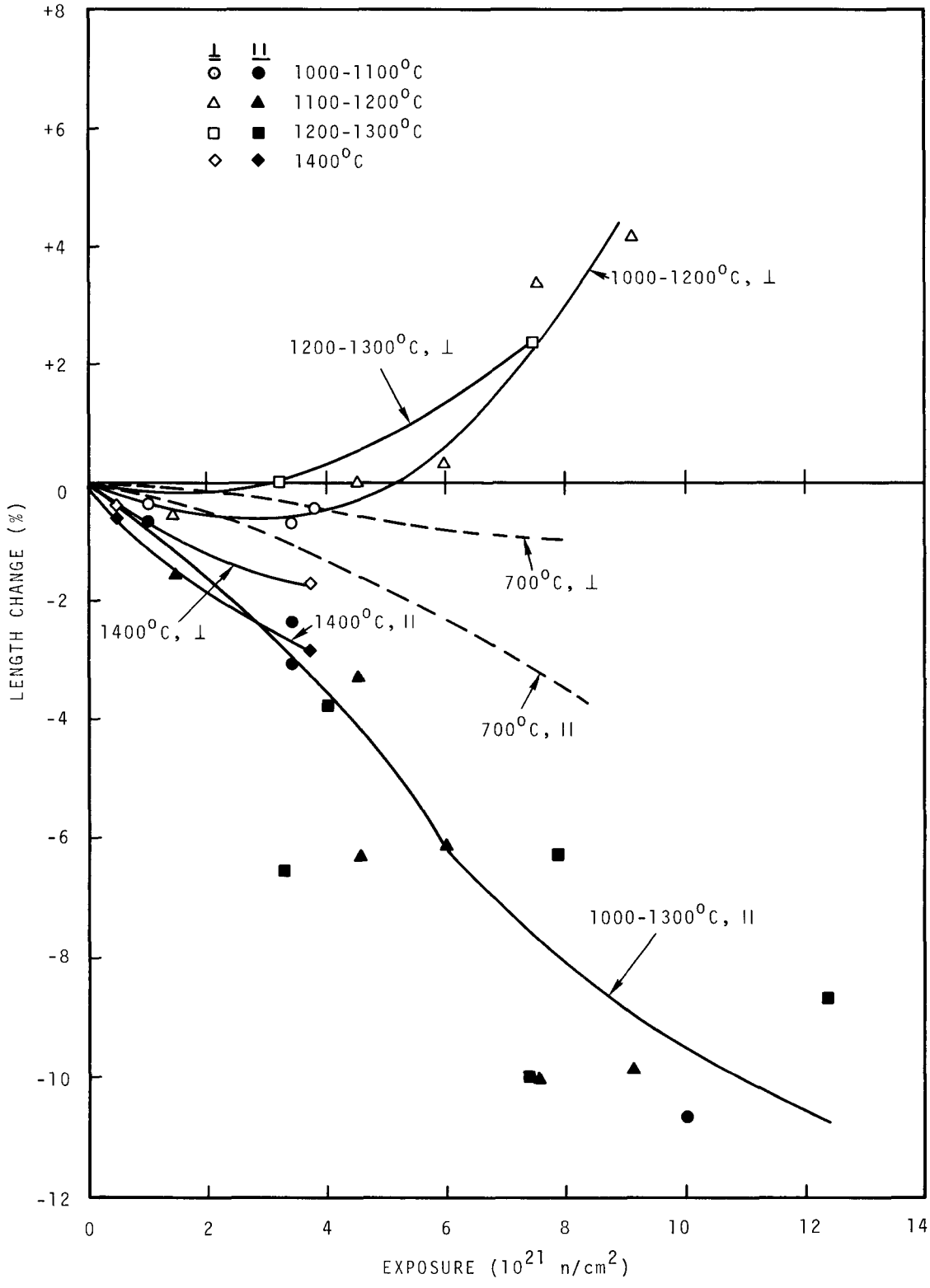

FIGURE 5. Length Change of TSX.

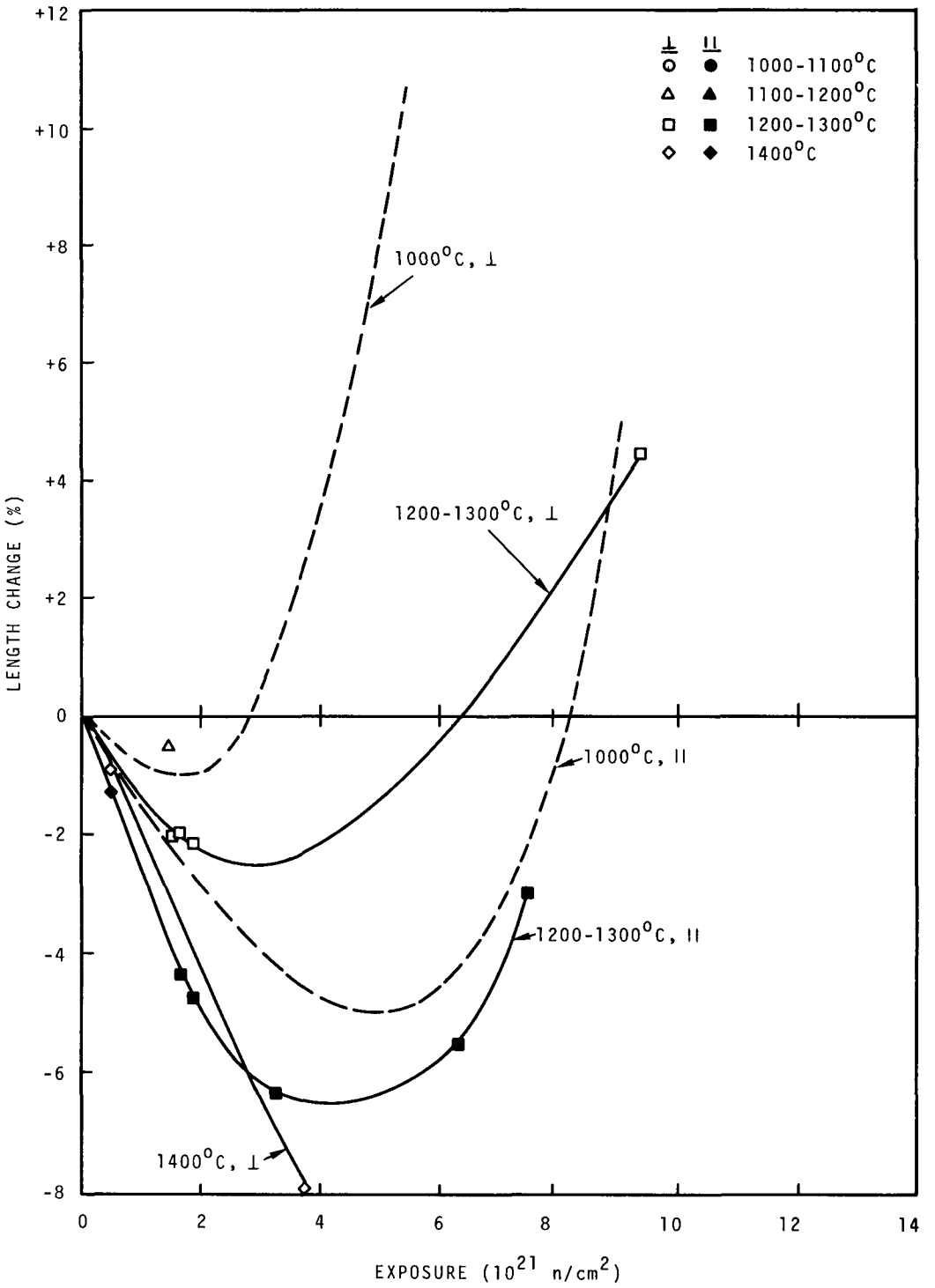

FIGURE 6. Length Change of TSGBF.

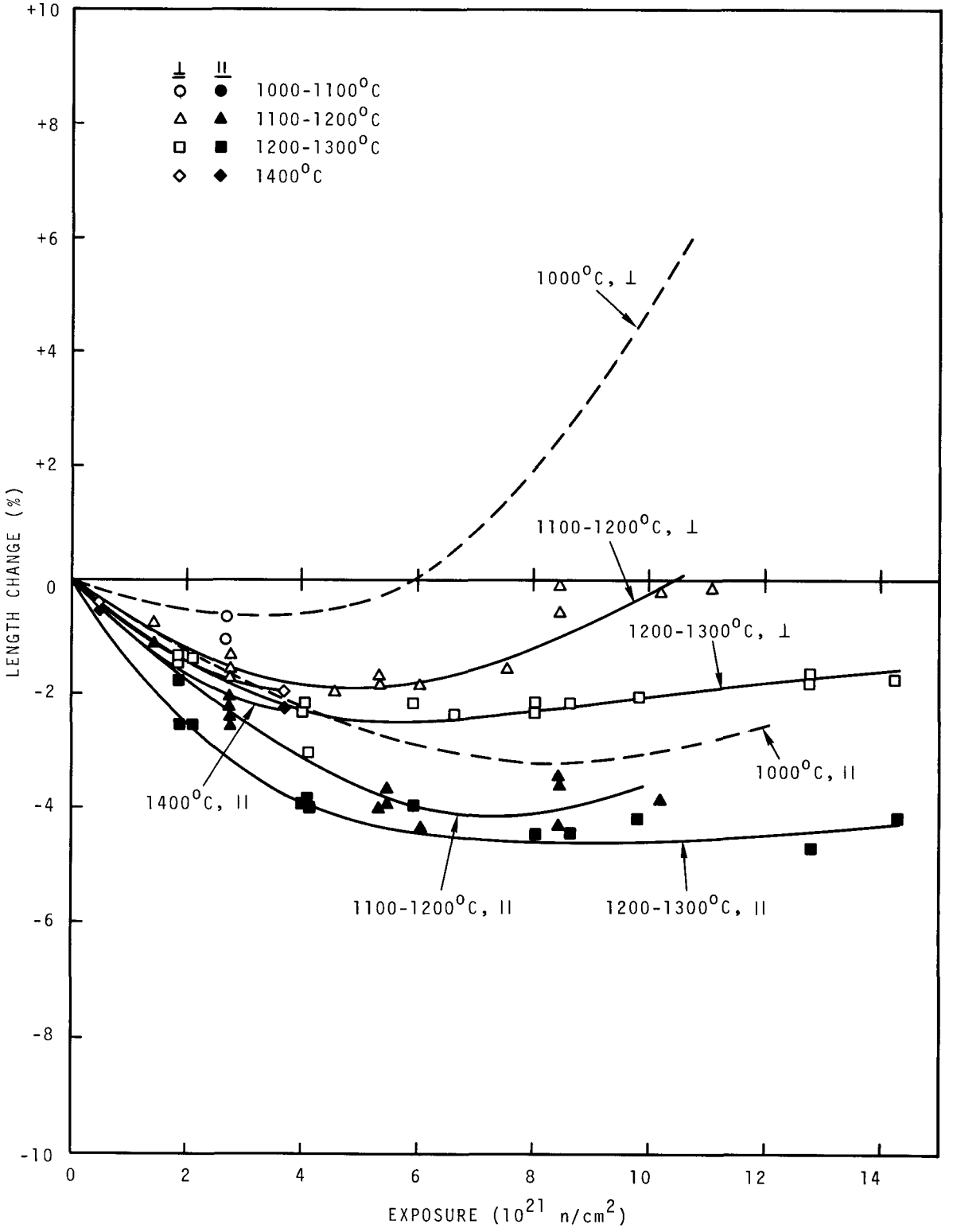

FIGURE 7. Length Change of RP4.

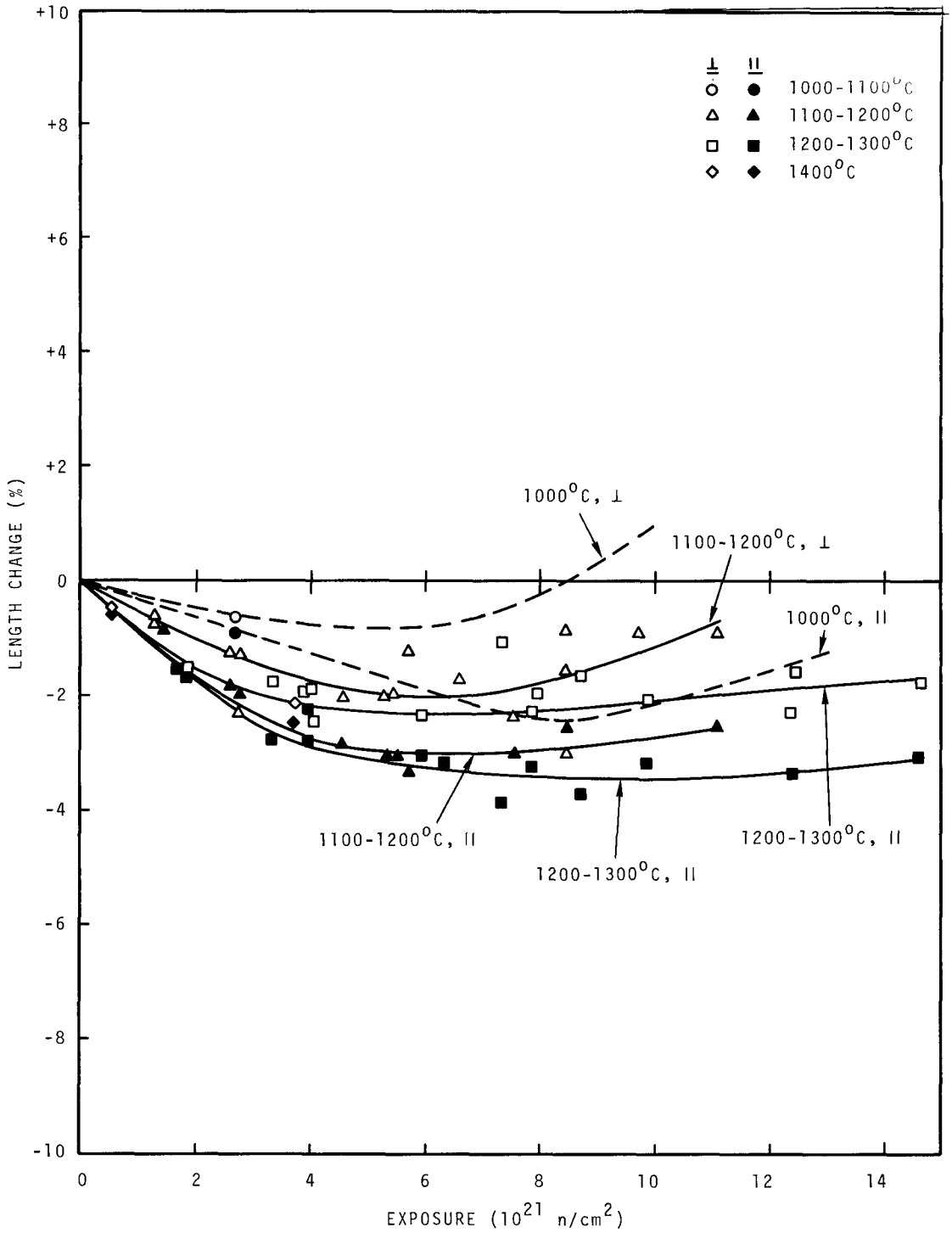

FIGURE 8. Length Change of RC5.

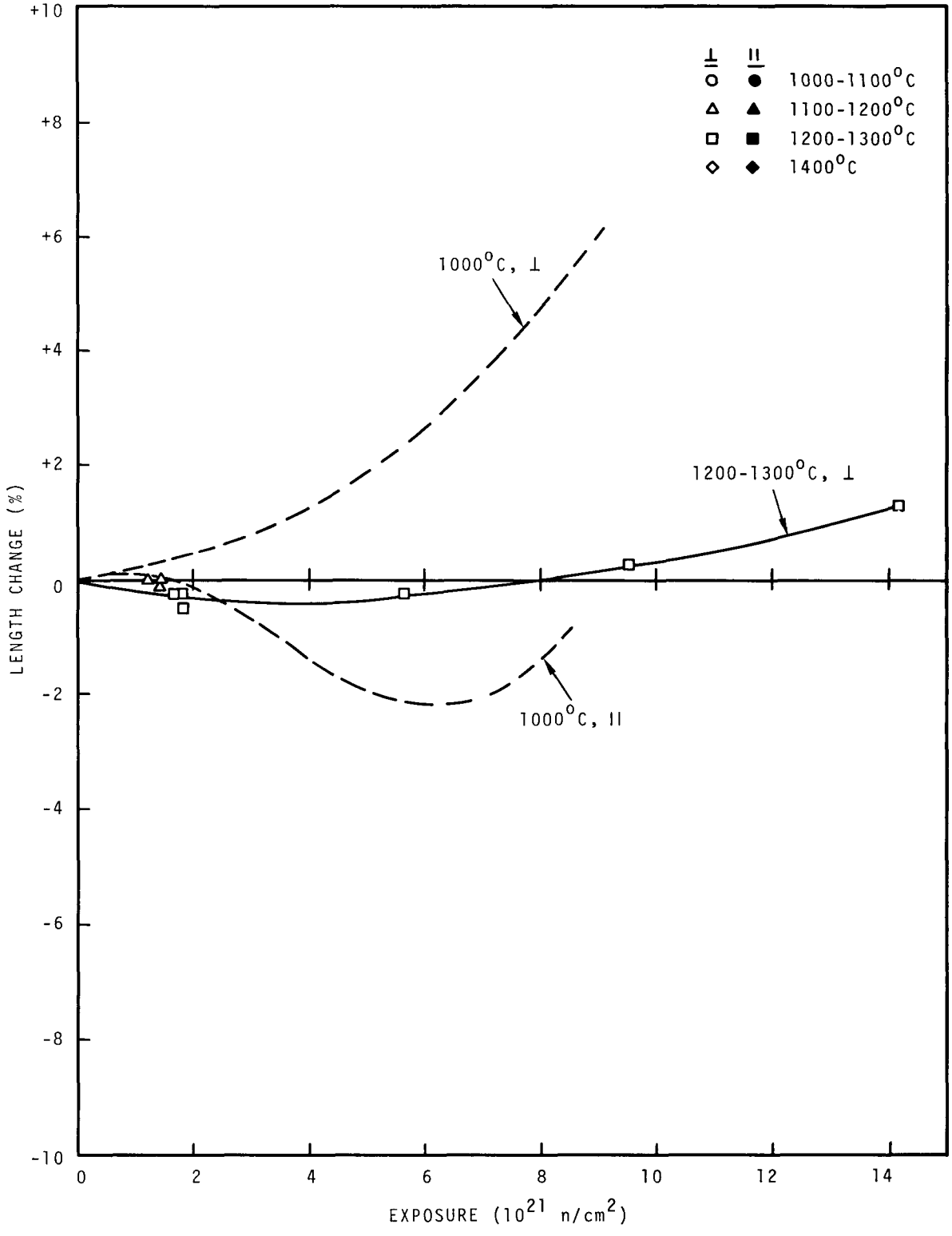

FIGURE 9. Length Change of JOZ.

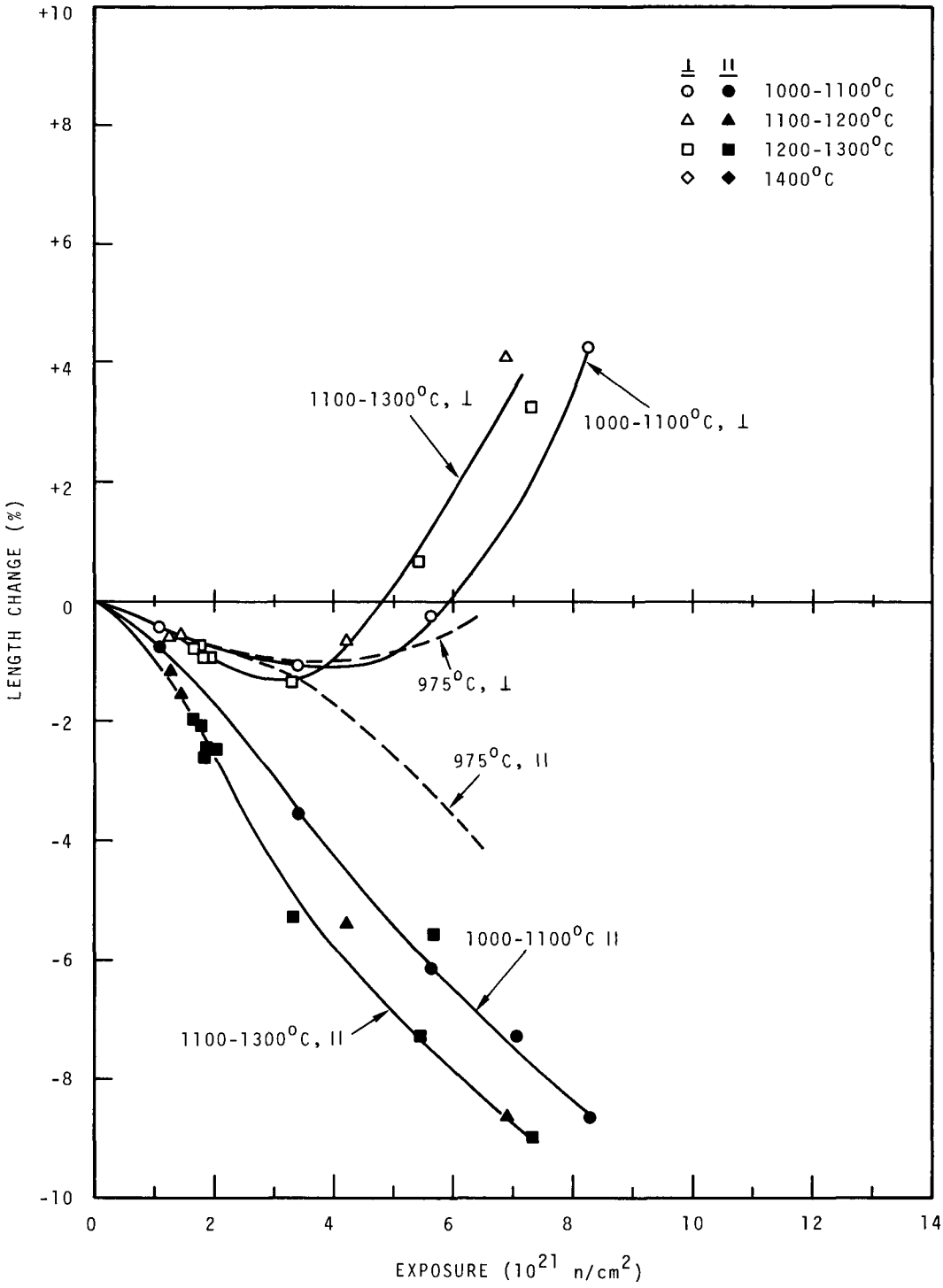

FIGURE 10. Length Change of H327.

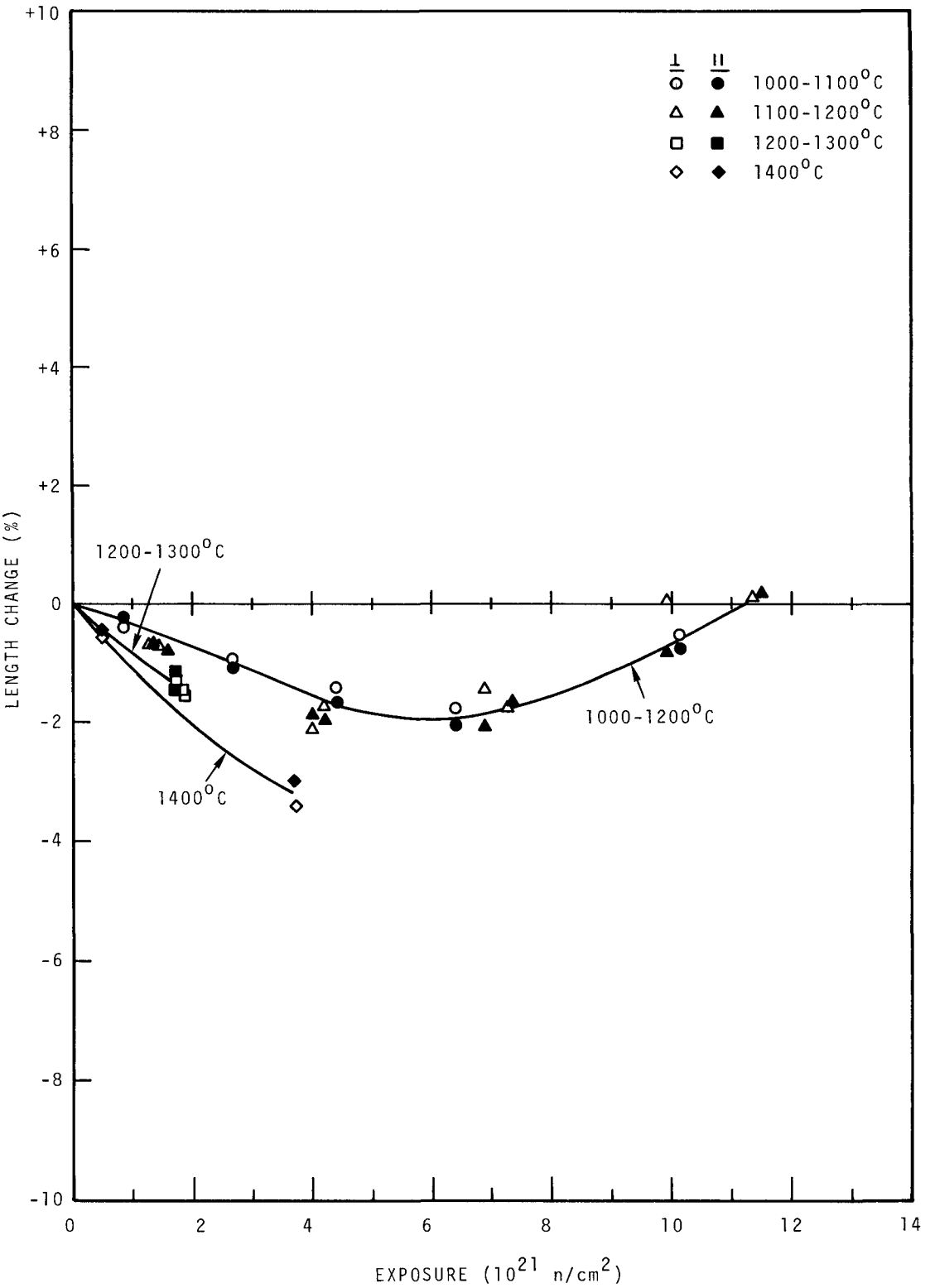

FIGURE 11. Length Change of H328.

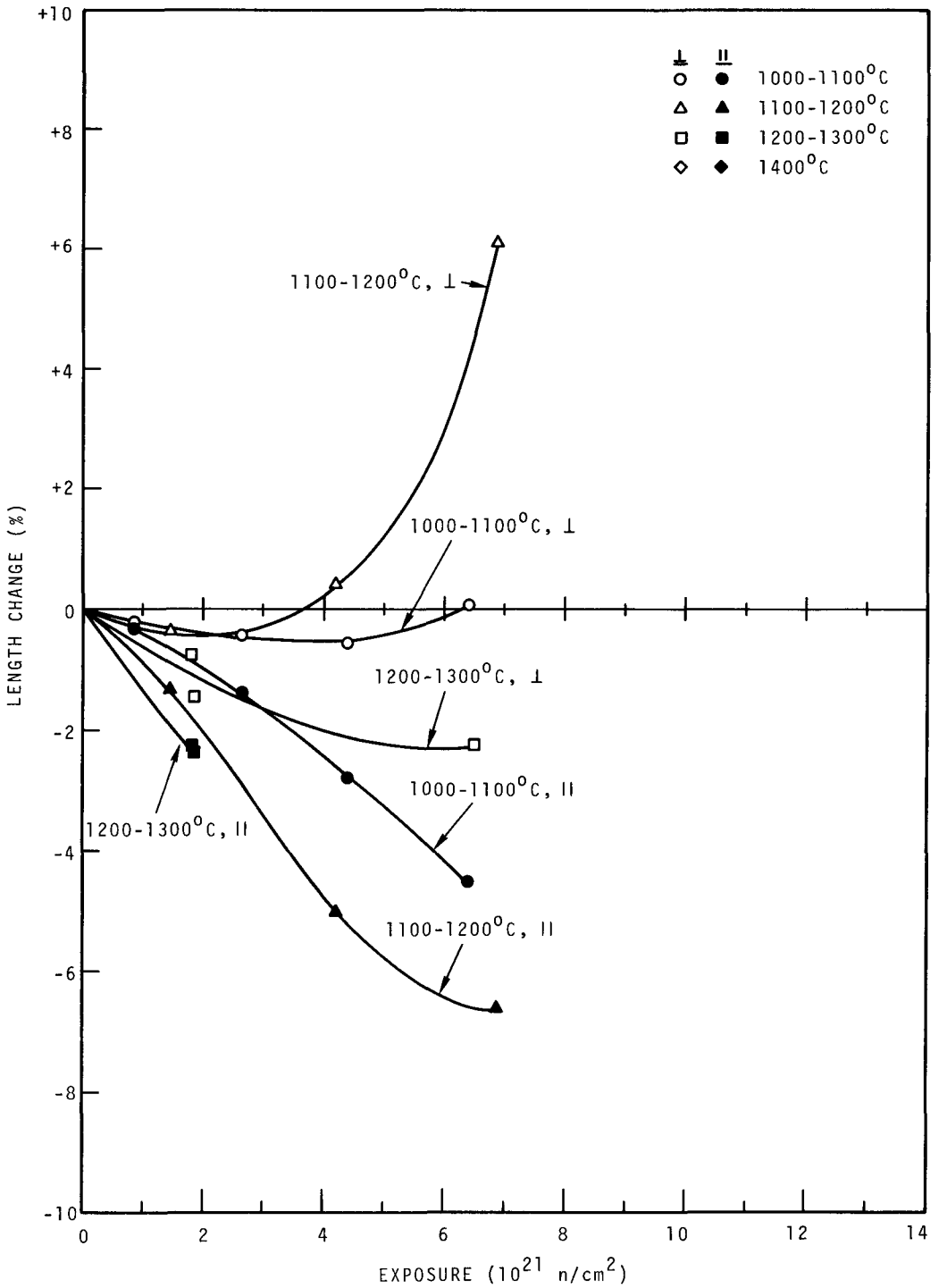

FIGURE 12. Length Change of 9567.

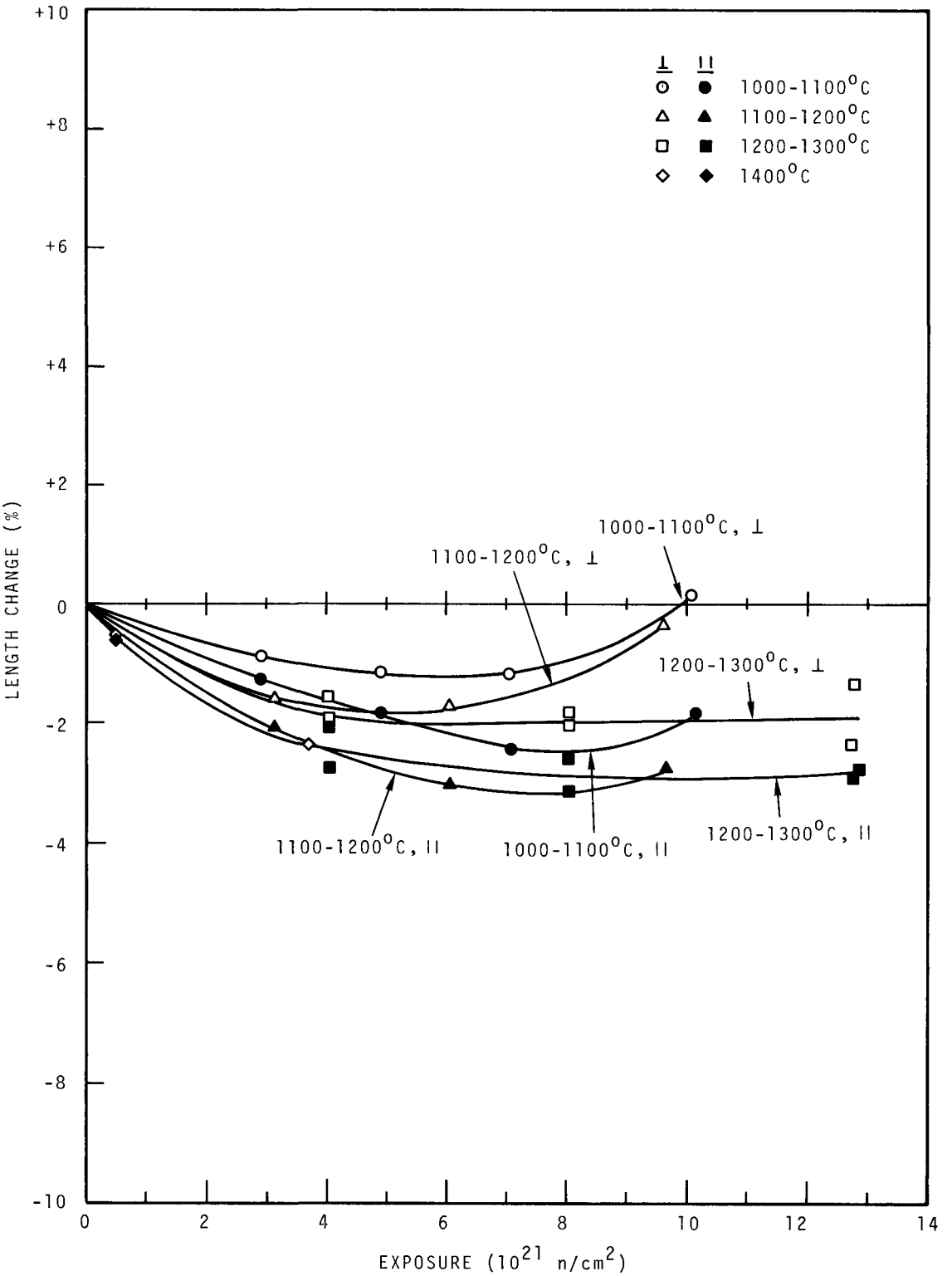

FIGURE 13. Length Change of 9640.

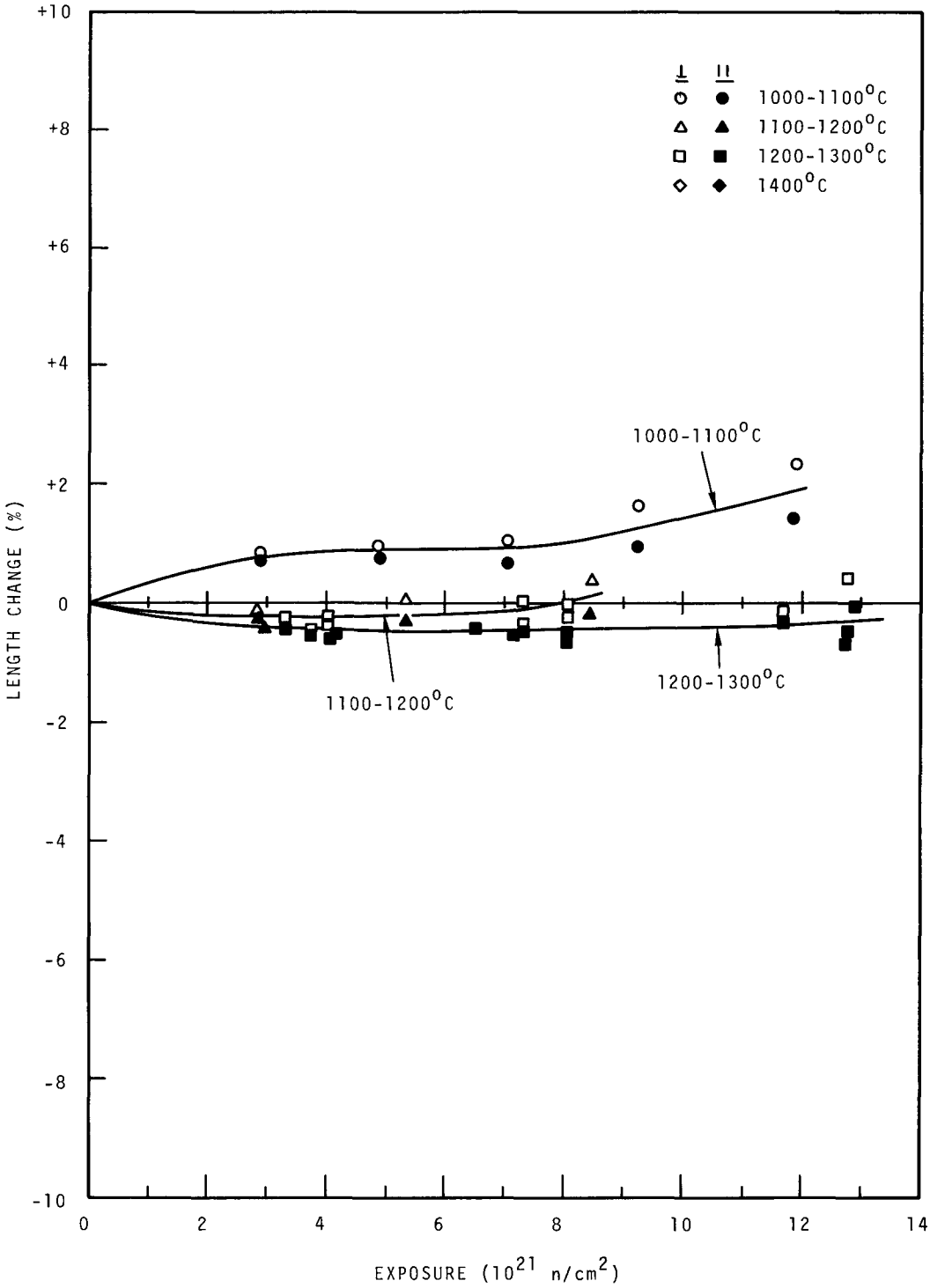

FIGURE 14. Length Change of 9650.

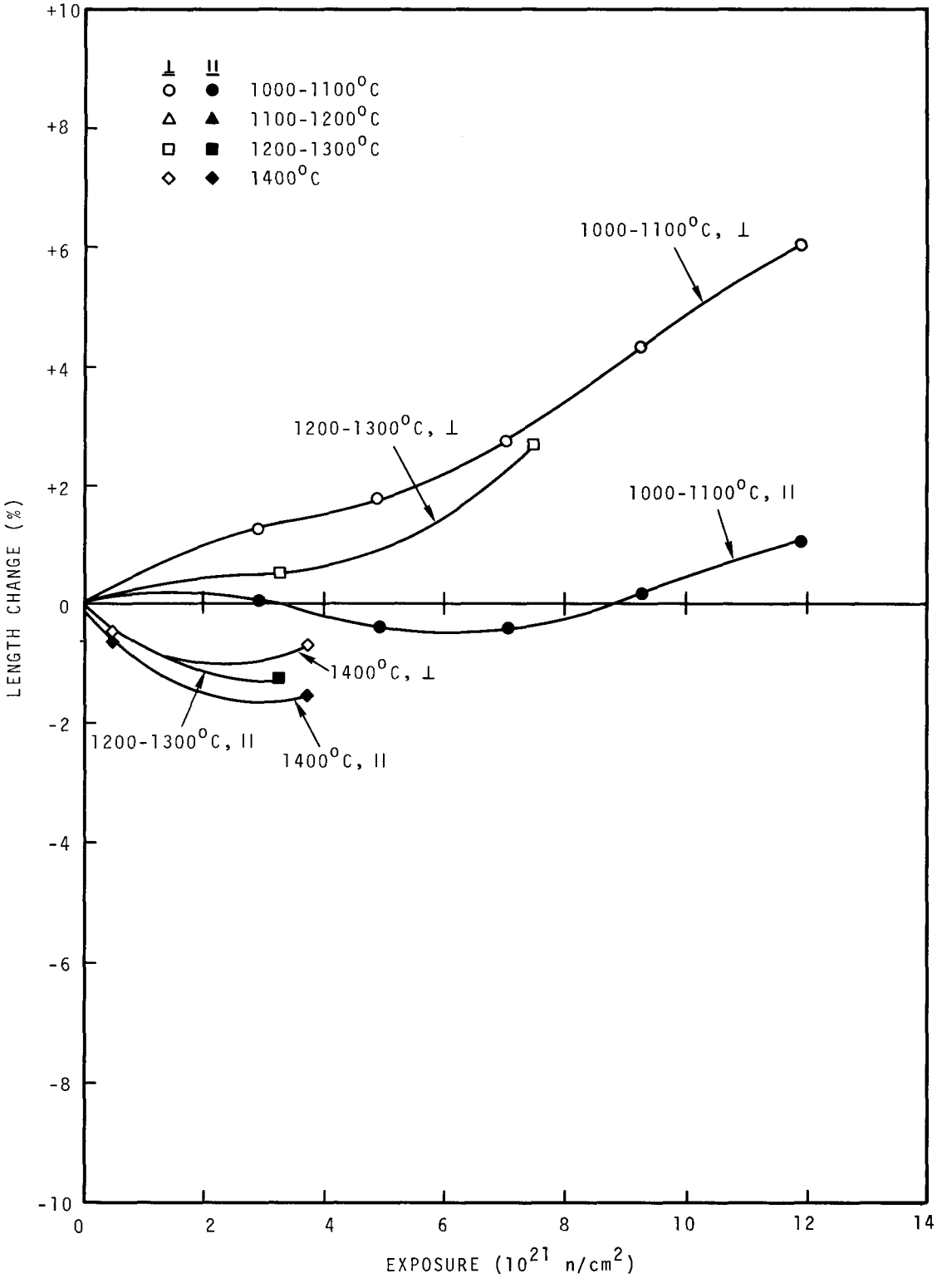

FIGURE 15. Length Change of 9751.

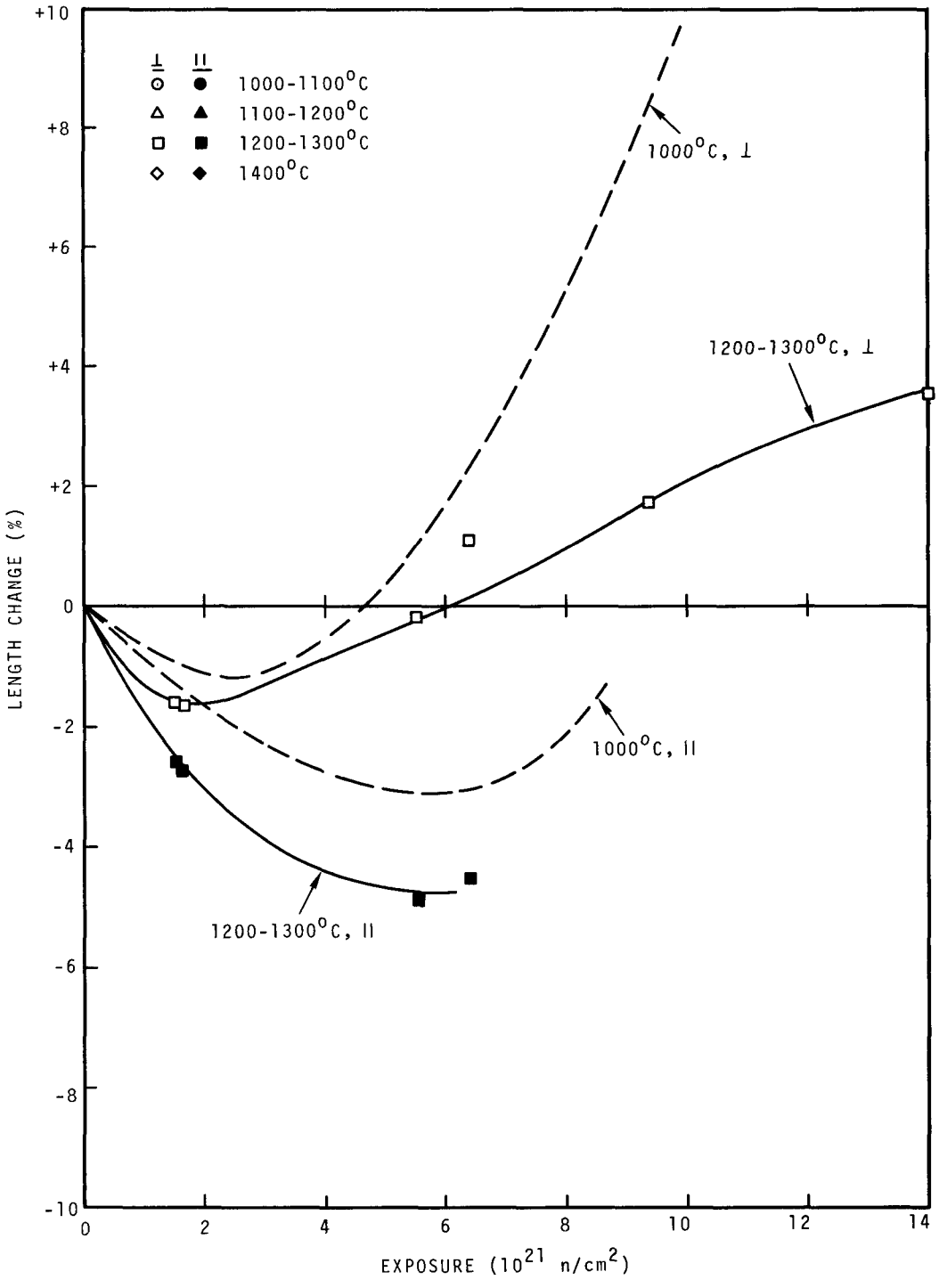

FIGURE 16. Length Change of GN.

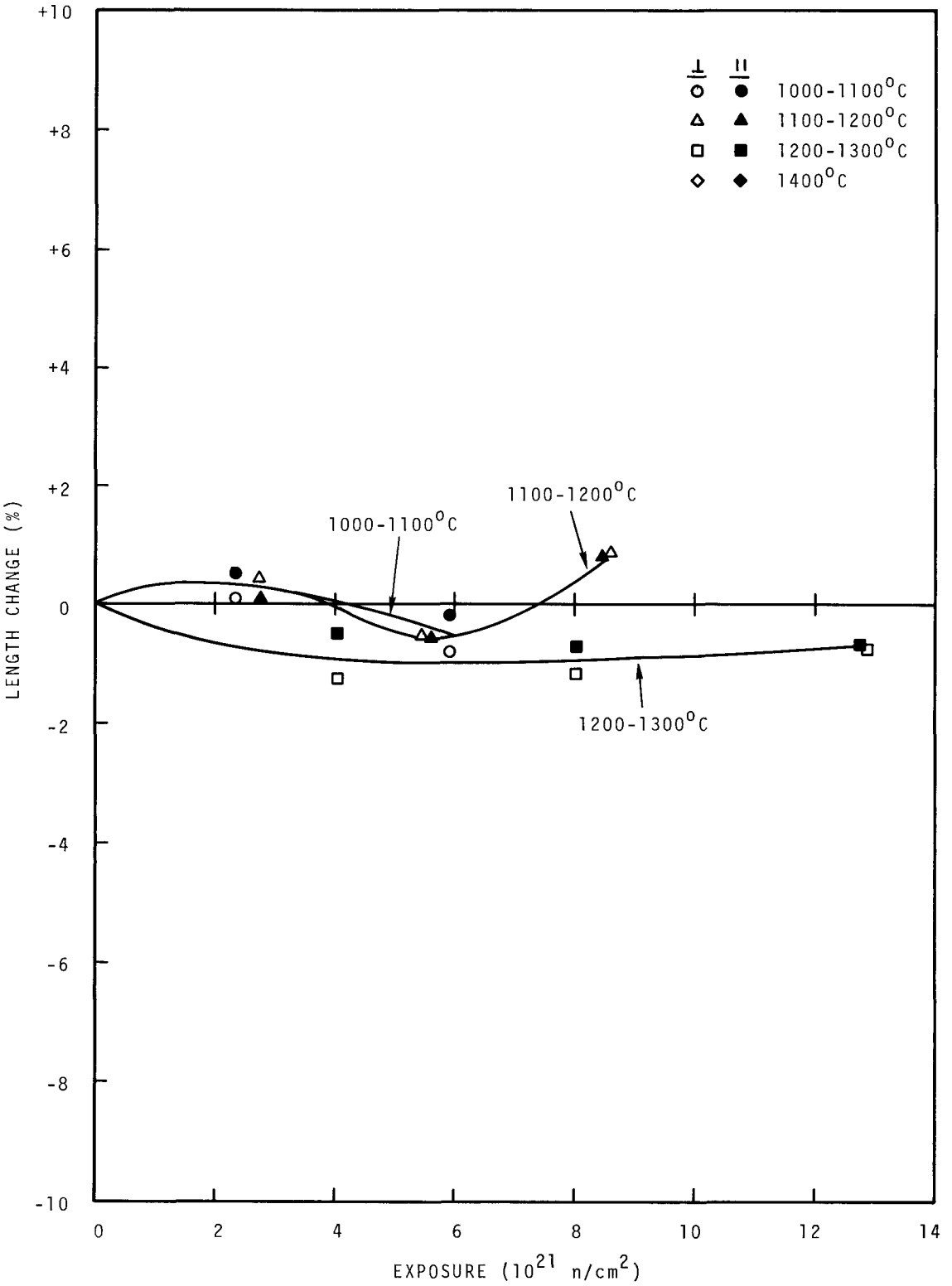

FIGURE 17. Length Change of AXF-Q1.

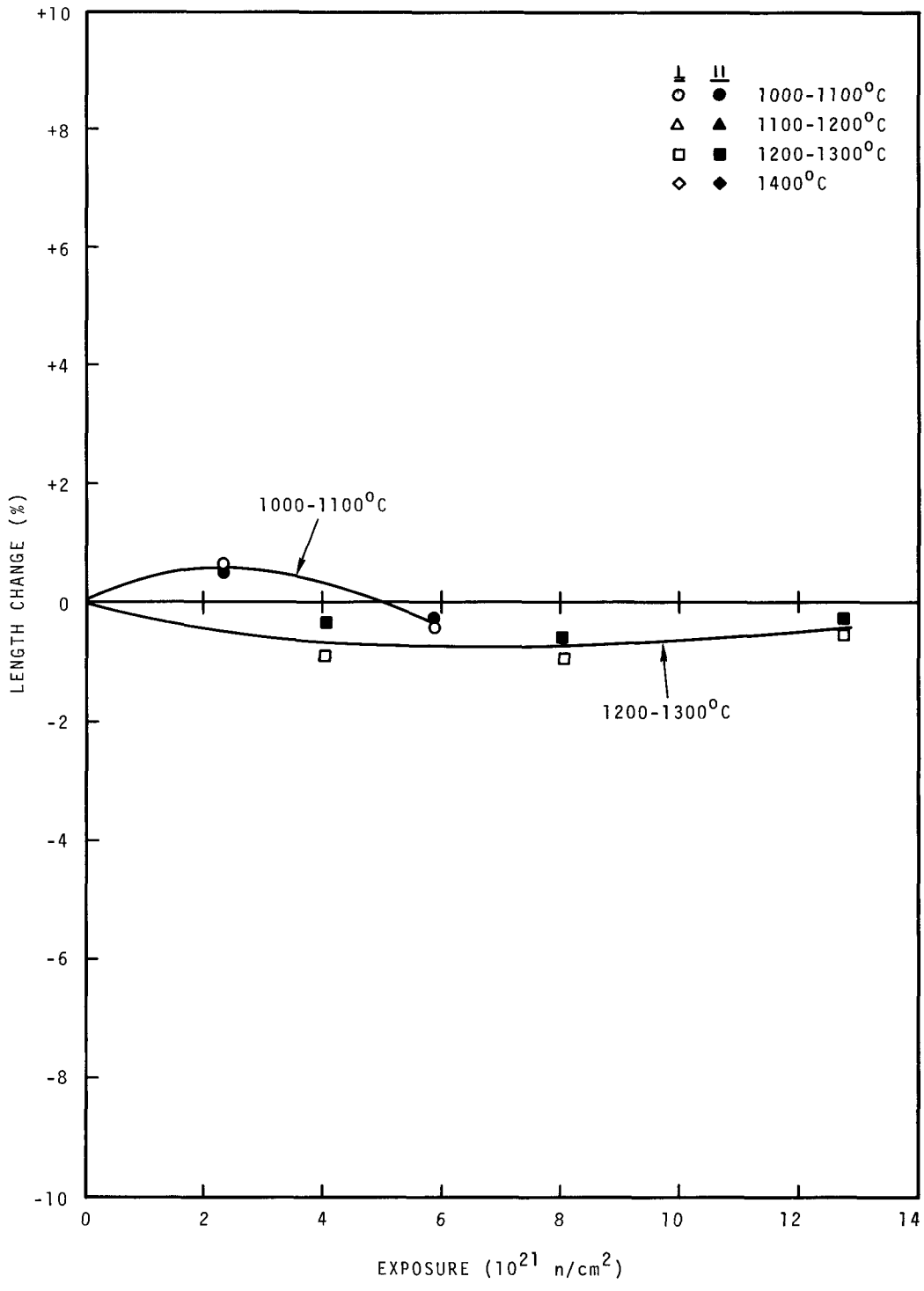

FIGURE 18. Length Change of AXF-5Q1.

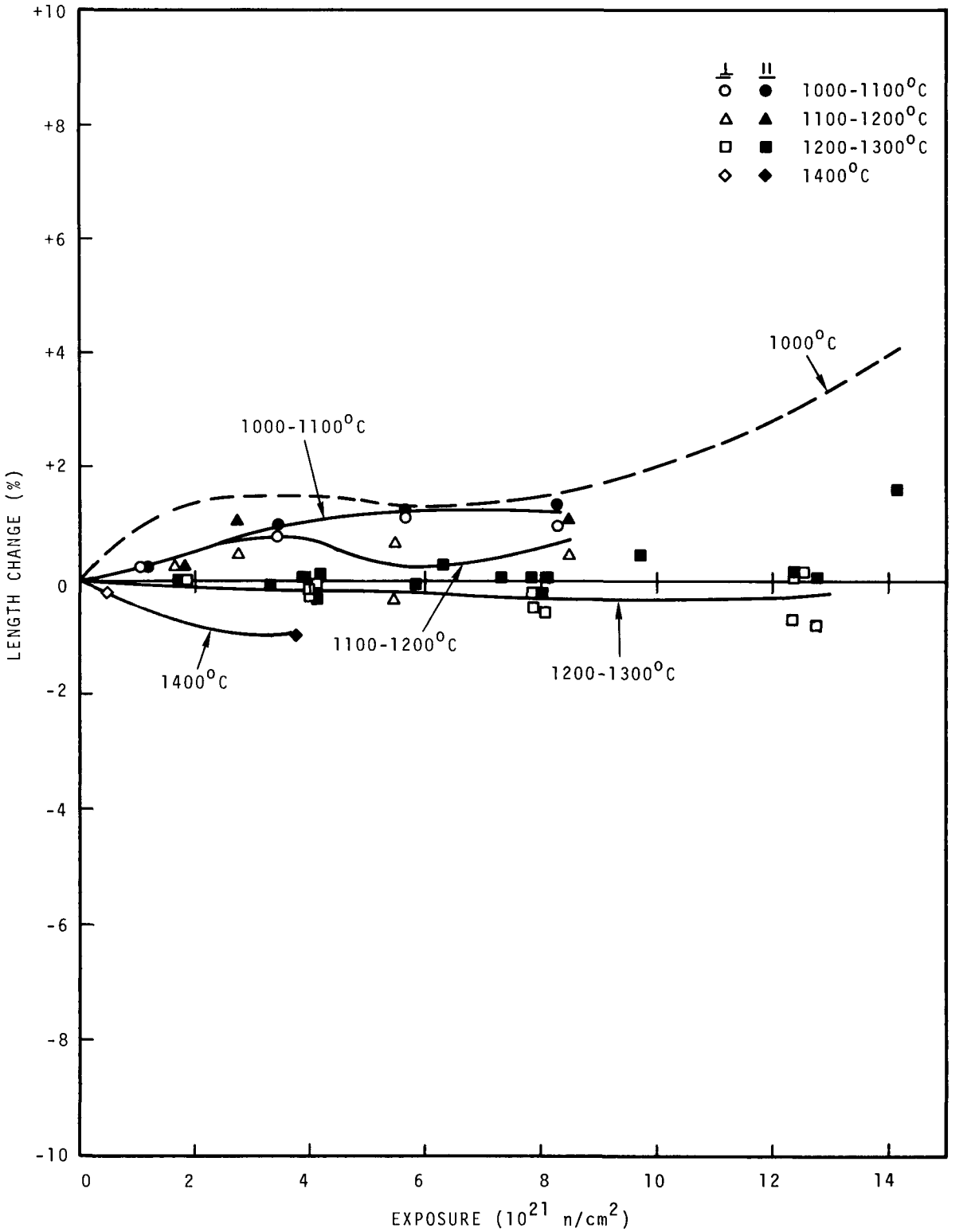

FIGURE 19. Length Change of AXF-8Q1.

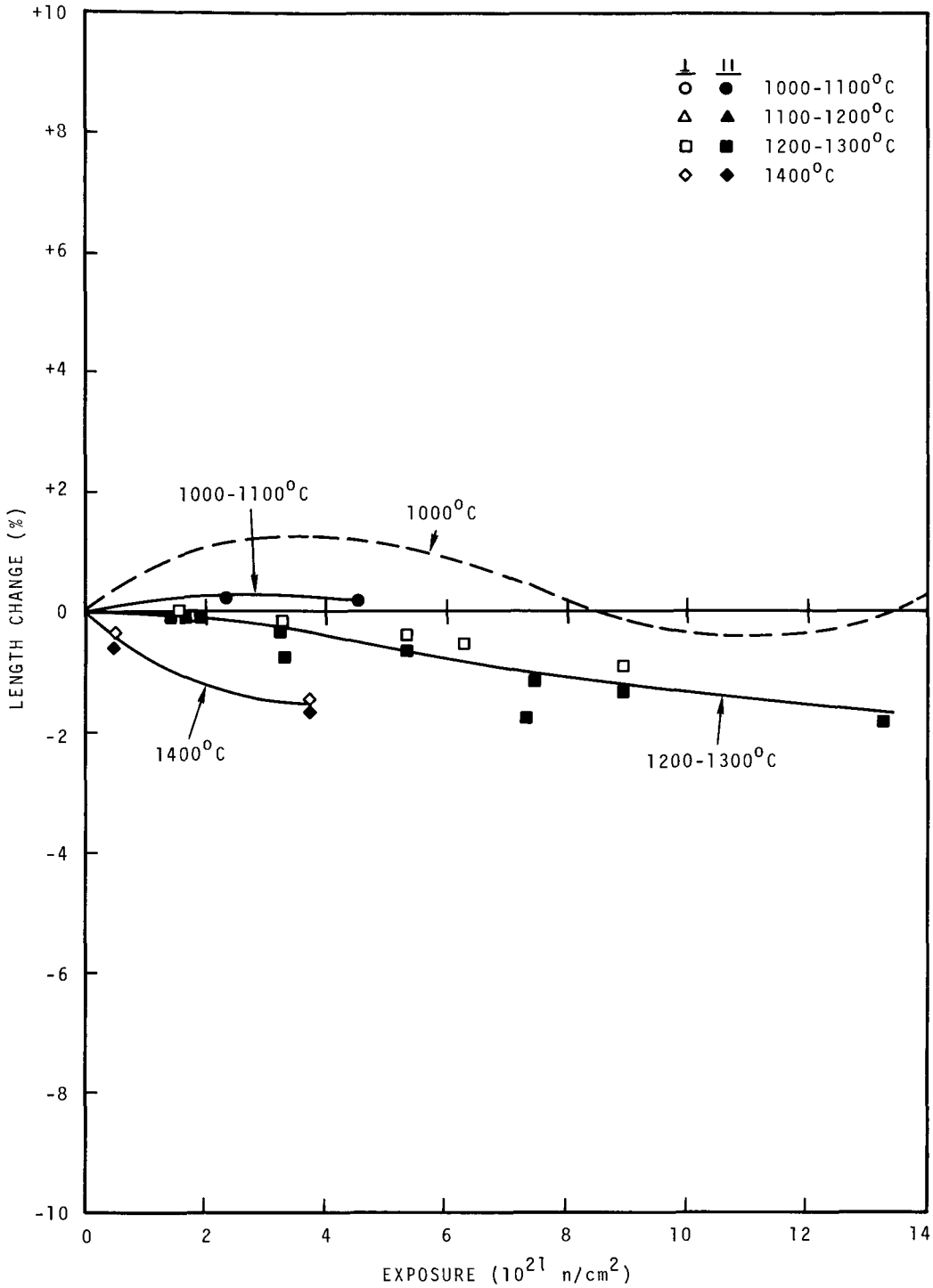

FIGURE 20. Length Change of AXZ-5Q1.

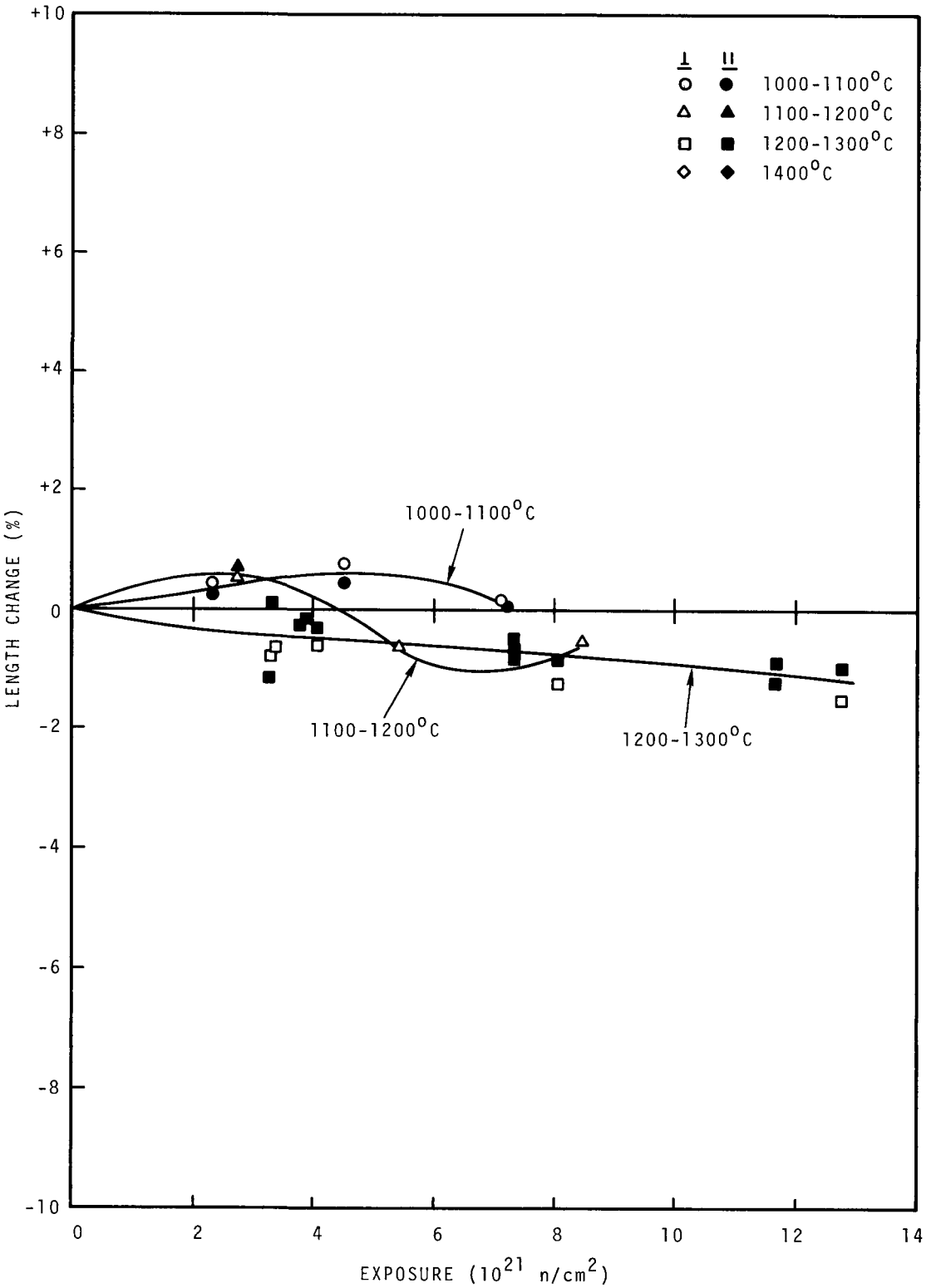

FIGURE 21. Length Change of AXZ-8Q1.

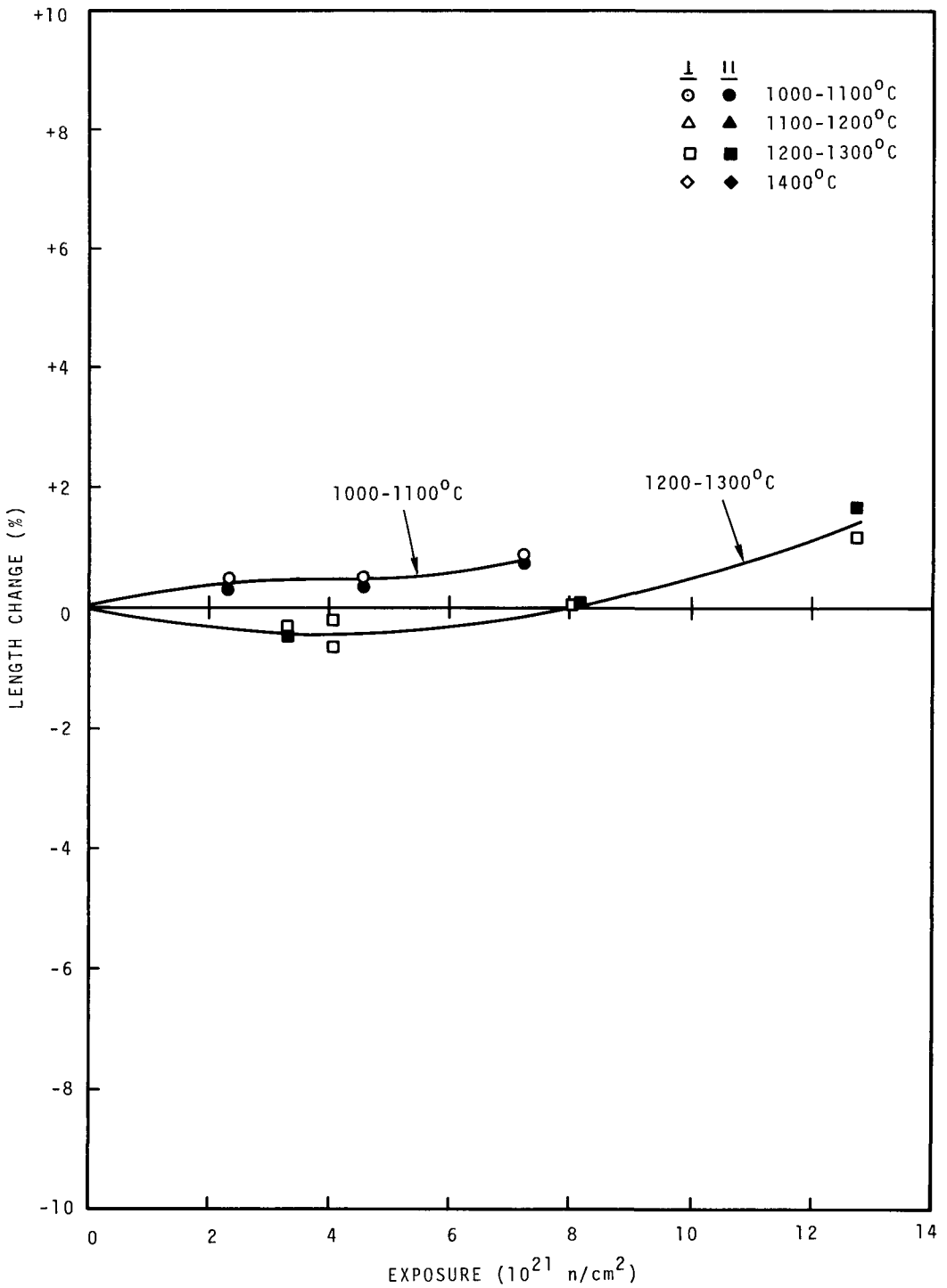

FIGURE 22. Length Change of AXF-5QBG1.

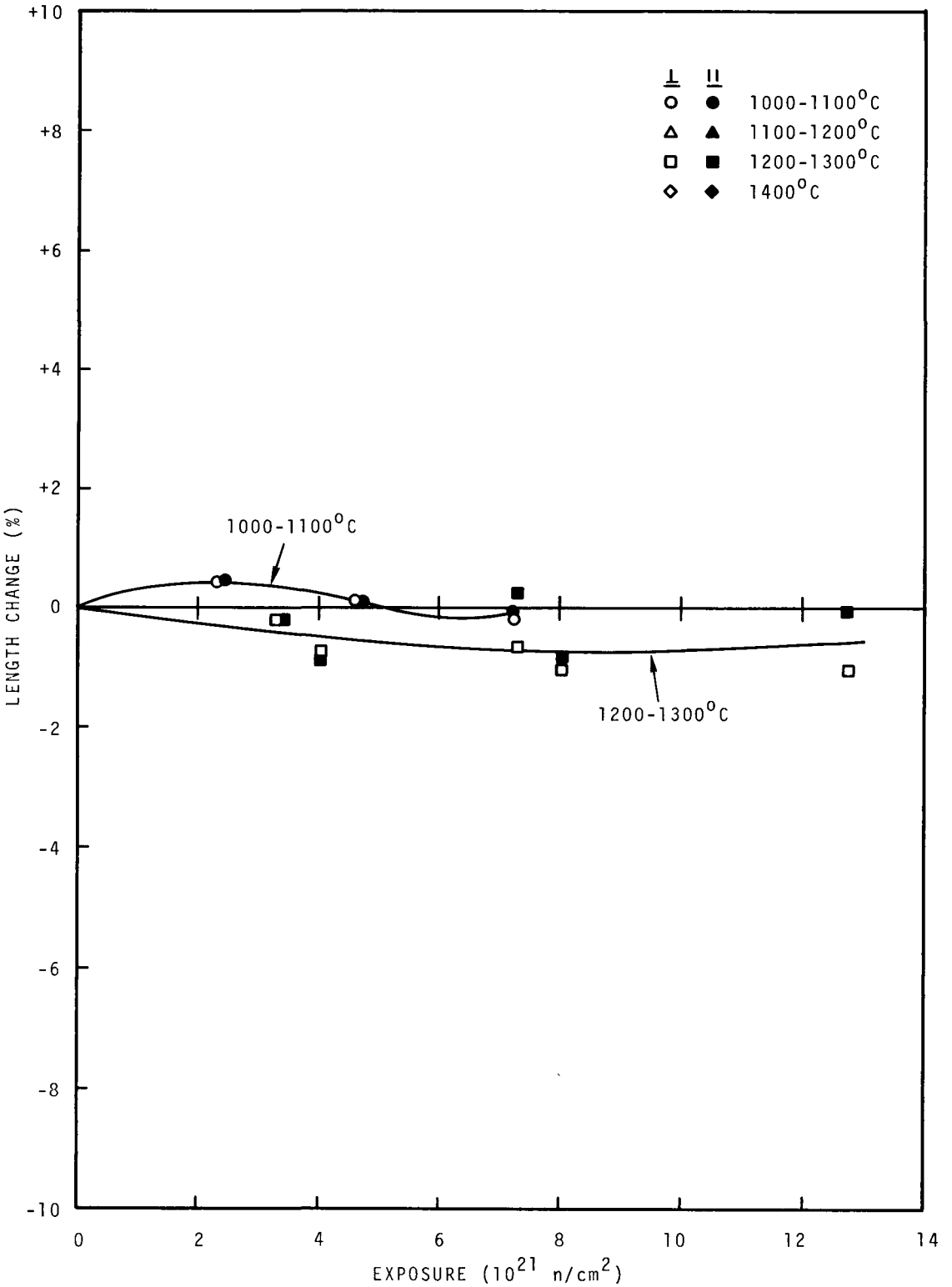

FIGURE 23. Length Change of AXZ-8QBG1.

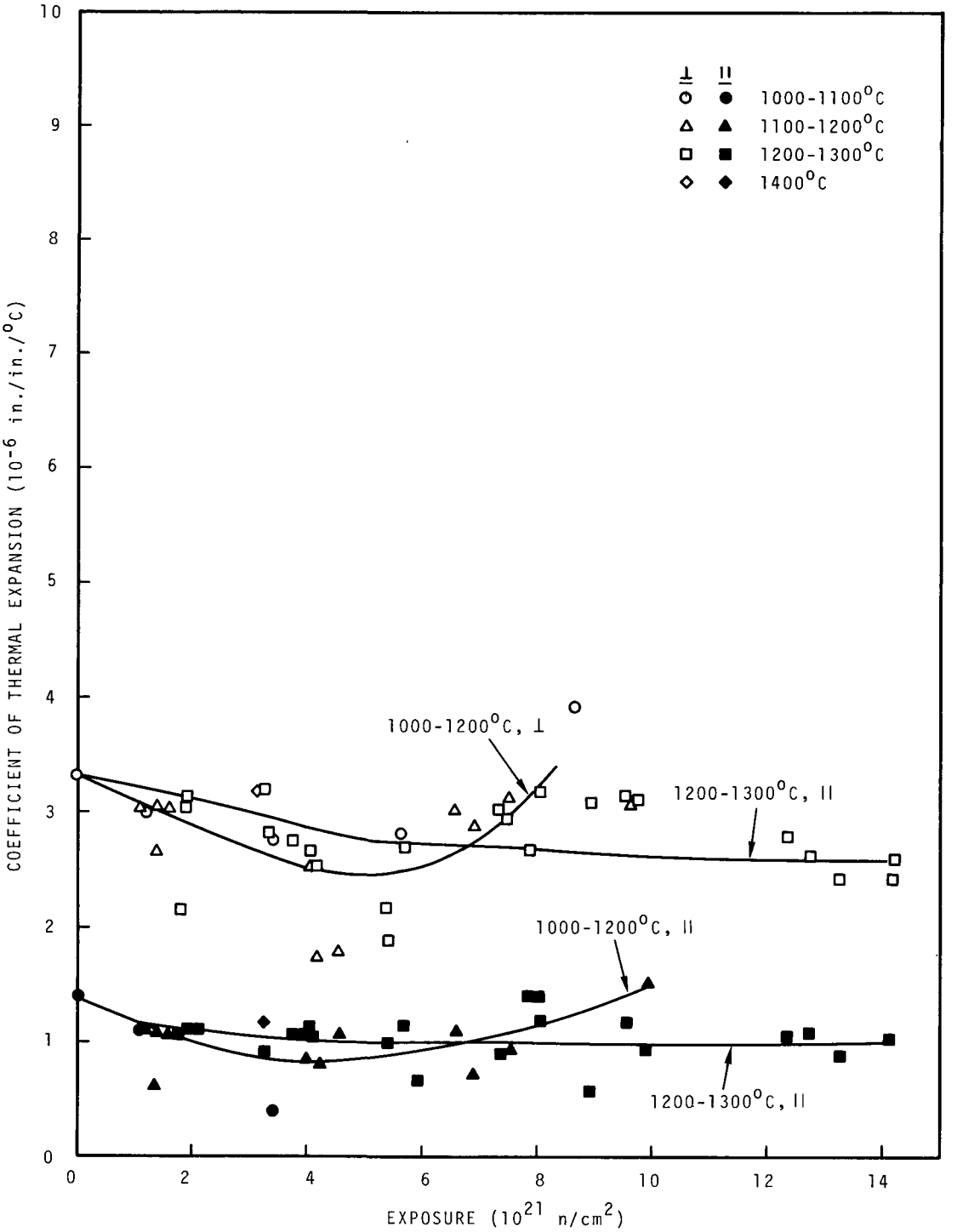

FIGURE 24. Coefficient of Thermal Expansion of EGCR.

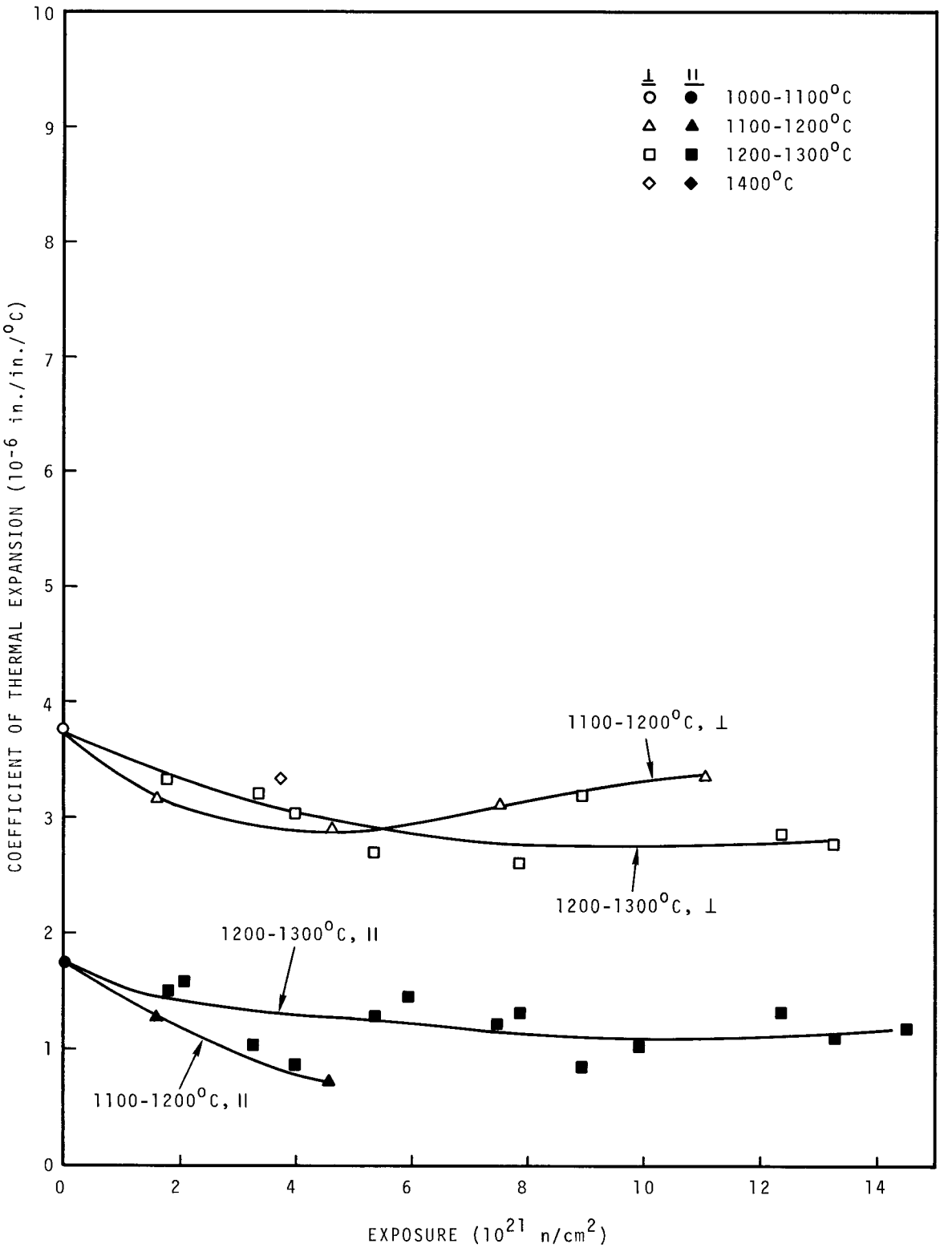

FIGURE 25. Coefficient of Thermal Expansion of CSF.

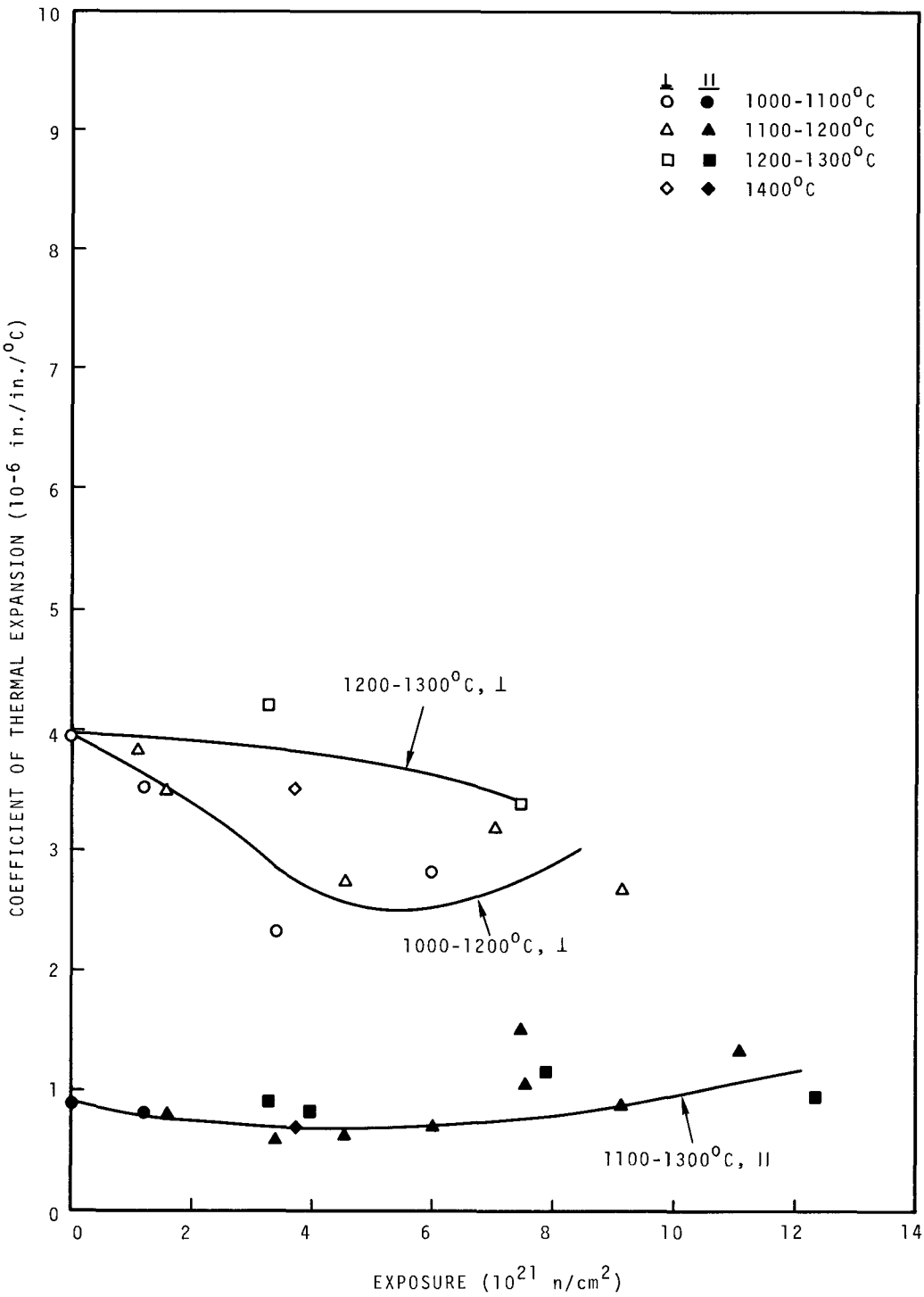

FIGURE 26. Coefficient of Thermal Expansion of TSX.

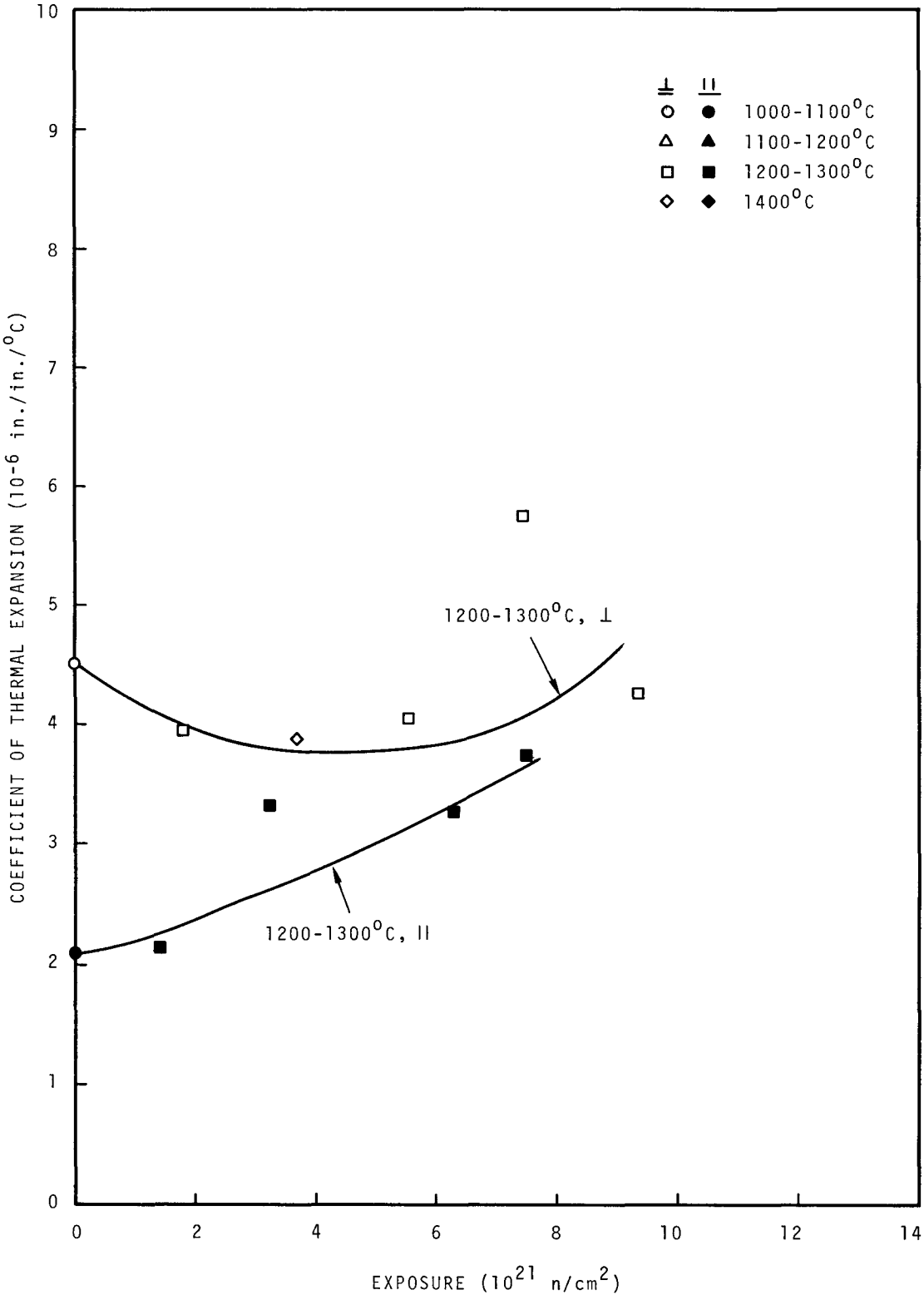

FIGURE 27. Coefficient of Thermal Expansion of TSGBF.

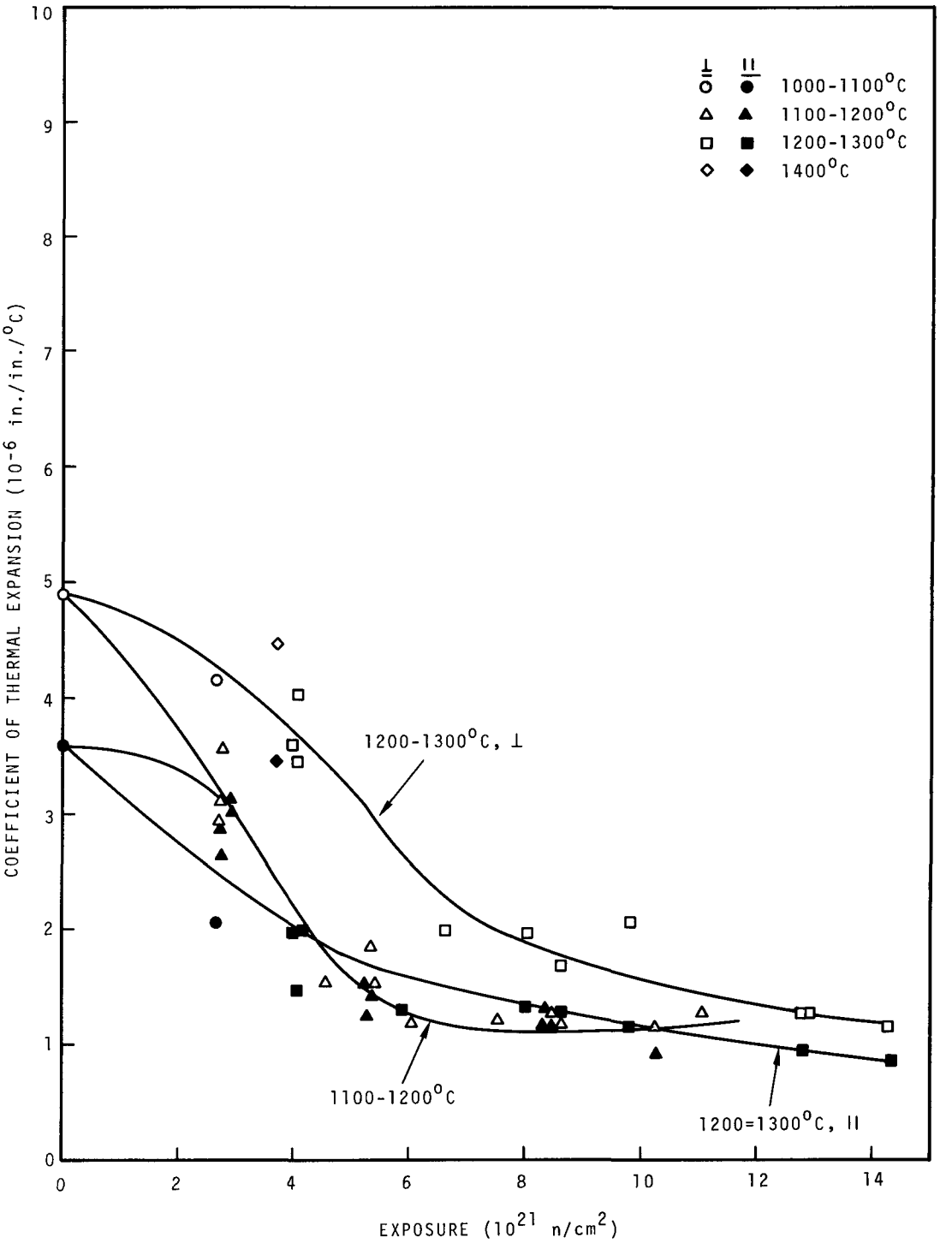

FIGURE 28. Coefficient of Thermal Expansion of RP4.

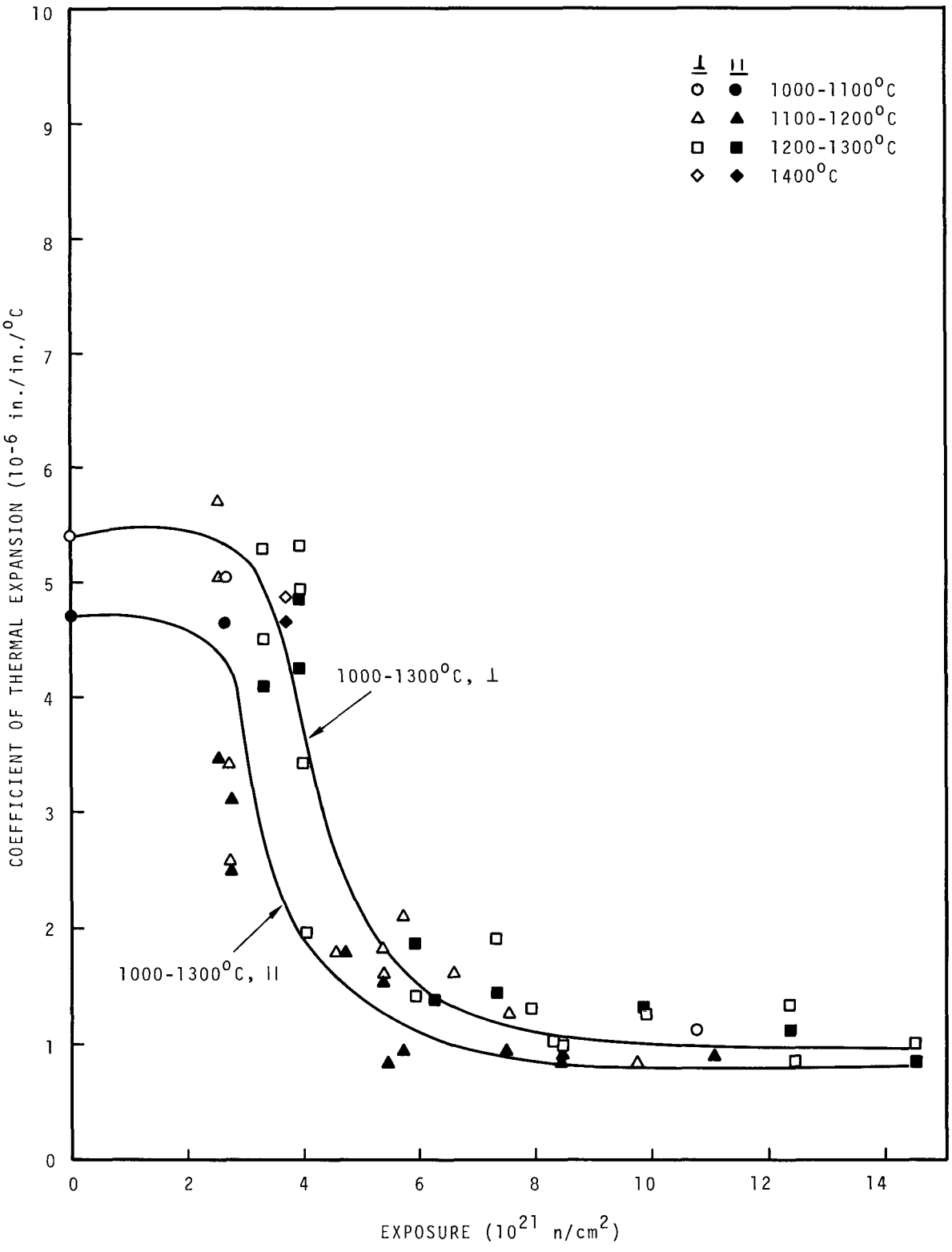

FIGURE 29. Coefficient of Thermal Expansion of RC5.

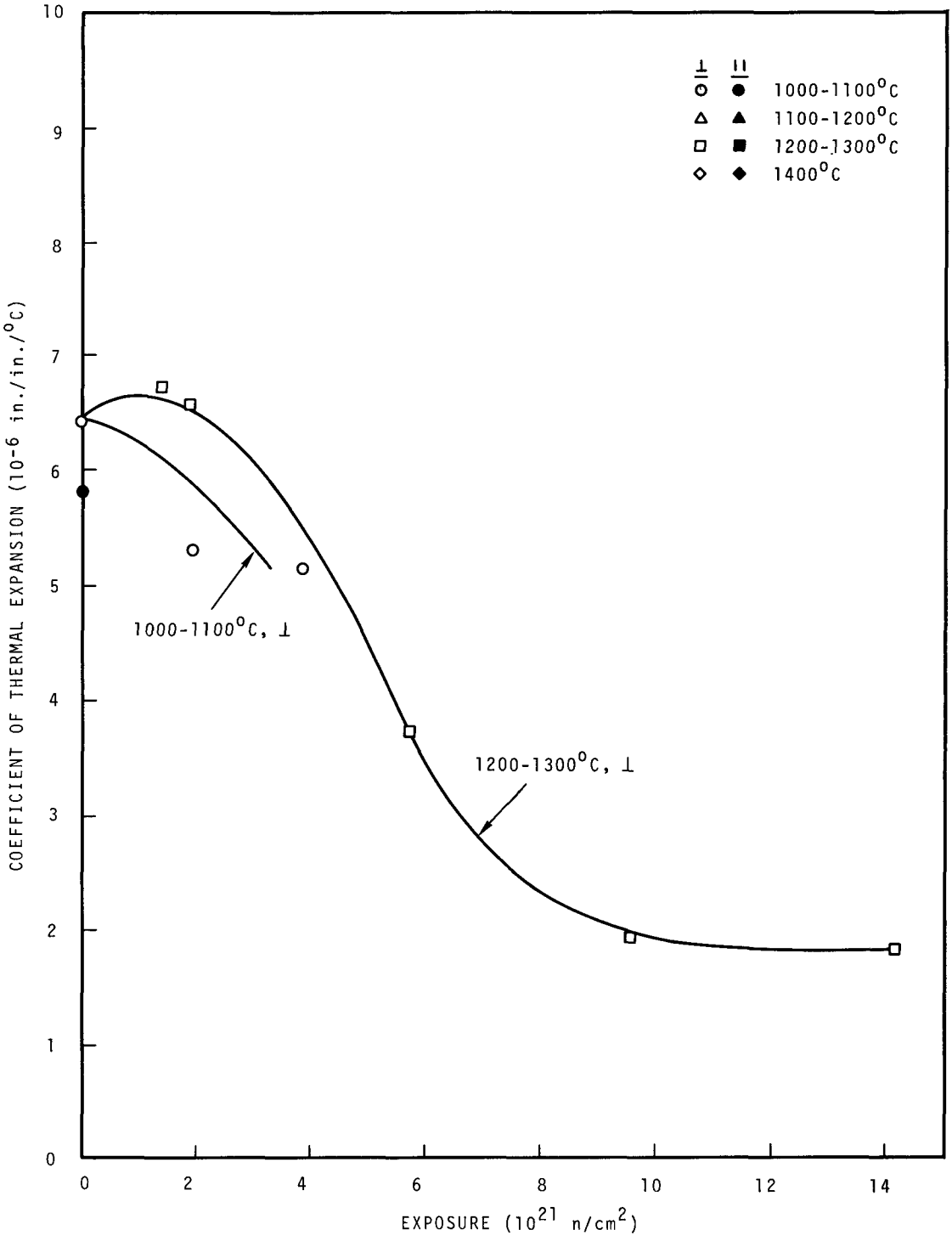

FIGURE 30. Coefficient of Thermal Expansion of JOZ.

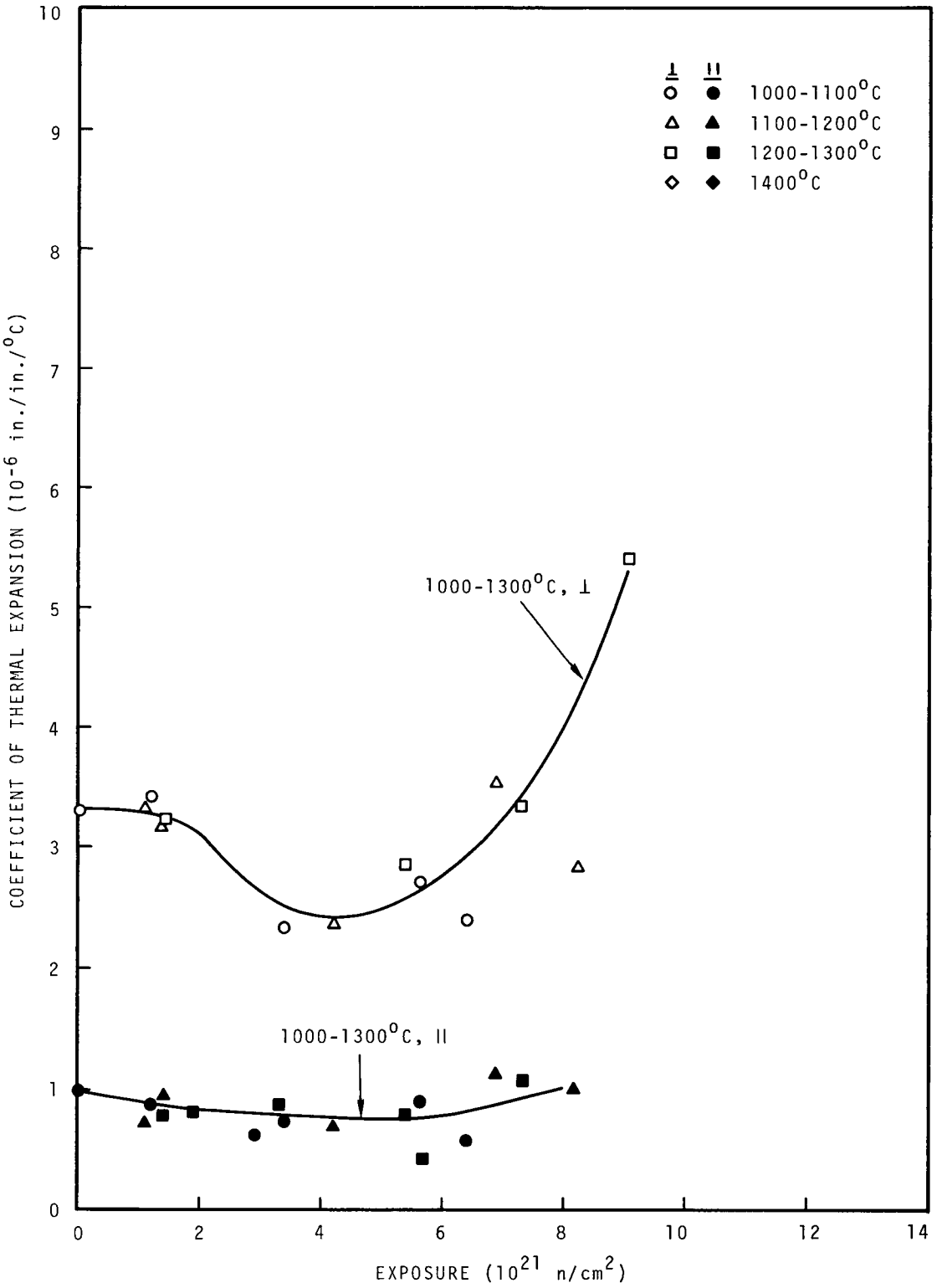

FIGURE 31. Coefficient of Thermal Expansion of H327.

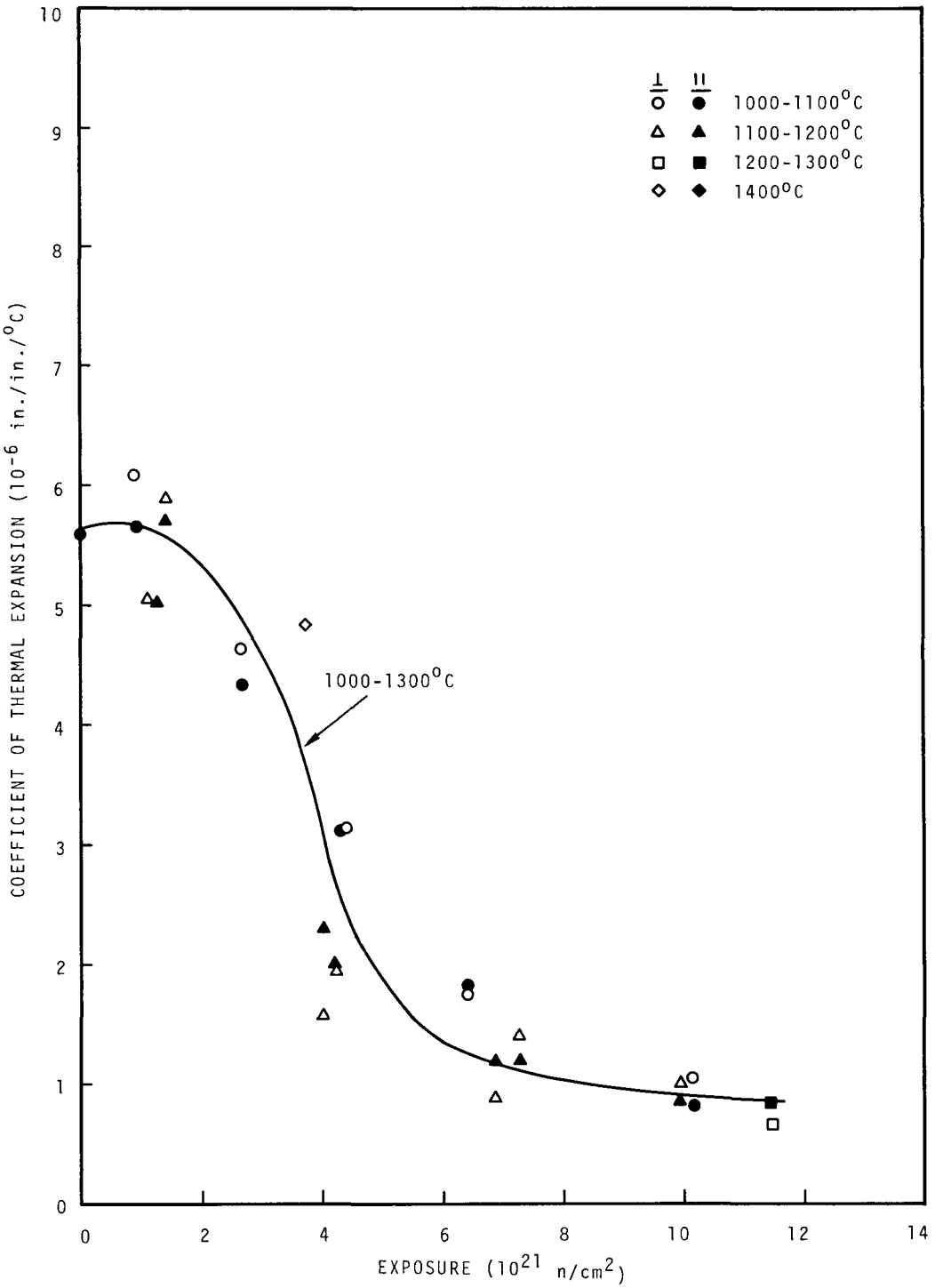

FIGURE 32. Coefficient of Thermal Expansion of H328.

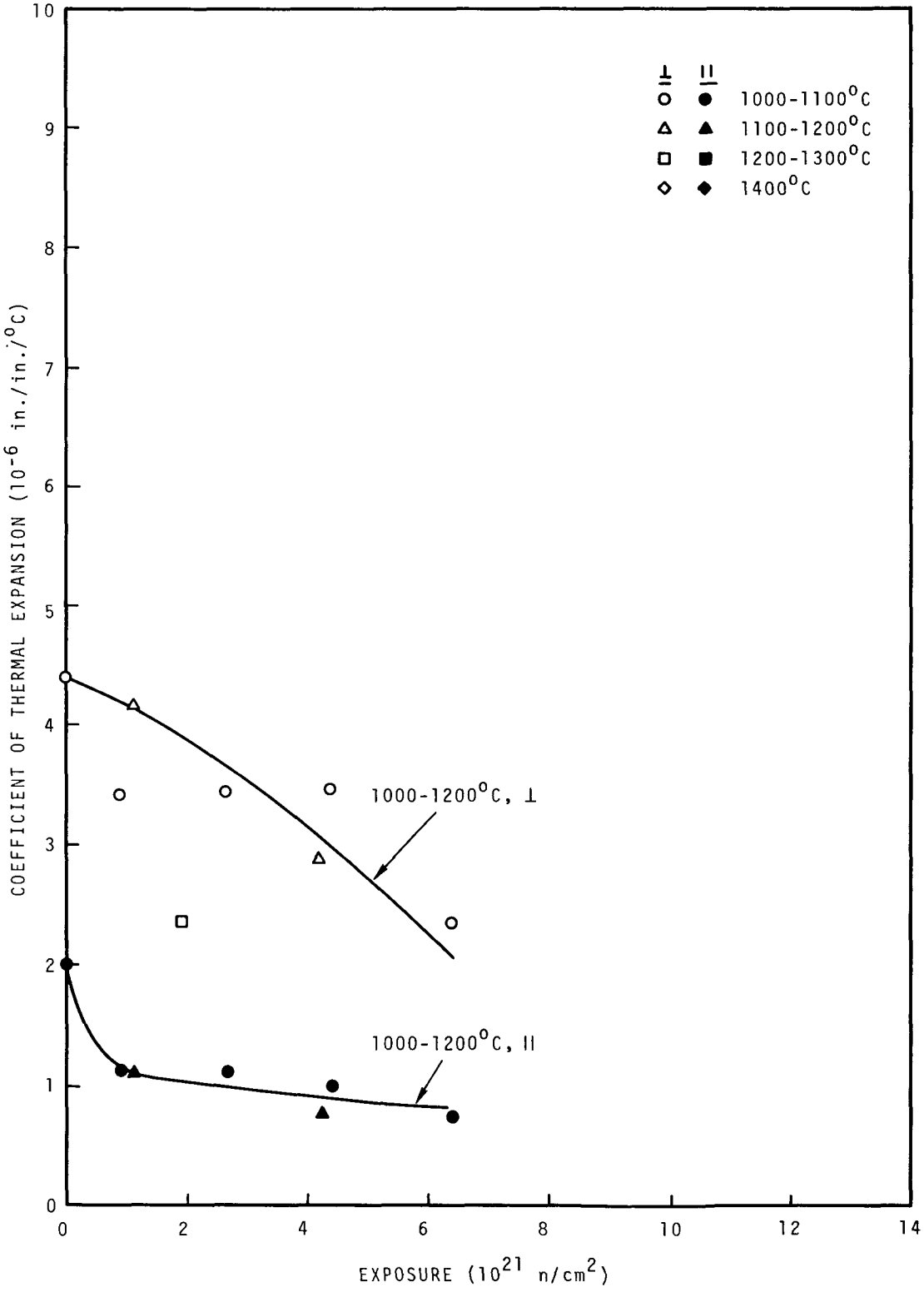

FIGURE 33. Coefficient of Thermal Expansion of 9567.

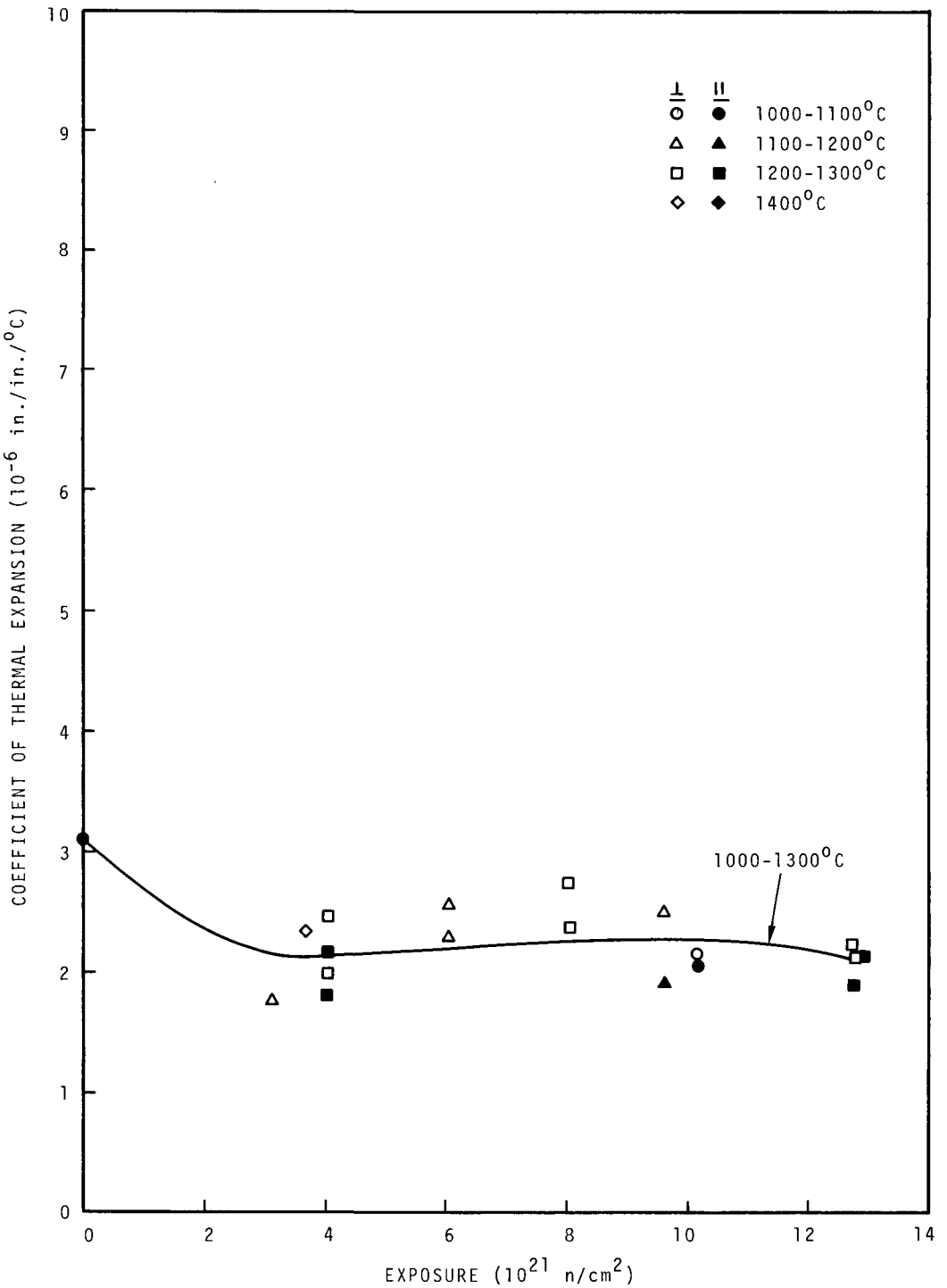

FIGURE 34. Coefficient of Thermal Expansion of 9640.

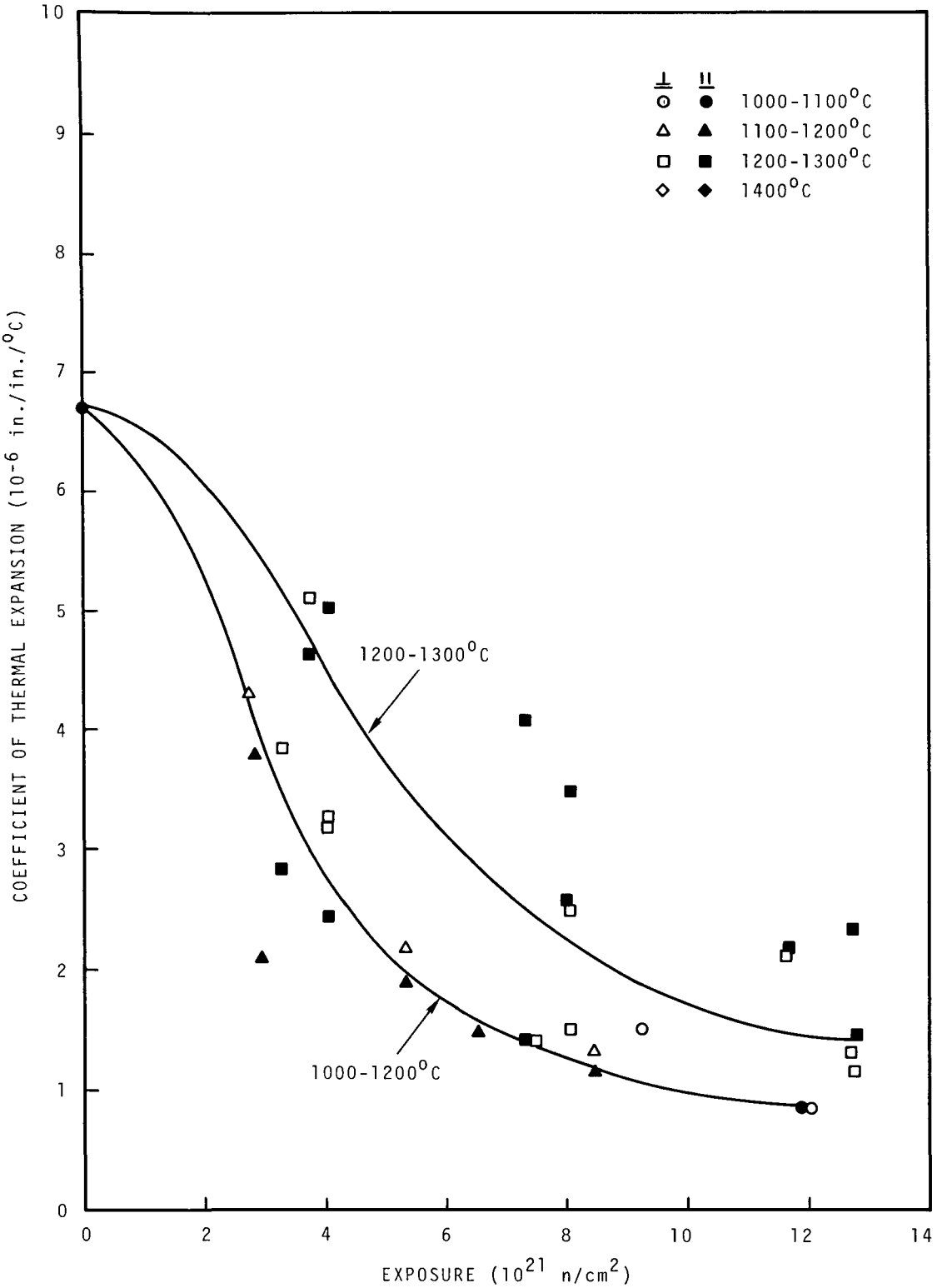

FIGURE 35. Coefficient of Thermal Expansion of 9650.

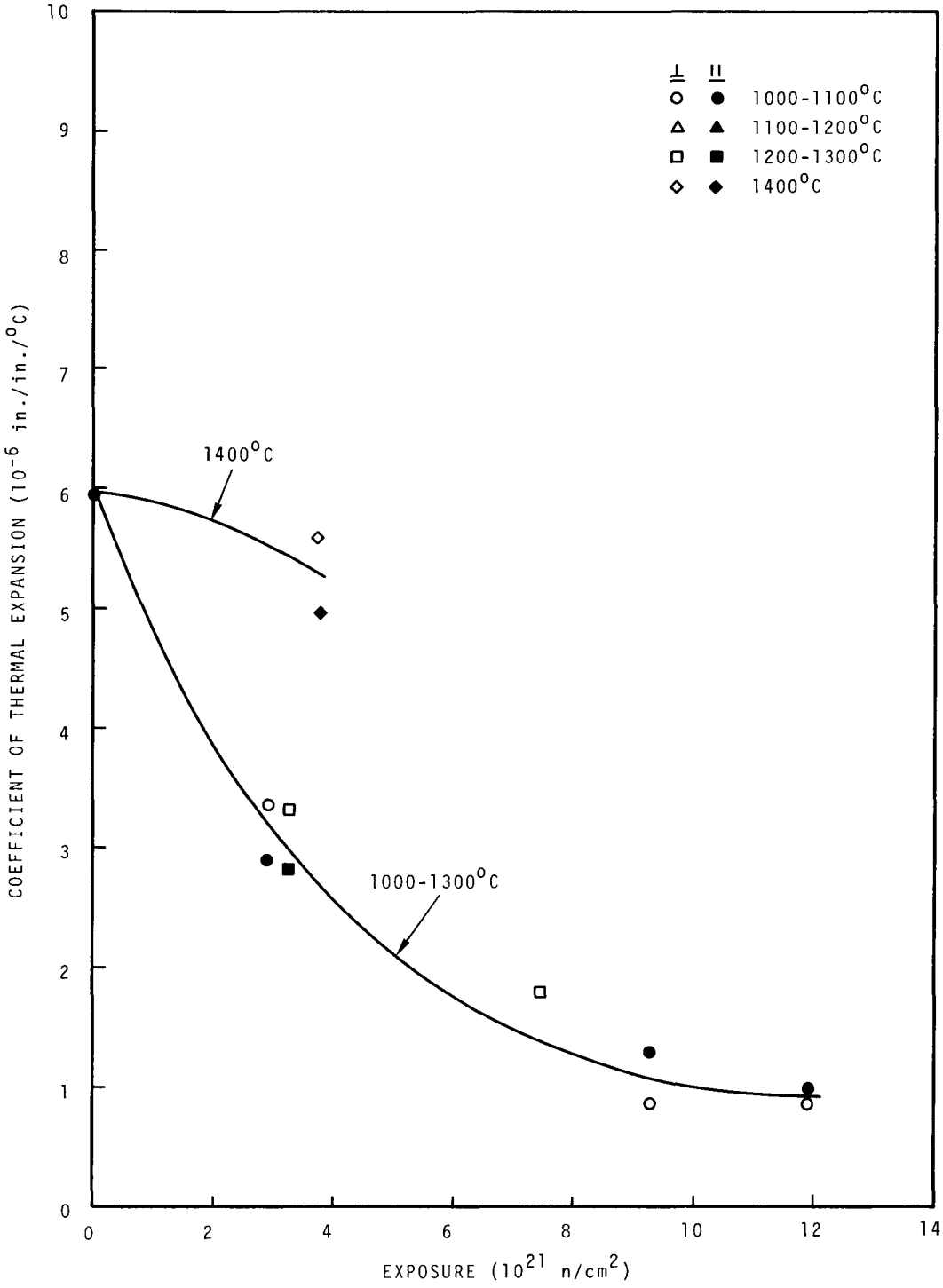

FIGURE 36. Coefficient of Thermal Expansion of 9751.

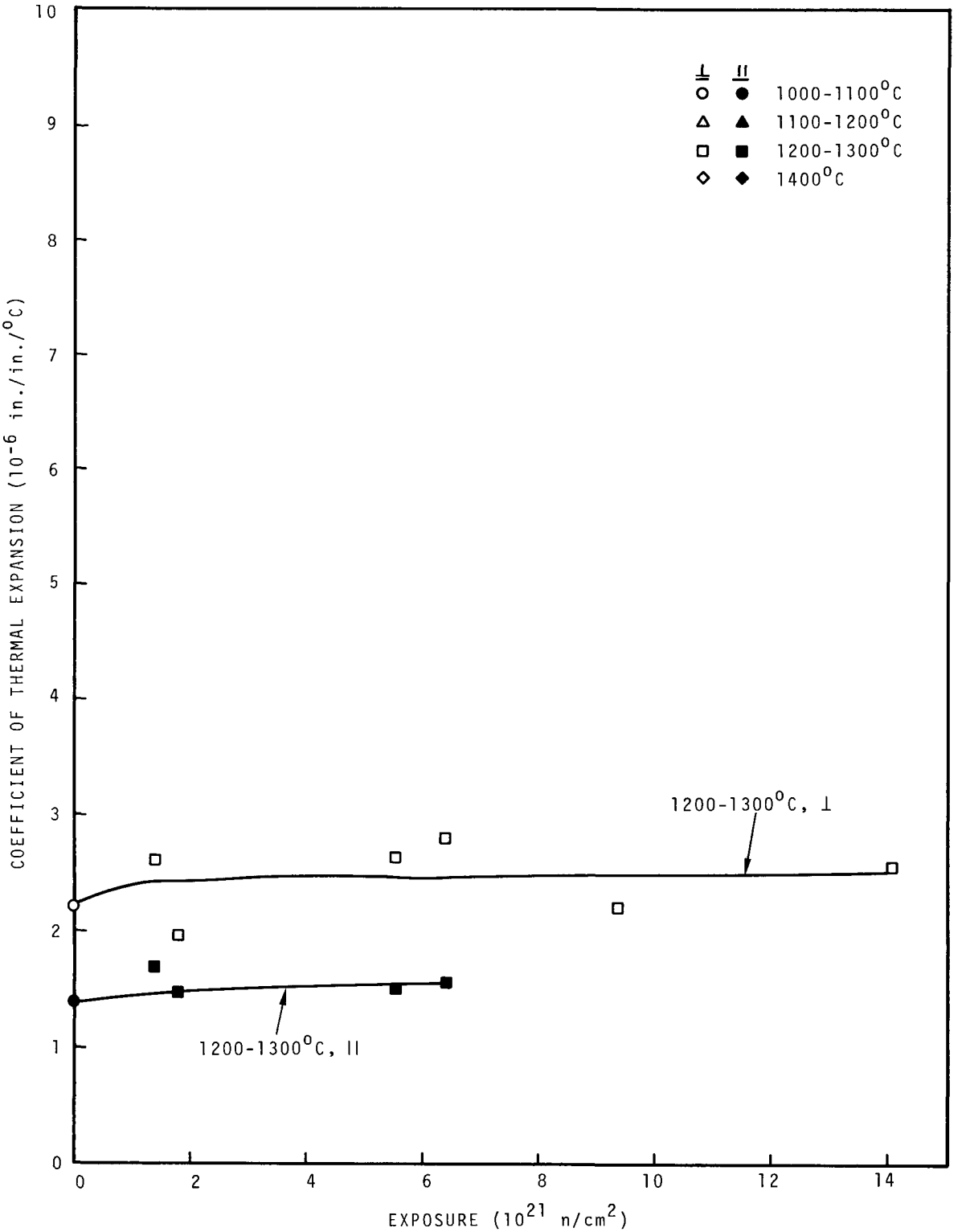

FIGURE 37. Coefficient of Thermal Expansion of GN.

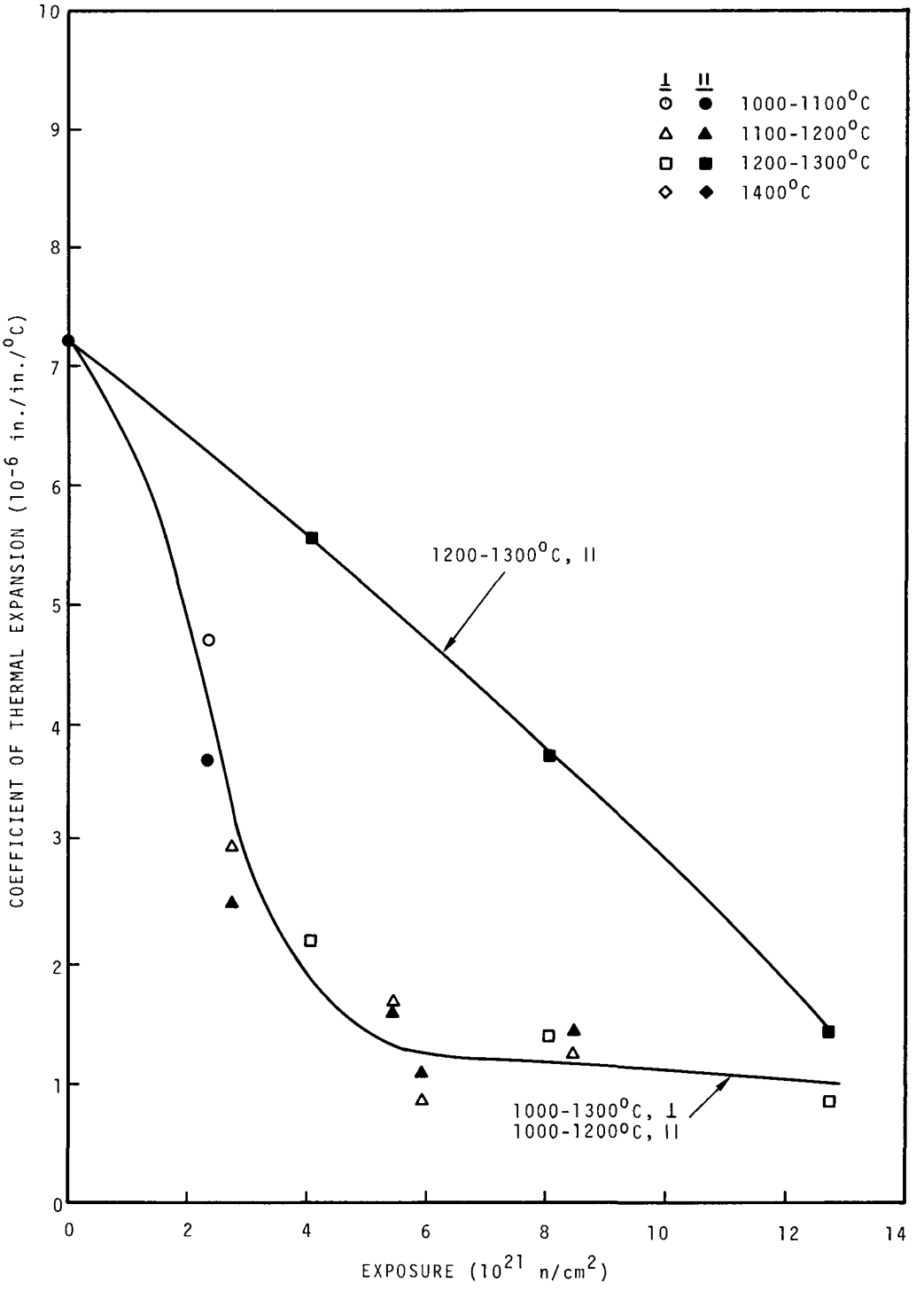

FIGURE 38. Coefficient of Thermal Expansion of AXF-Q1.

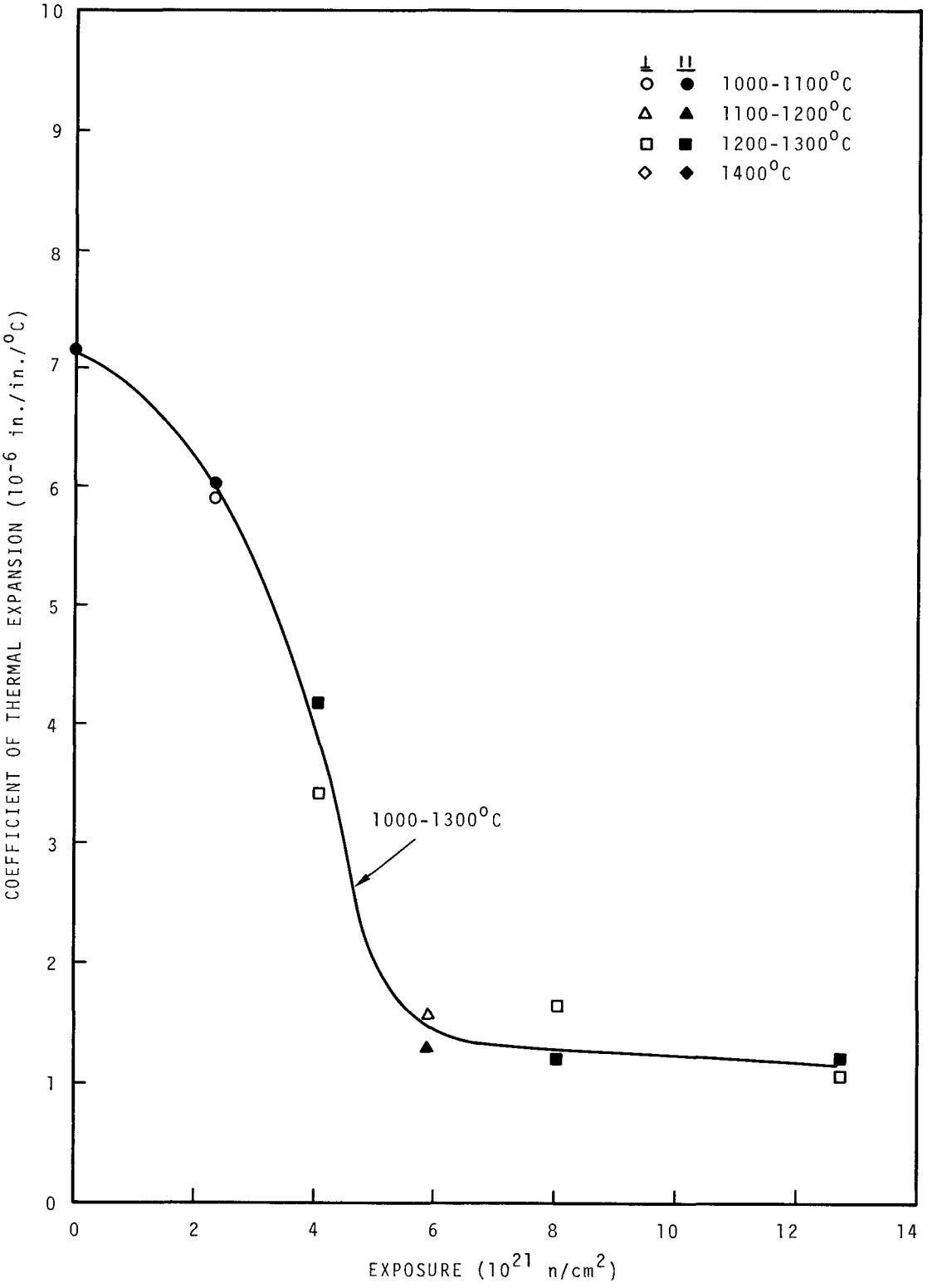

FIGURE 39. Coefficient of Thermal Expansion of AXF-5Q1.

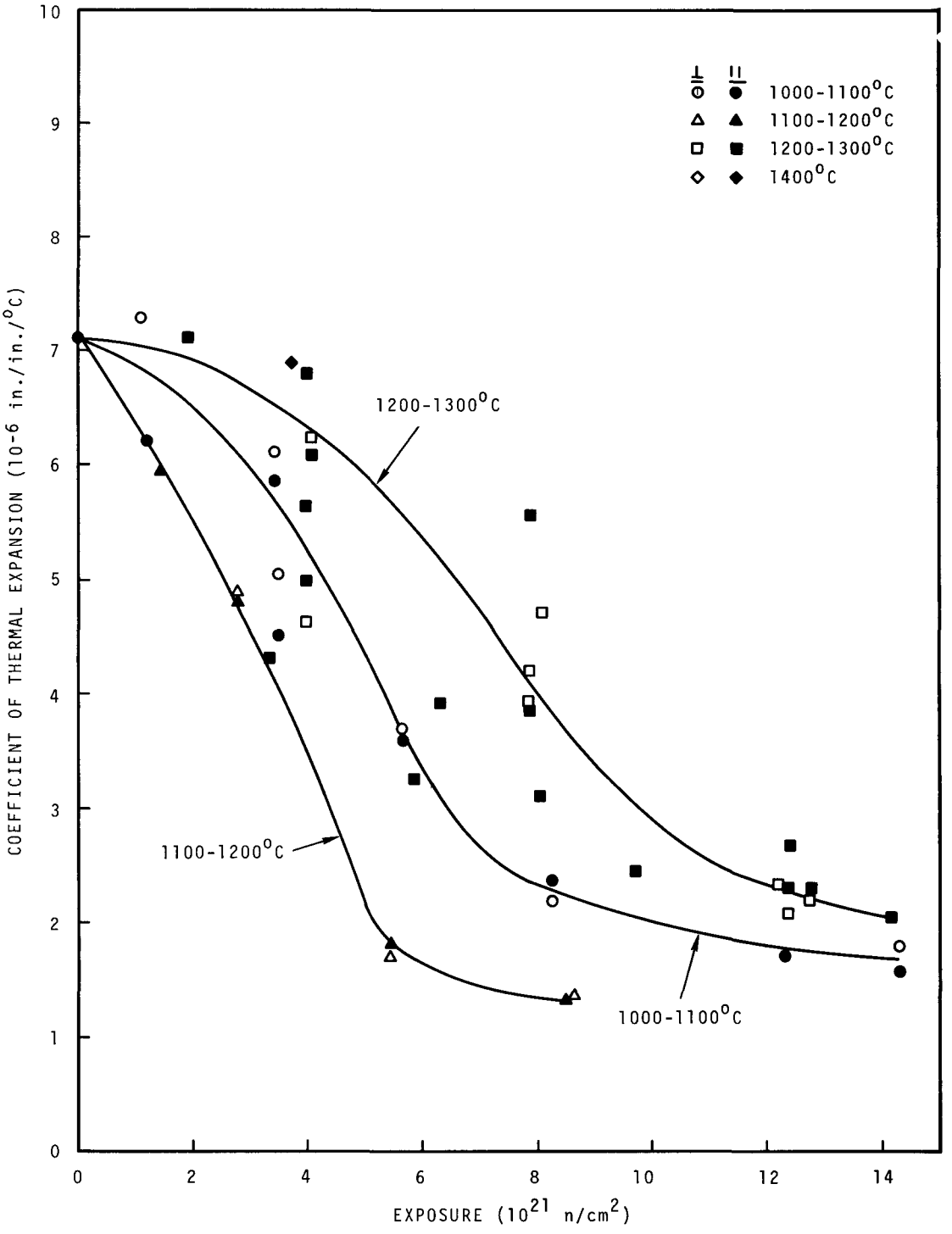

FIGURE 40. Coefficient of Thermal Expansion of AXF-8Q1.

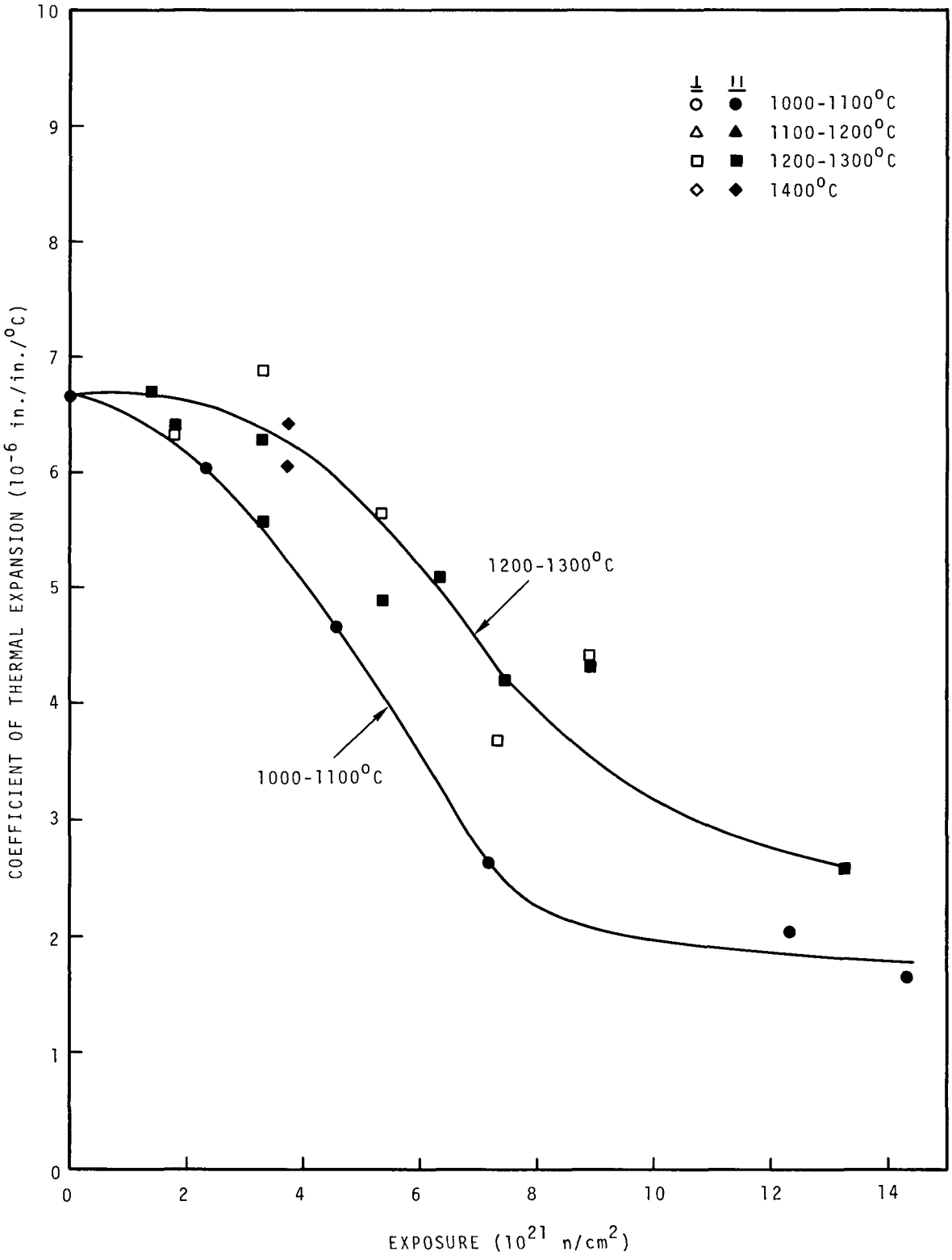

FIGURE 41. Coefficient of Thermal Expansion of AXZ-5Q1.

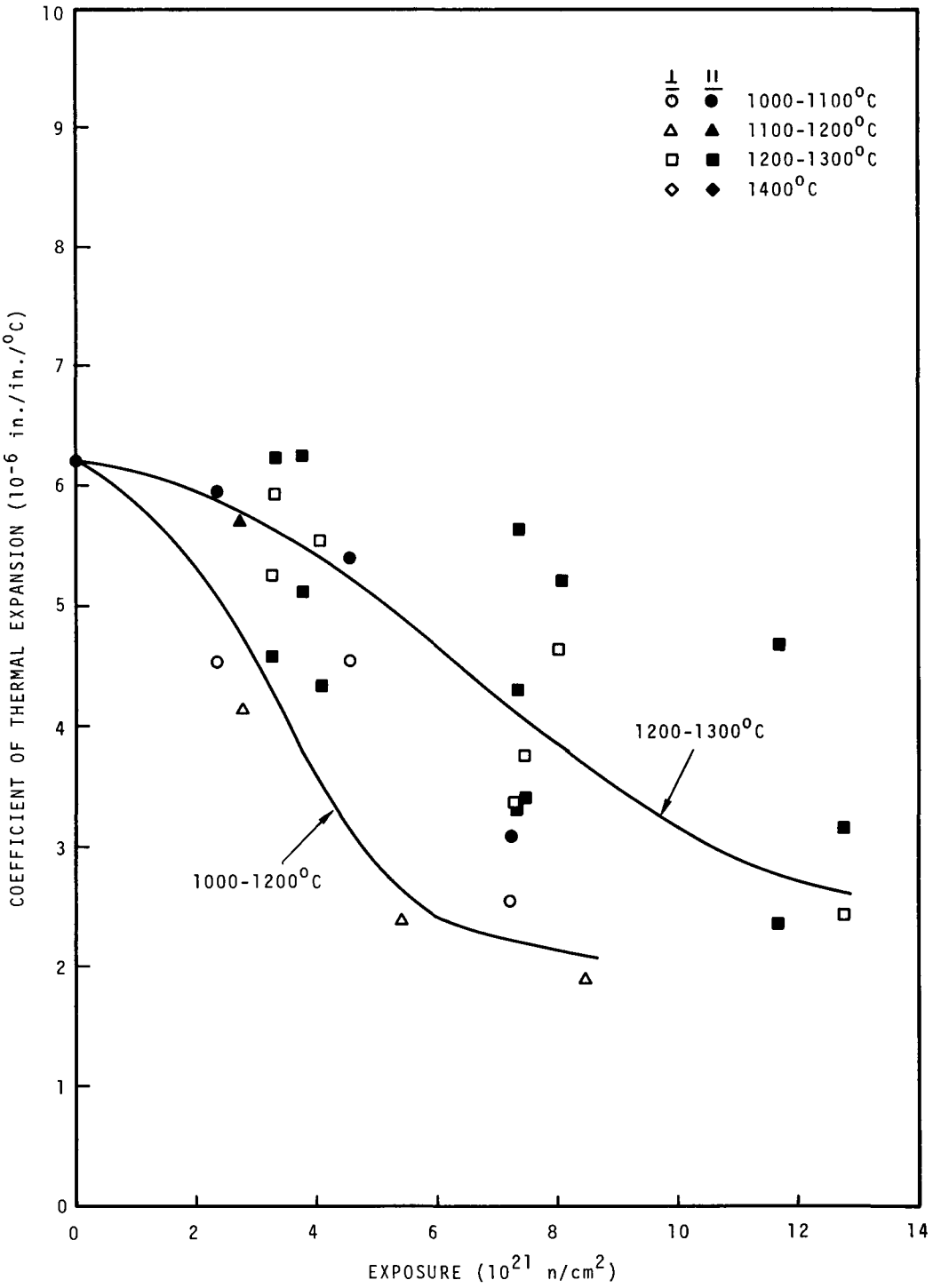

FIGURE 42. Coefficient of Thermal Expansion of AXZ-8Q1.

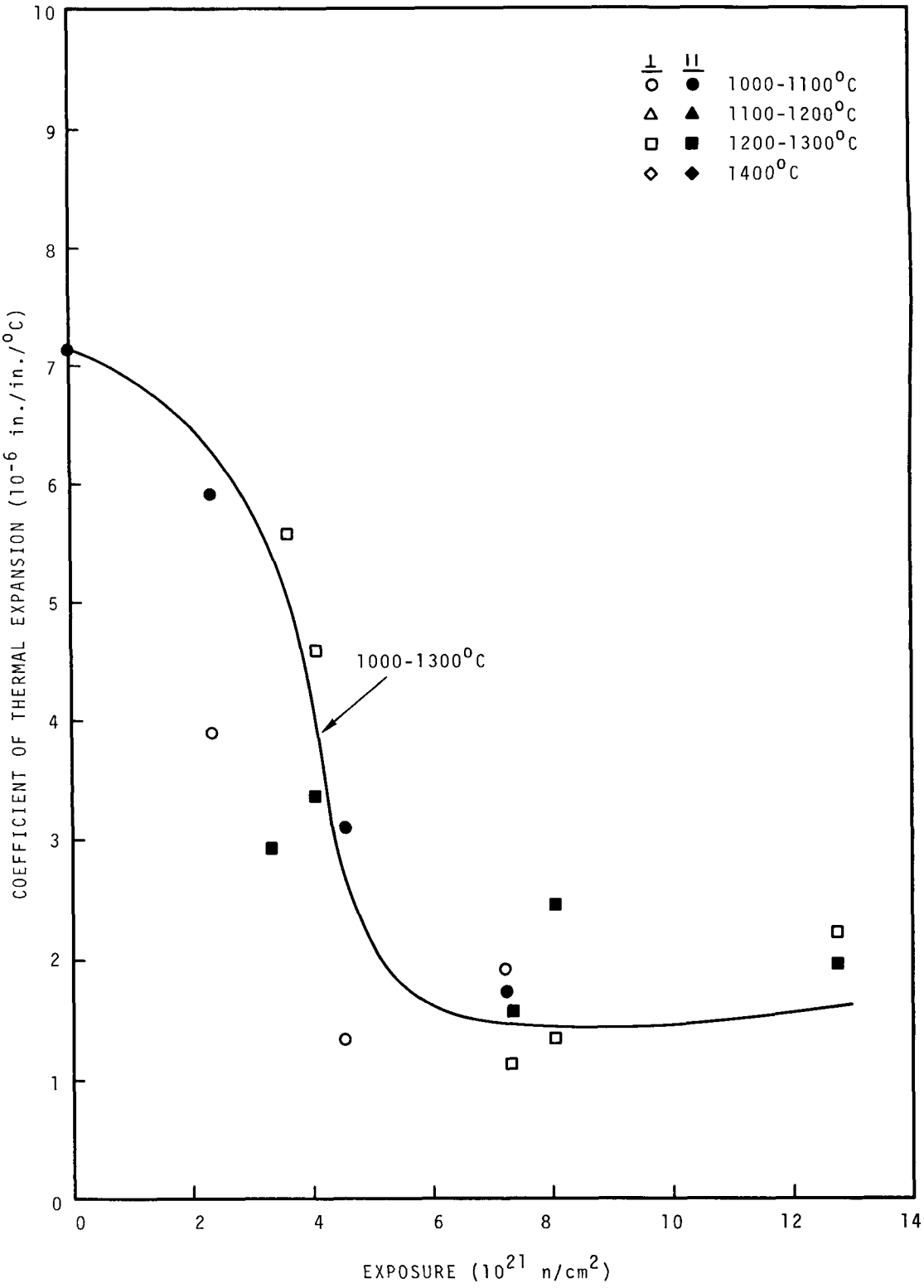

FIGURE 43. Coefficient of Thermal Expansion of AXF-5QBG1.

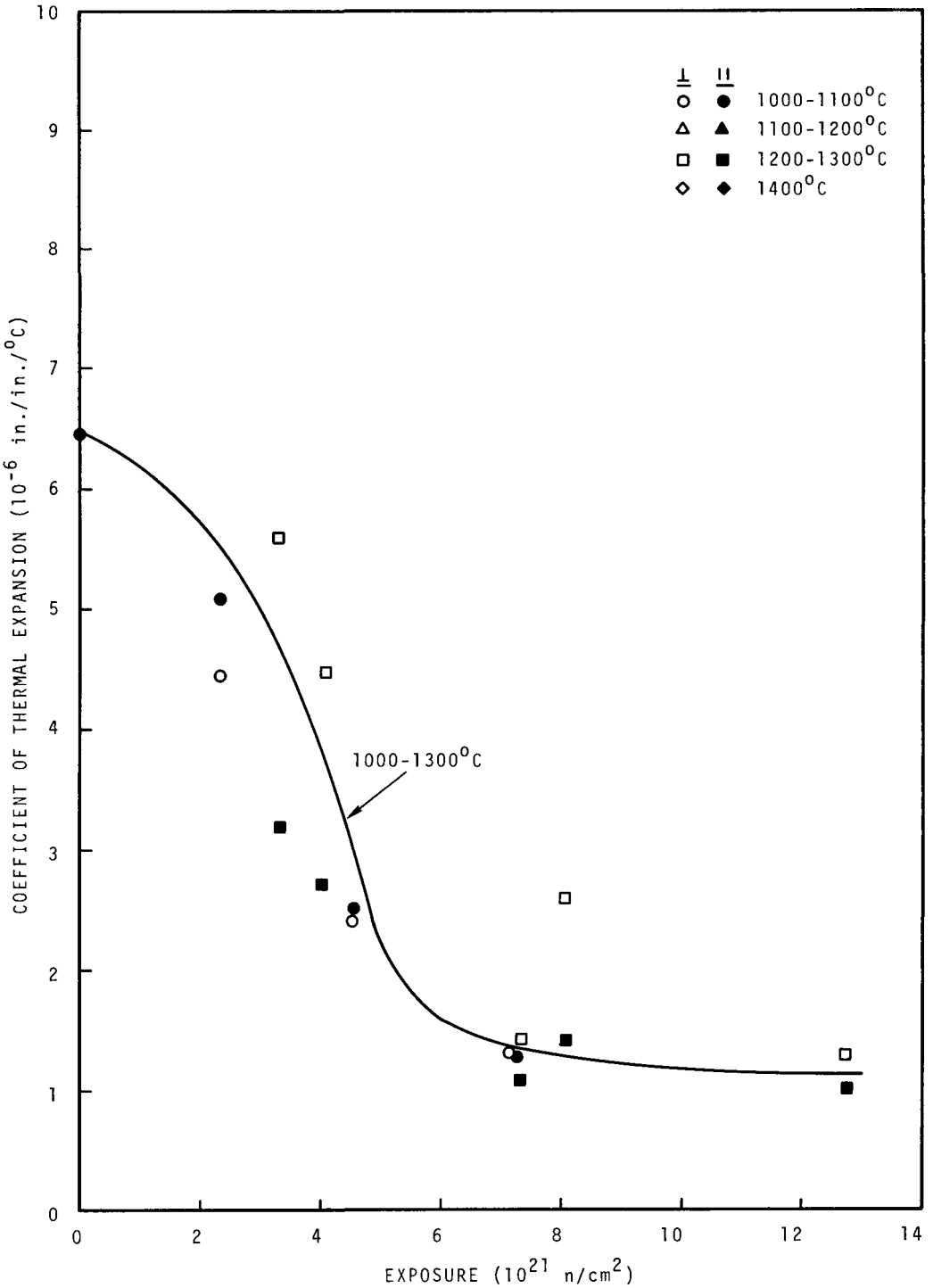

FIGURE 44. Coefficient of Thermal Expansion of AXF-8QBG1.

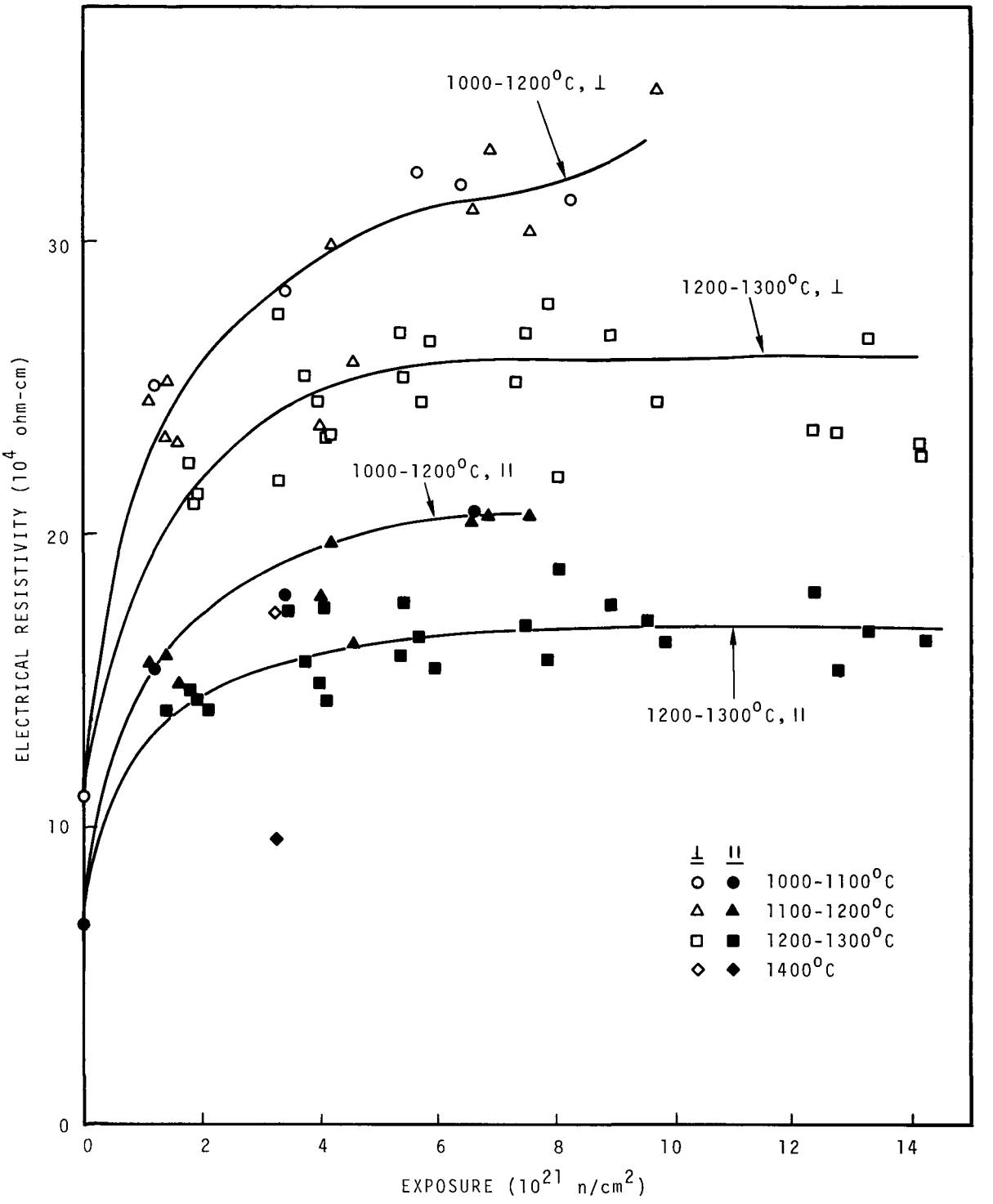

FIGURE 45. Electrical Resistivity of EGCR.

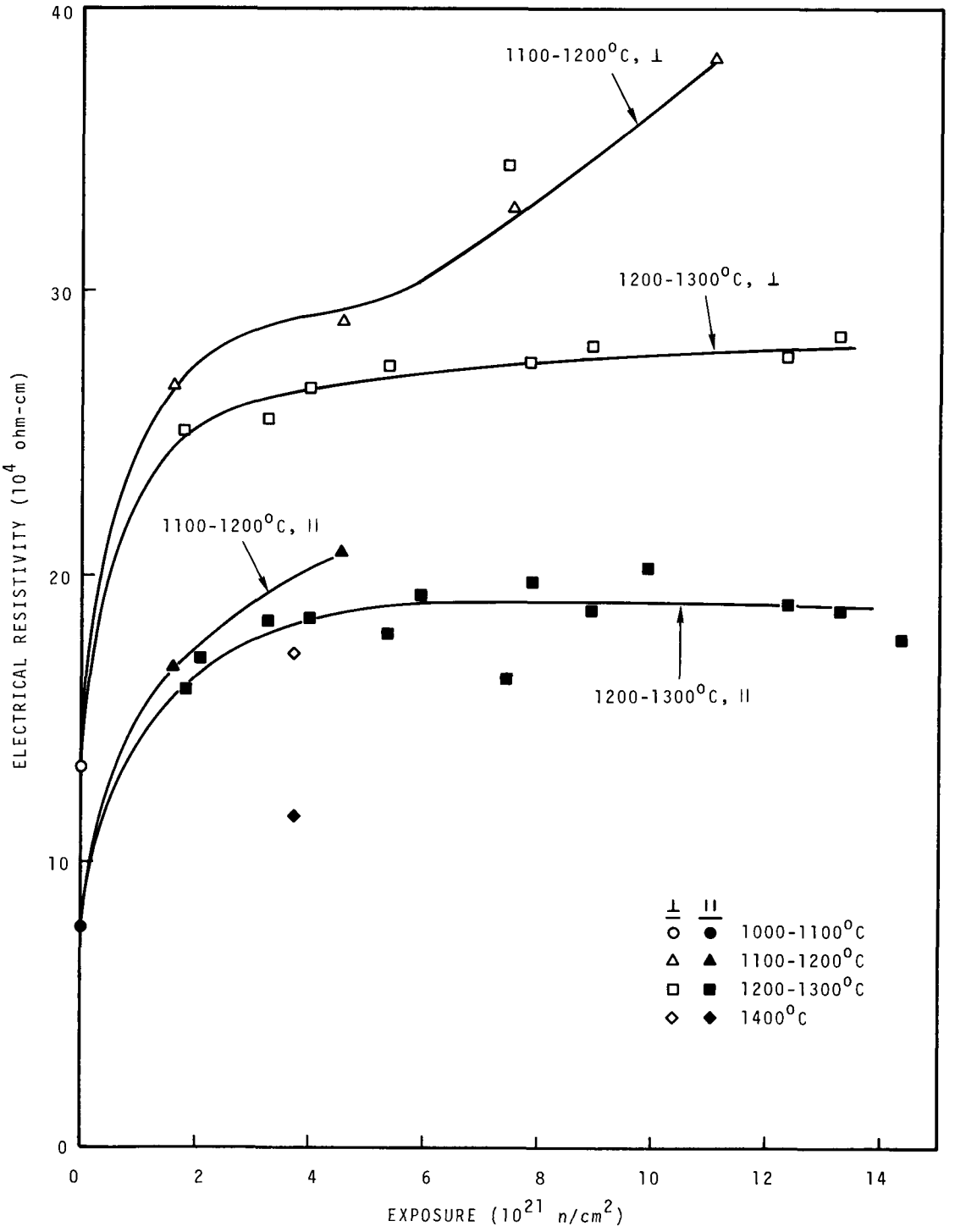

FIGURE 46. Electrical Resistivity of CSF.

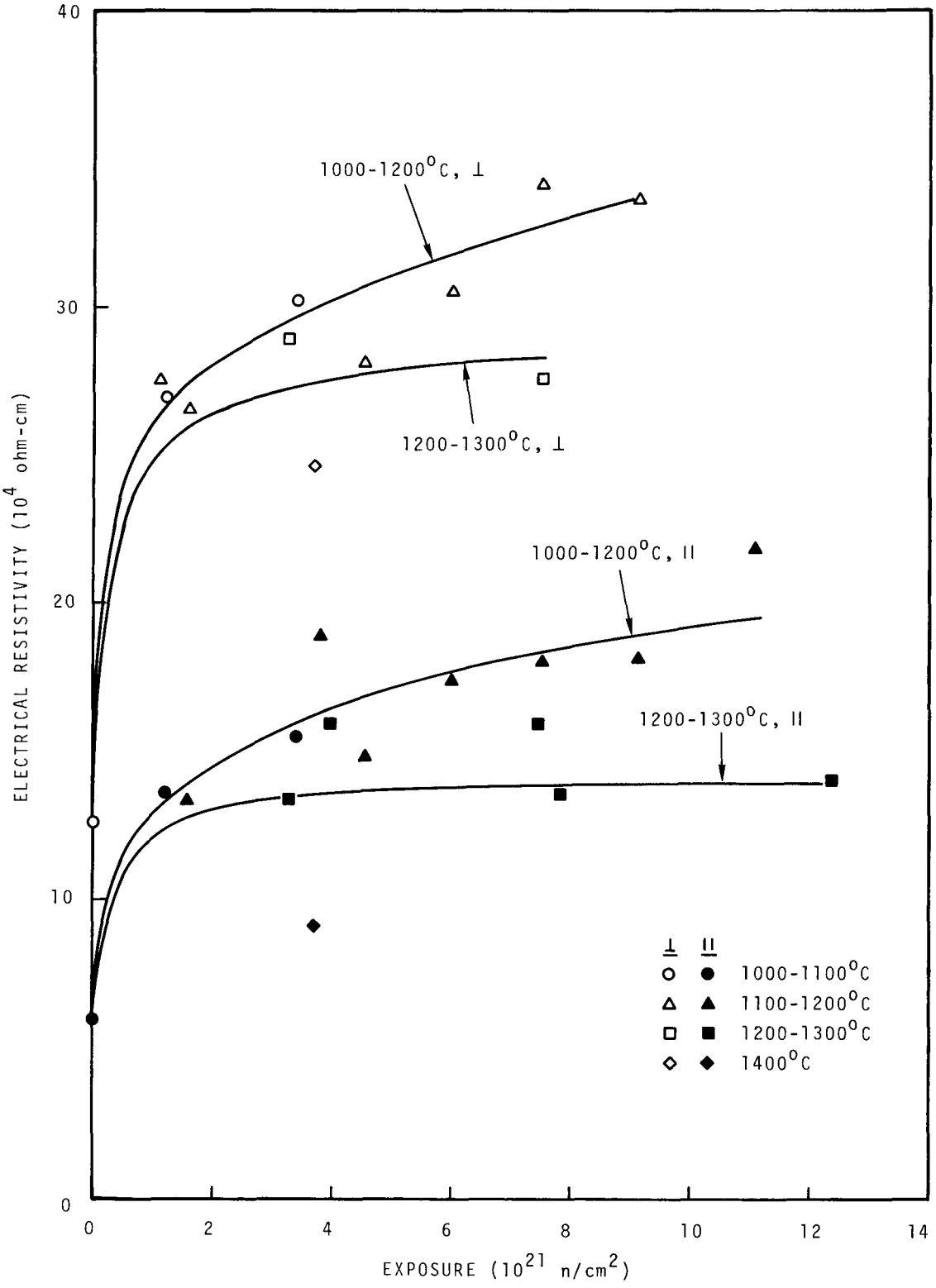

FIGURE 47. Electrical Resistivity of TSX.

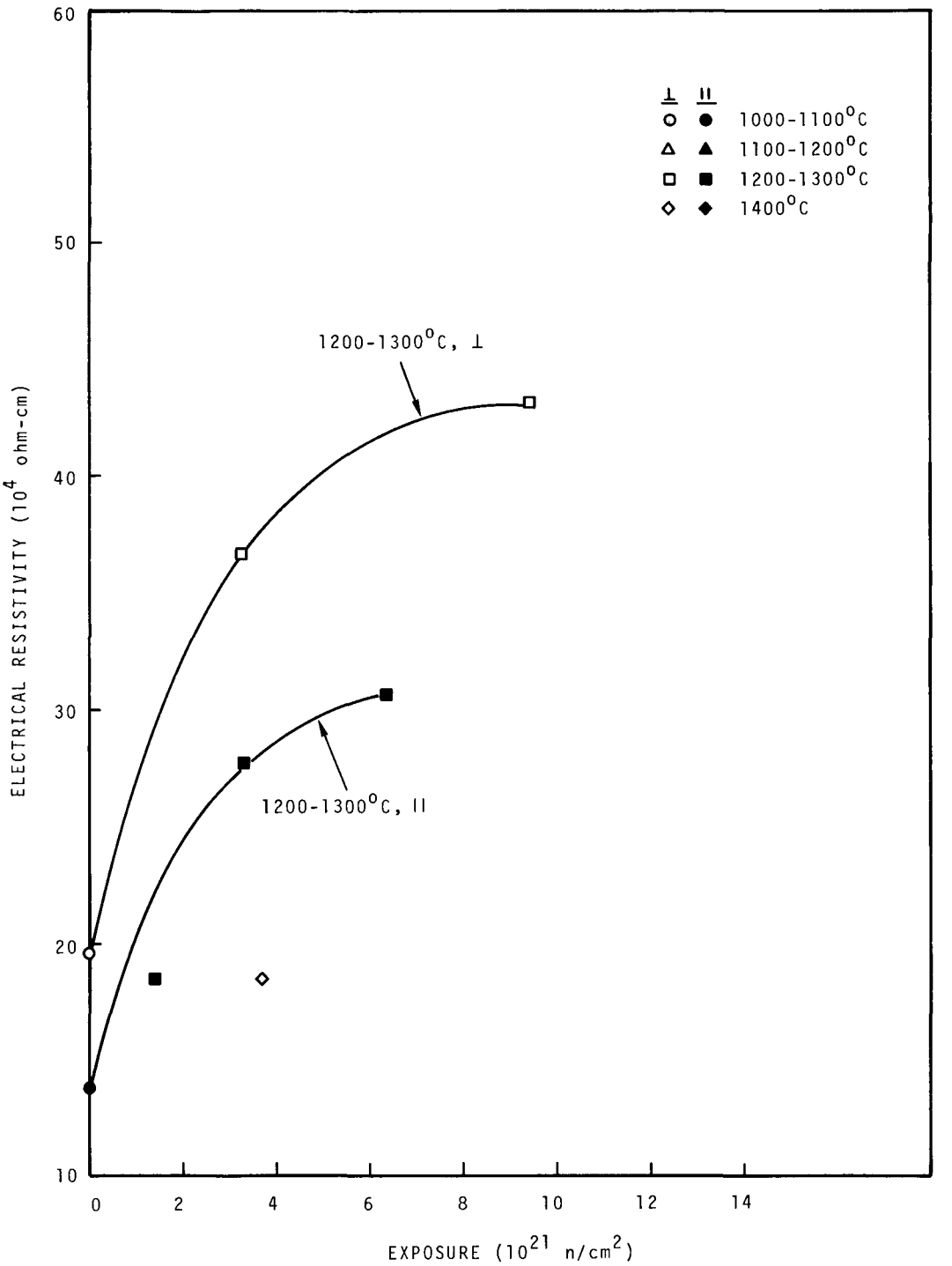

FIGURE 48. Electrical Resistivity of TSGBF.

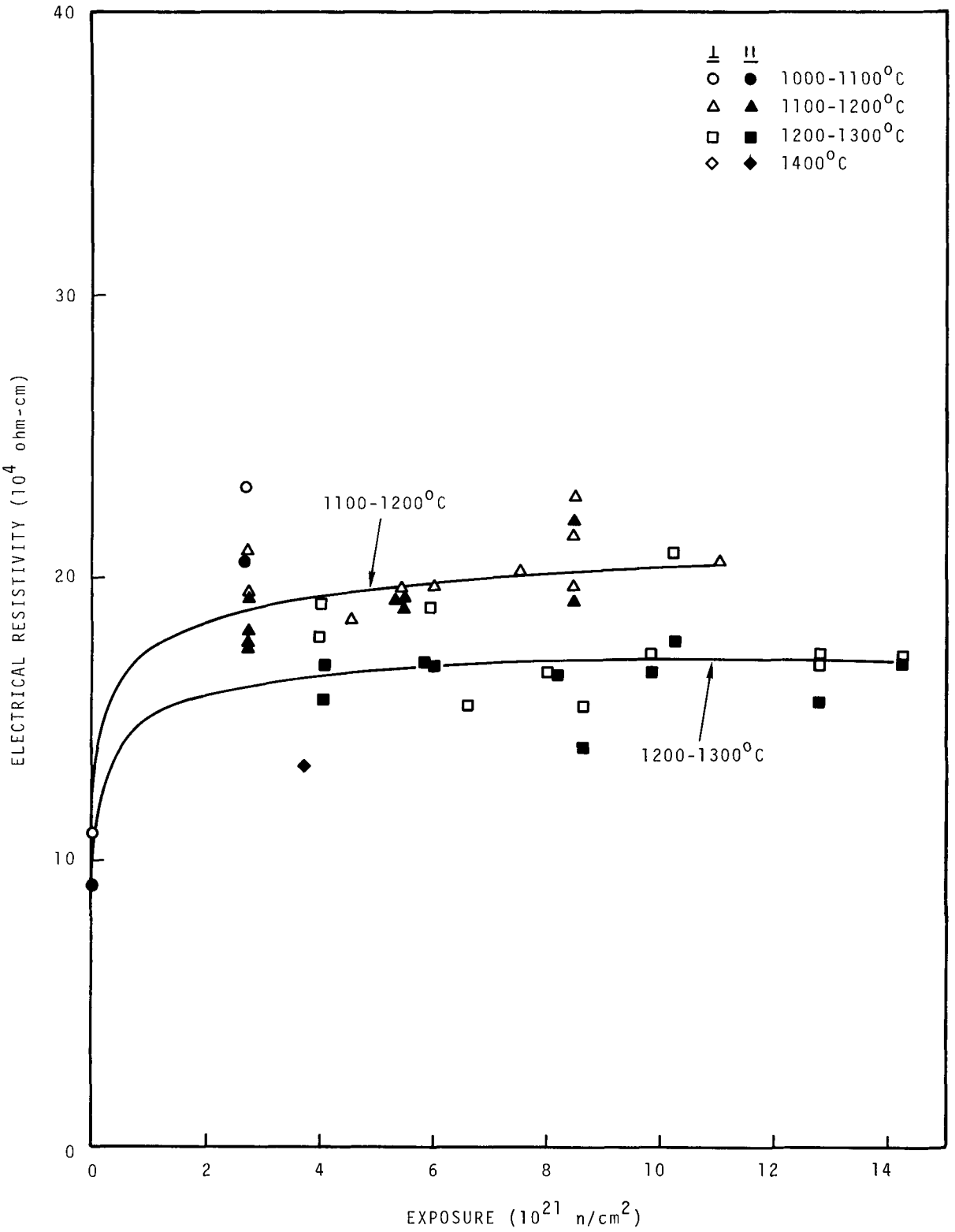

FIGURE 49. Electrical Resistivity of RP4.

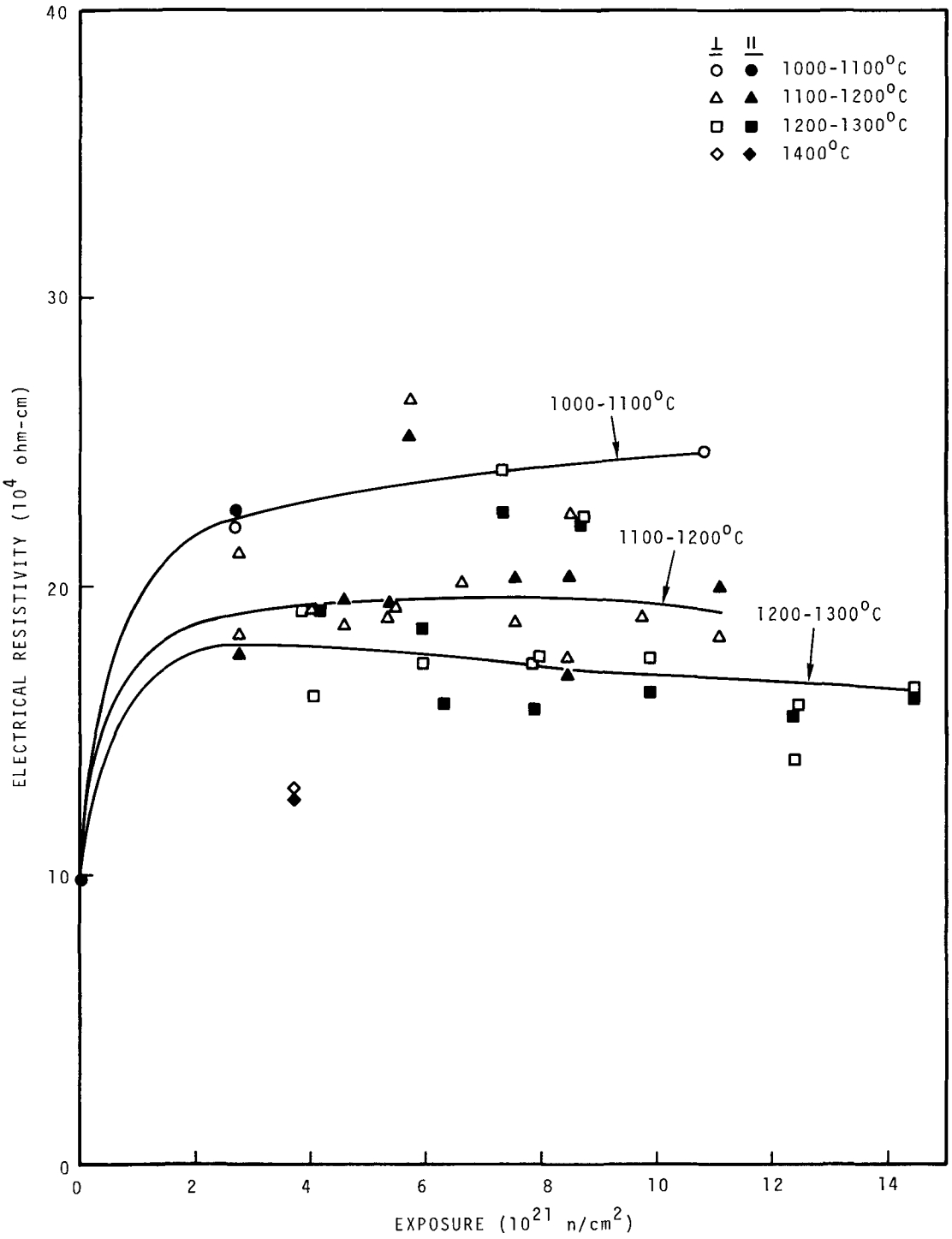

FIGURE 50. Electrical Resistivity of RC5.

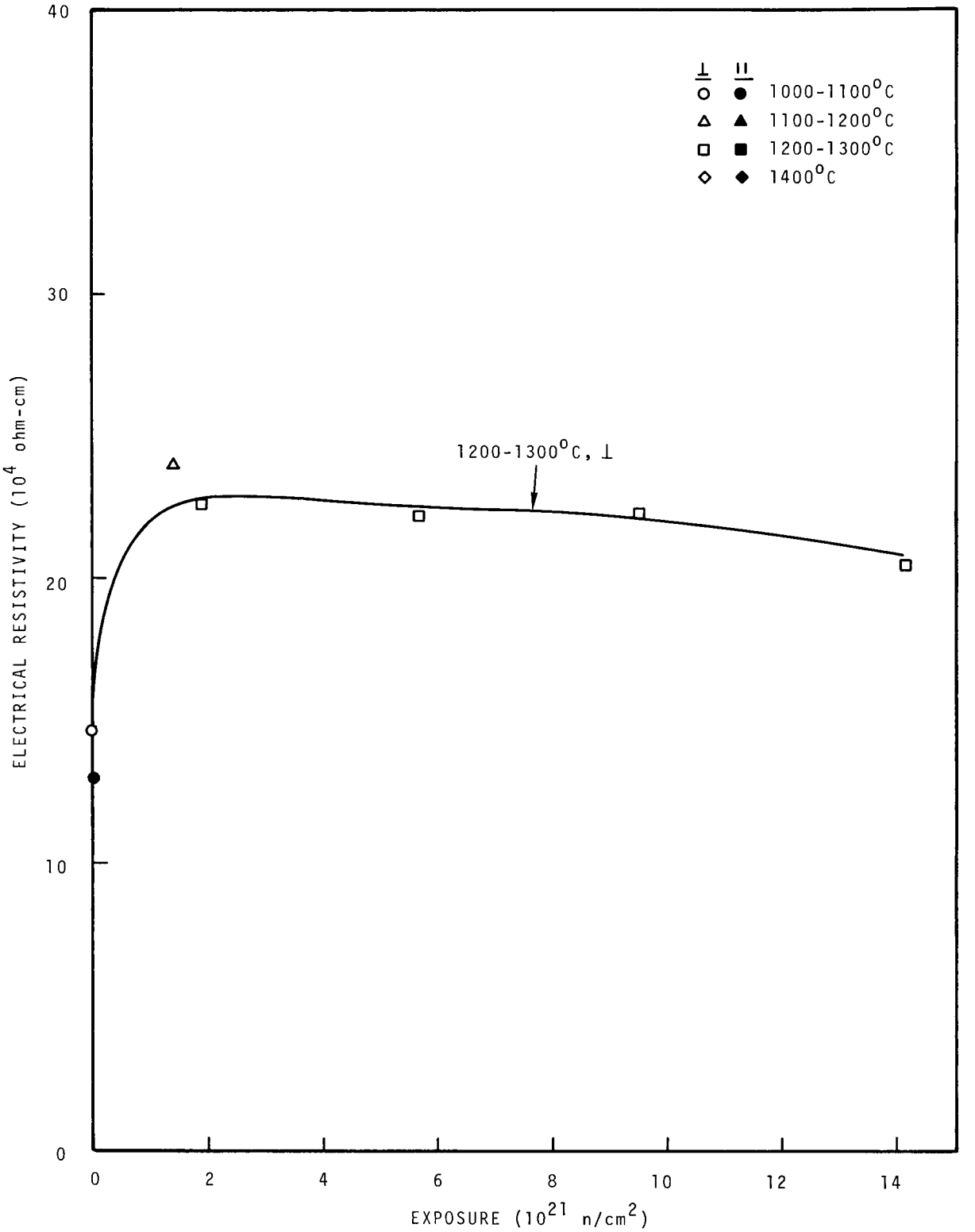

FIGURE 51. Electrical Resistivity of JOZ.

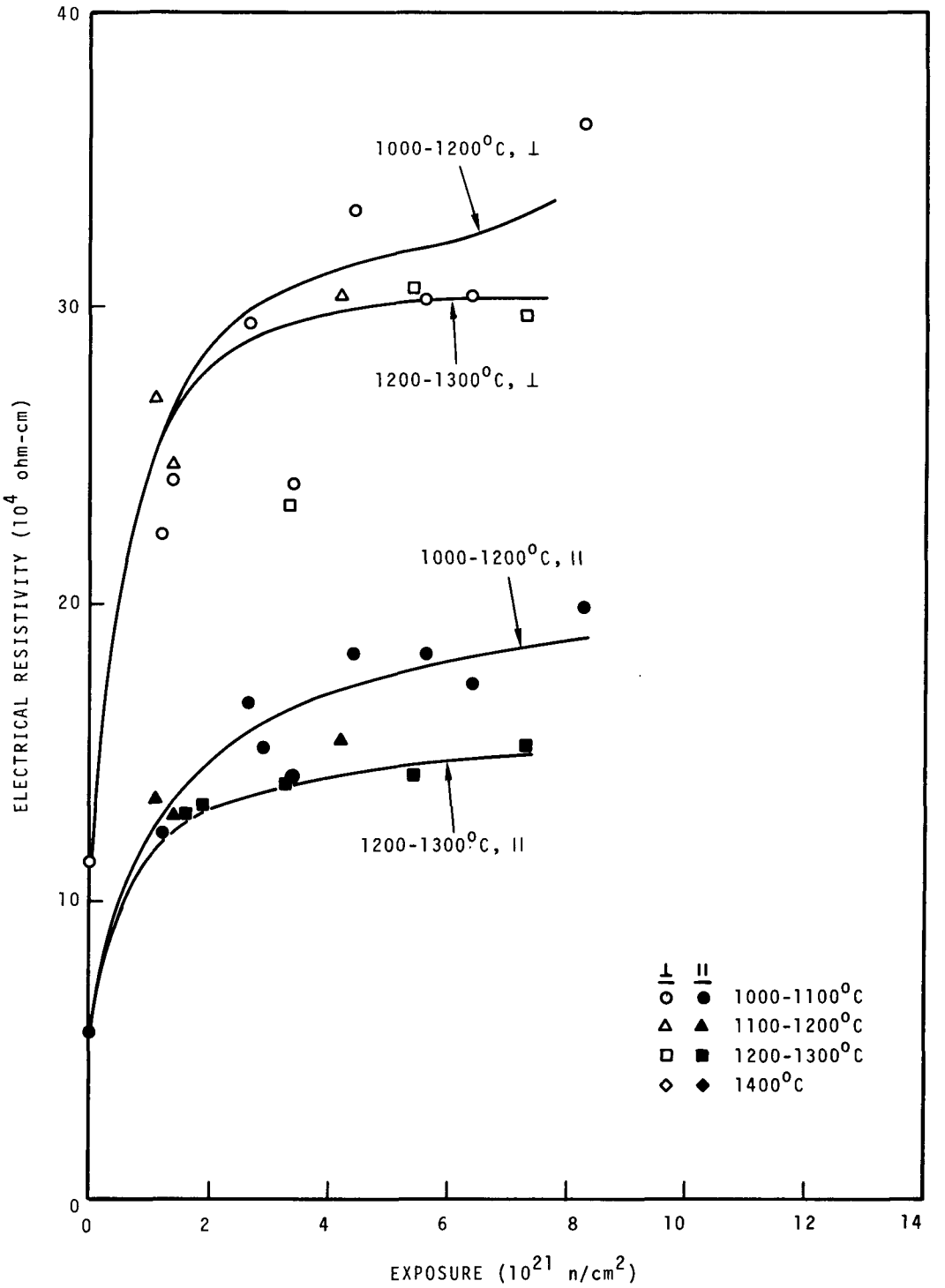

FIGURE 52. Electrical Resistivity of H327.

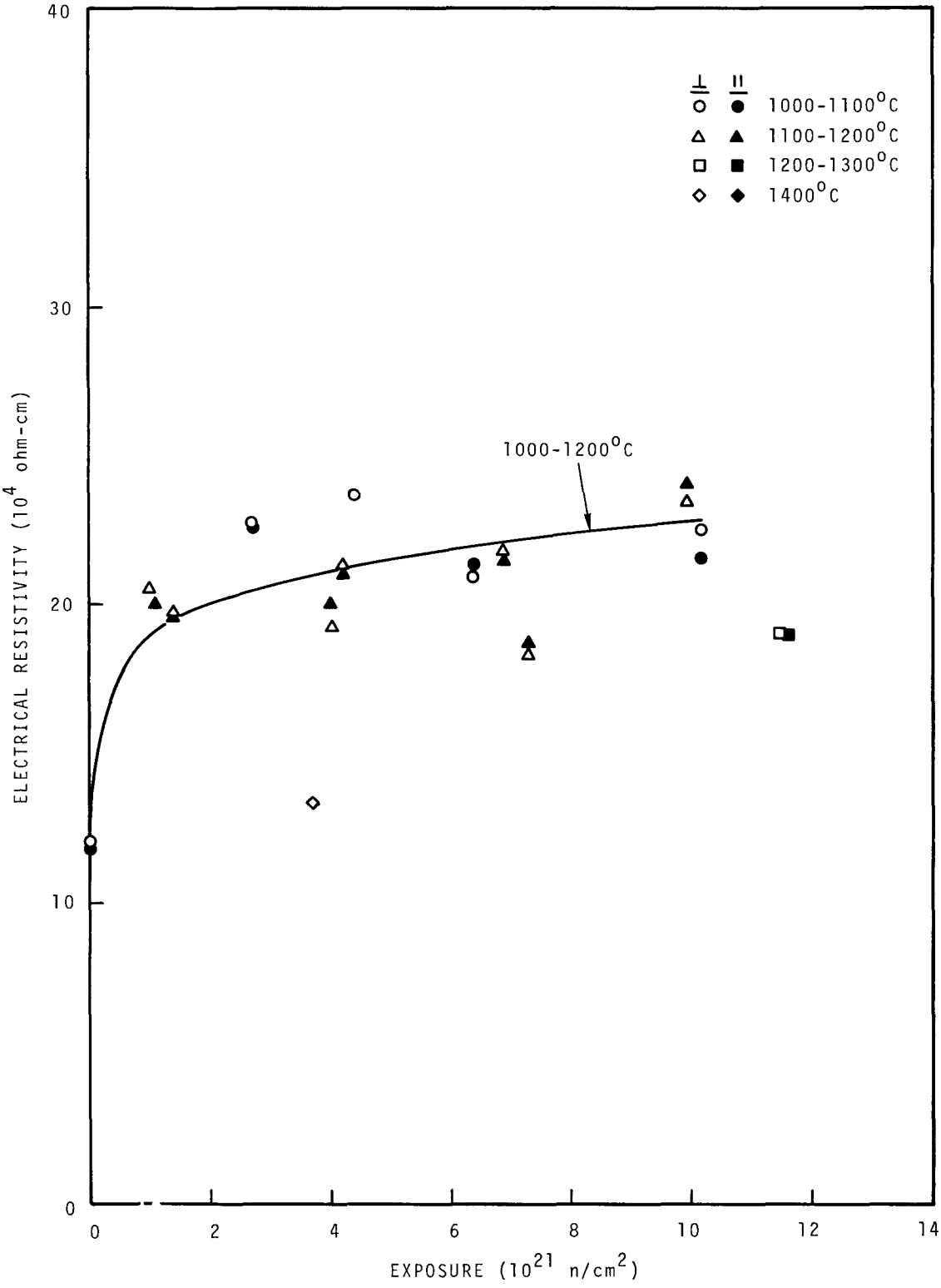

FIGURE 53. Electrical Resistivity of H328.

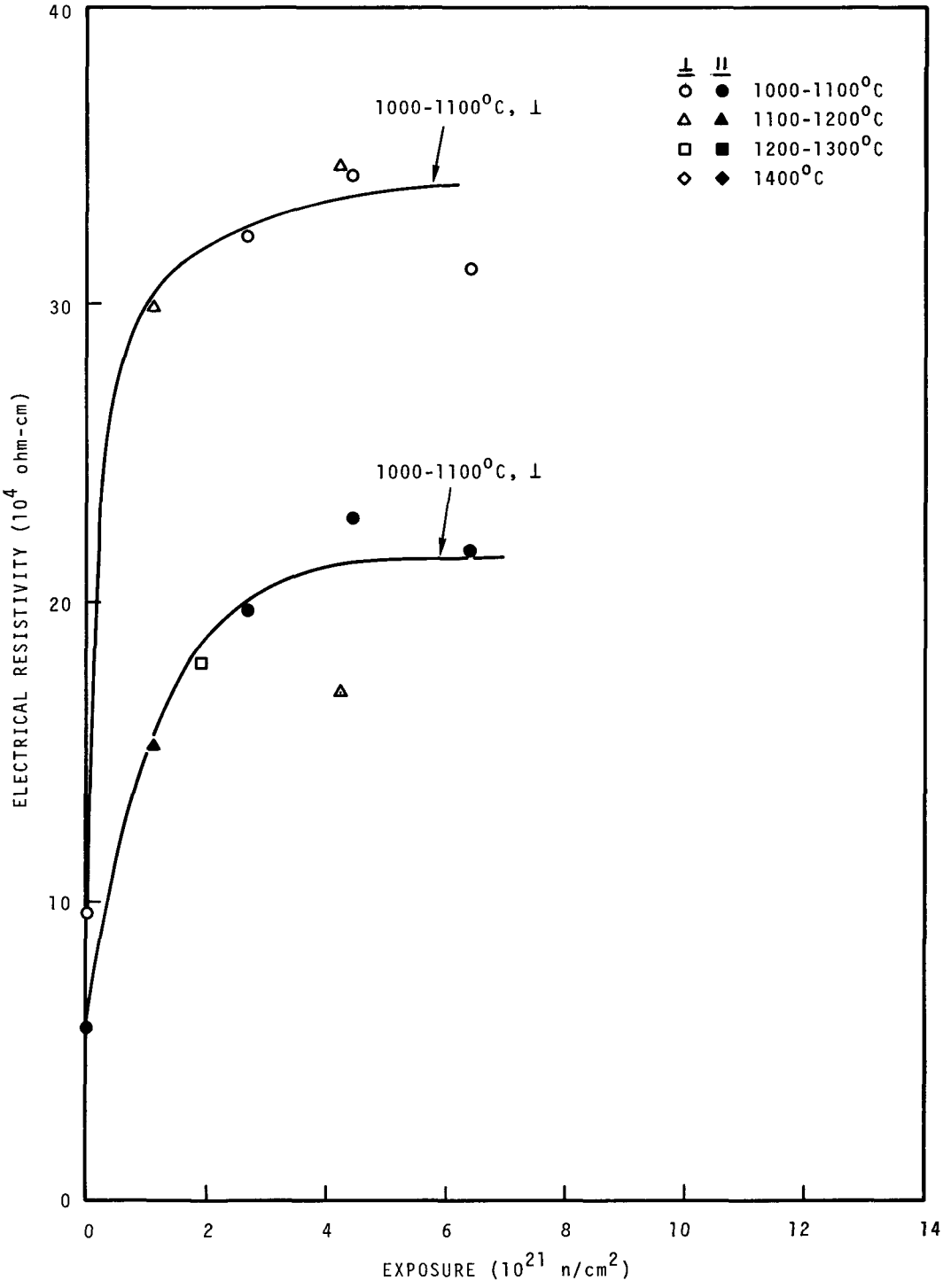

FIGURE 54. Electrical Resistivity of 9567.

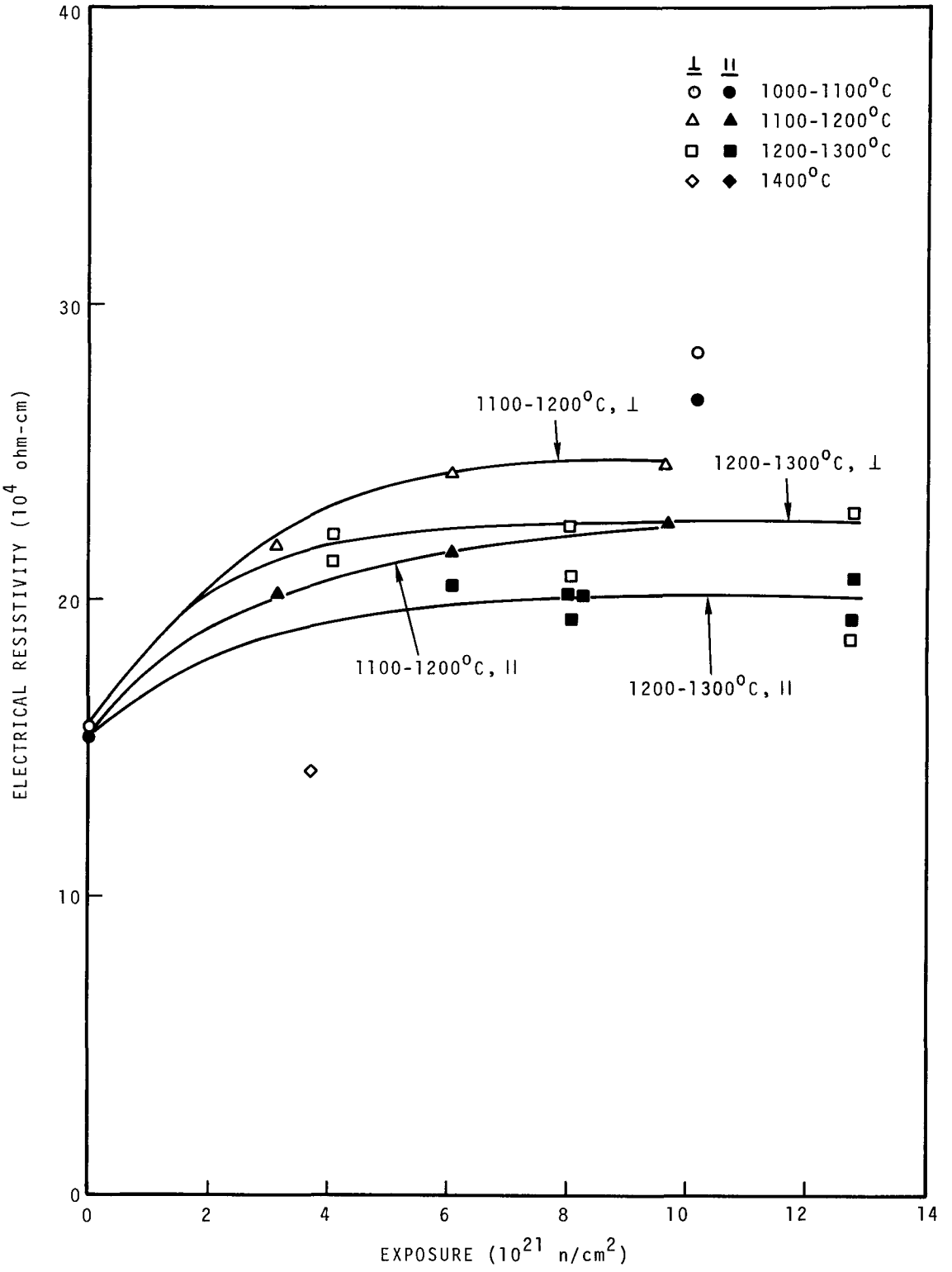

FIGURE 55. Electrical Resistivity of 9640.

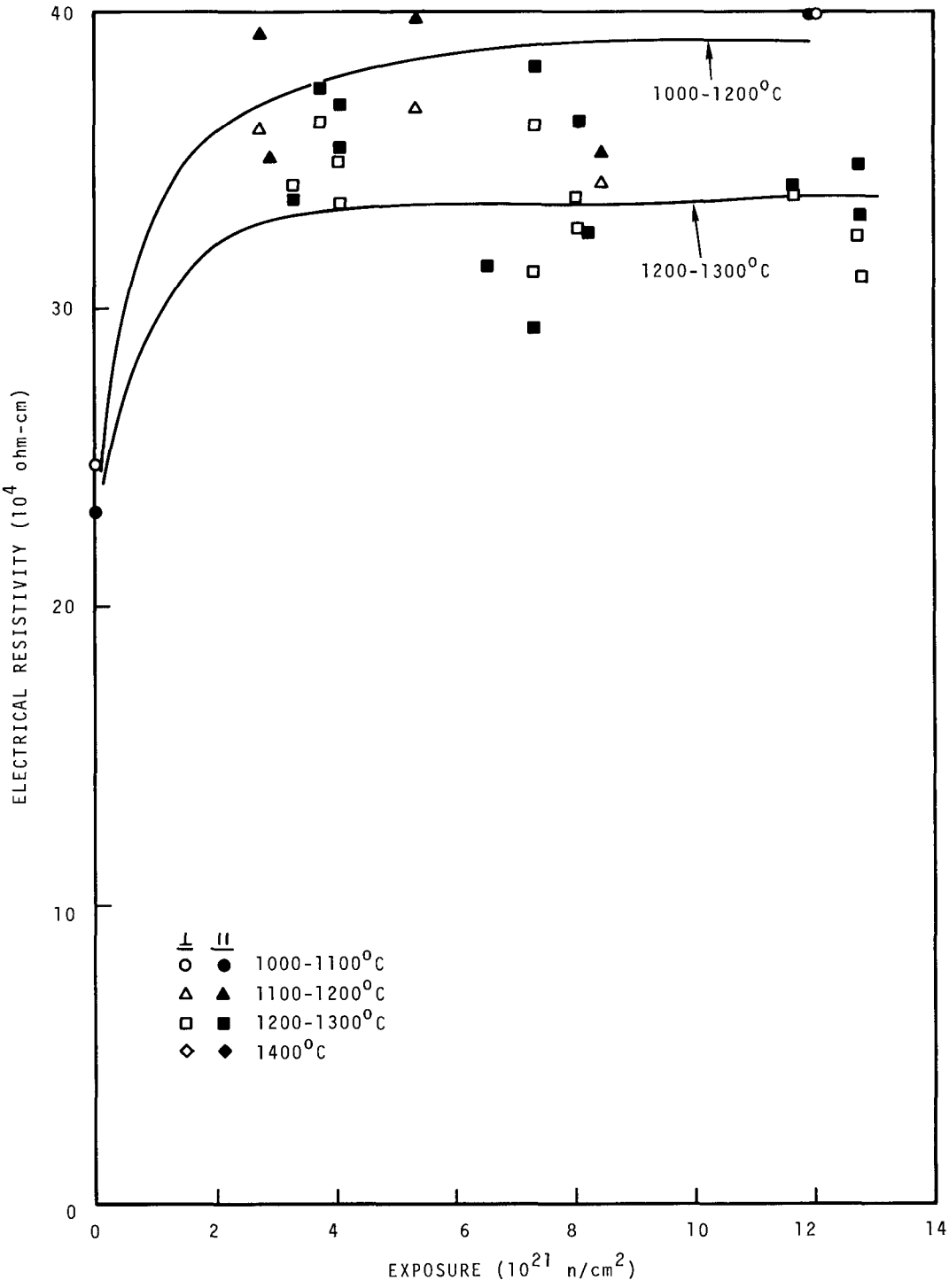

FIGURE 56. Electrical Resistivity of 9650.

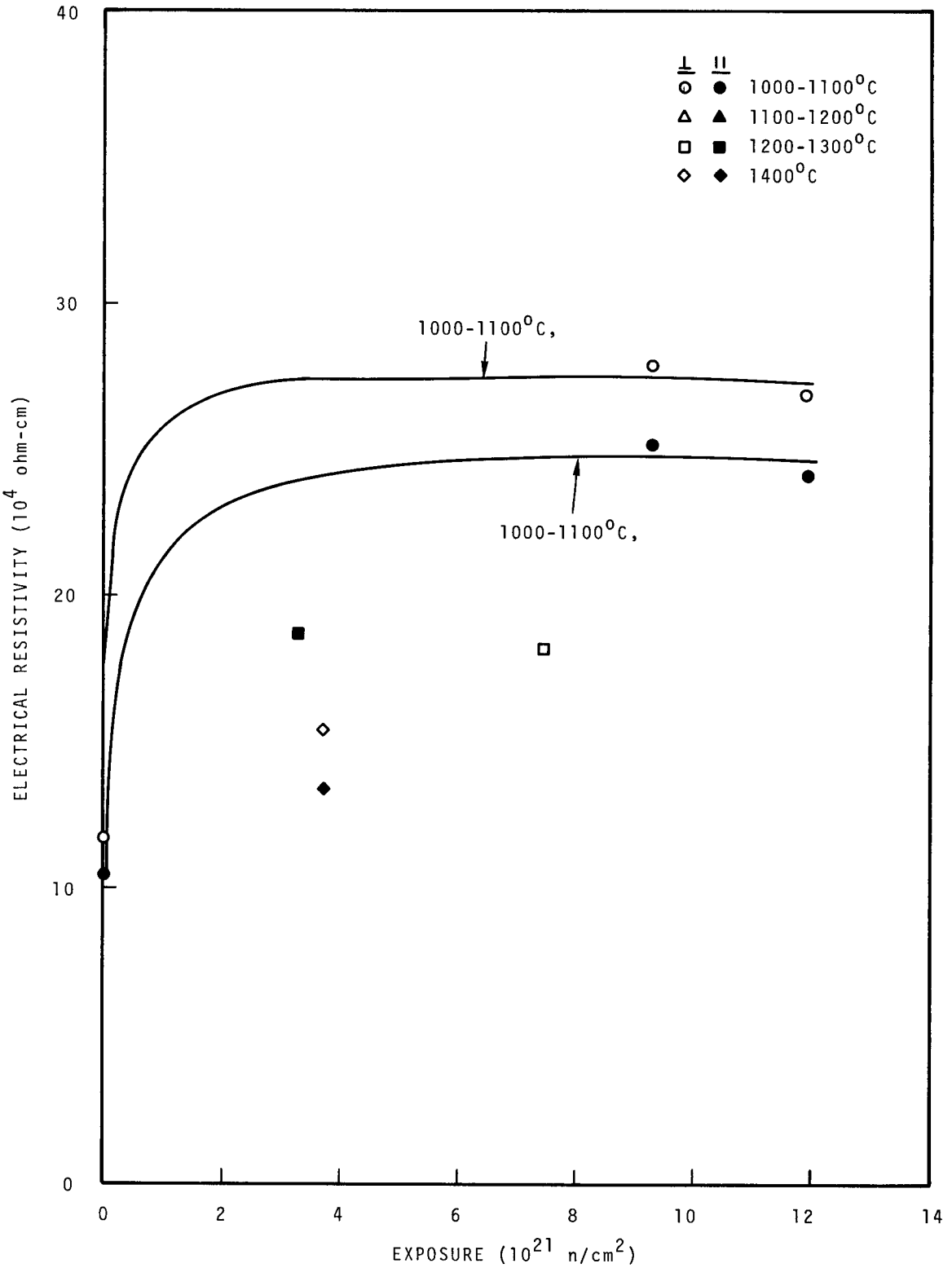

FIGURE 57. Electrical Resistivity of 9751.

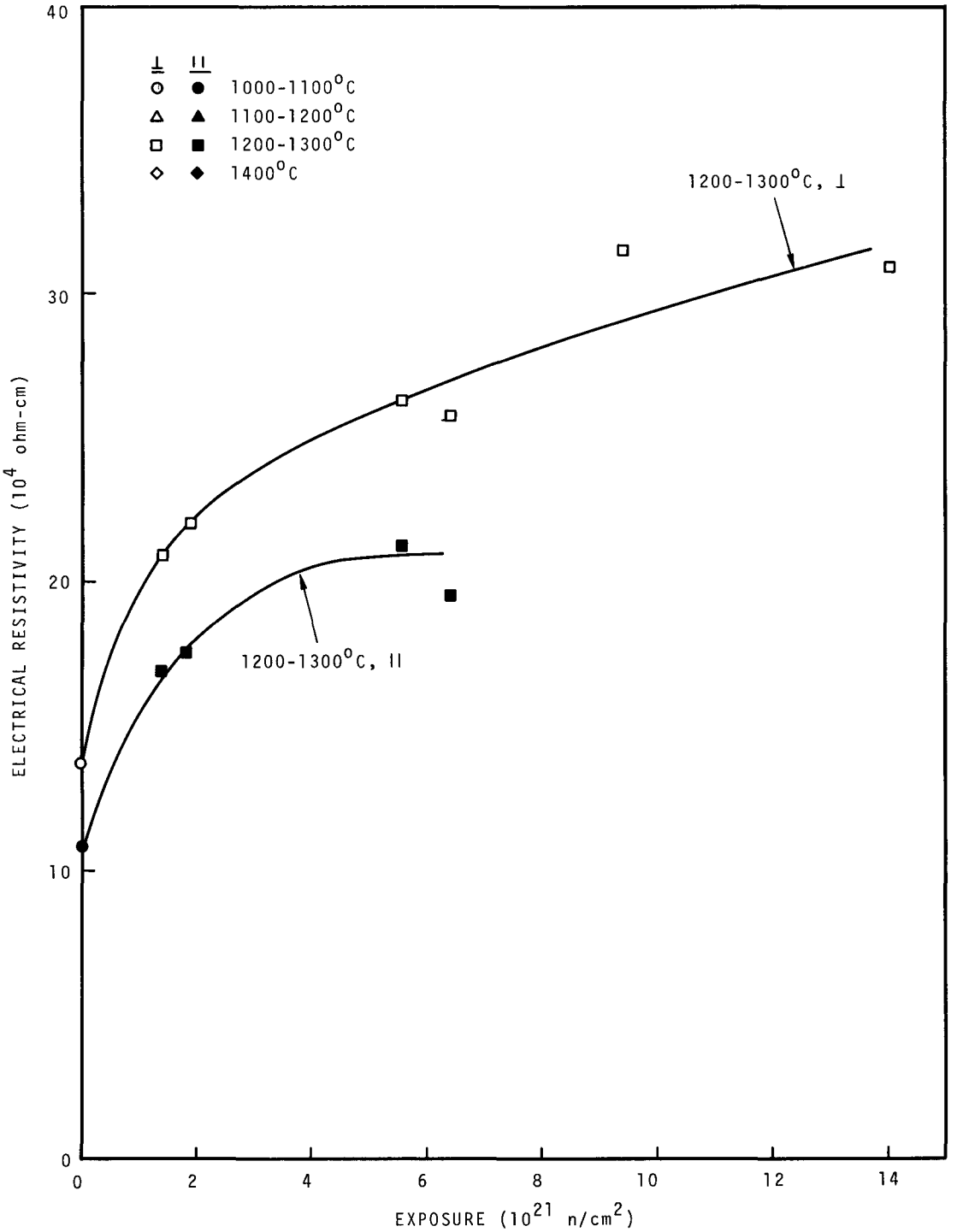

FIGURE 58. Electrical Resistivity of GN.

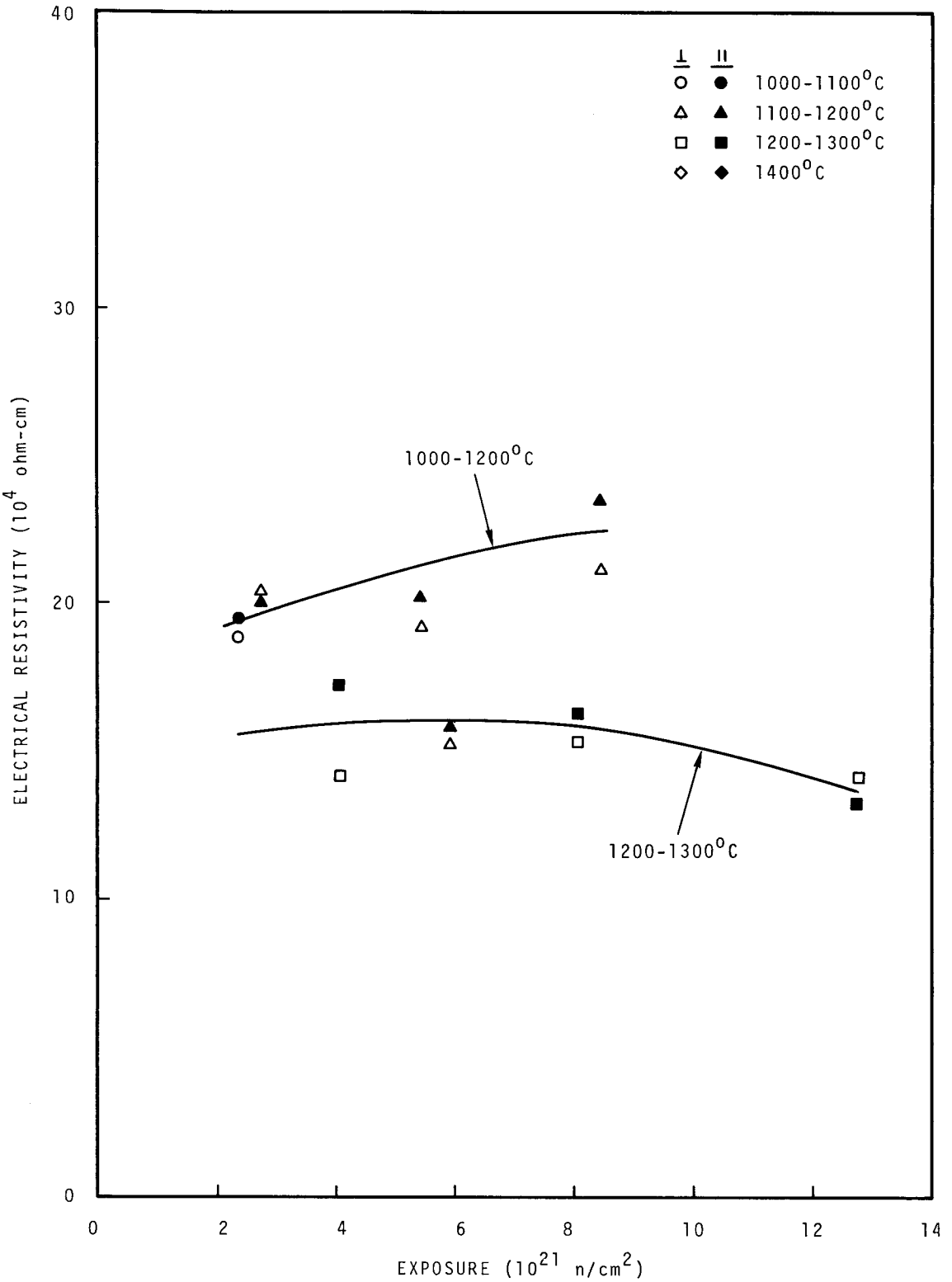

FIGURE 59. Electrical Resistivity of AXF-Q1.

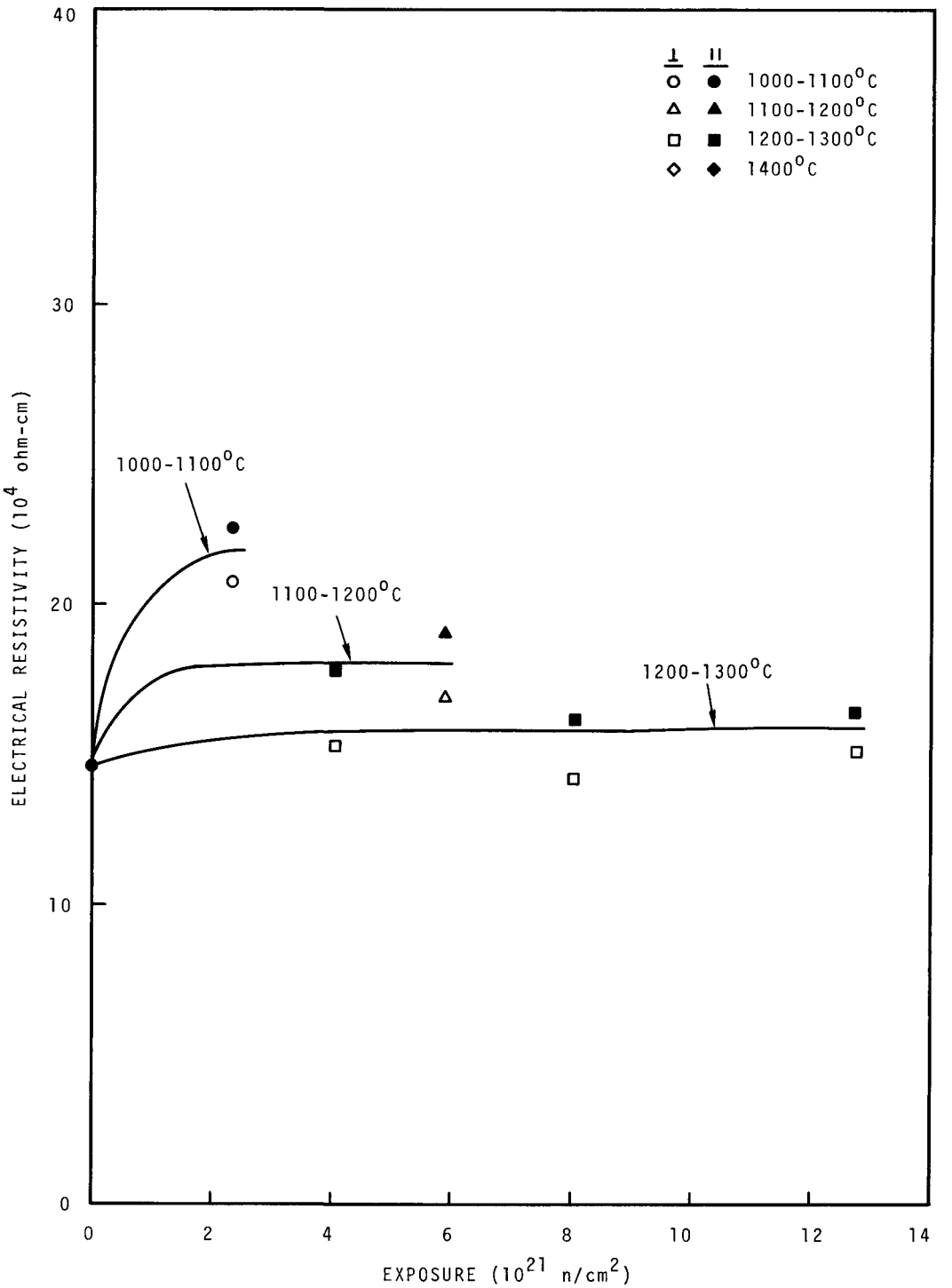

FIGURE 60. Electrical Resistivity of AXF-5Q1.

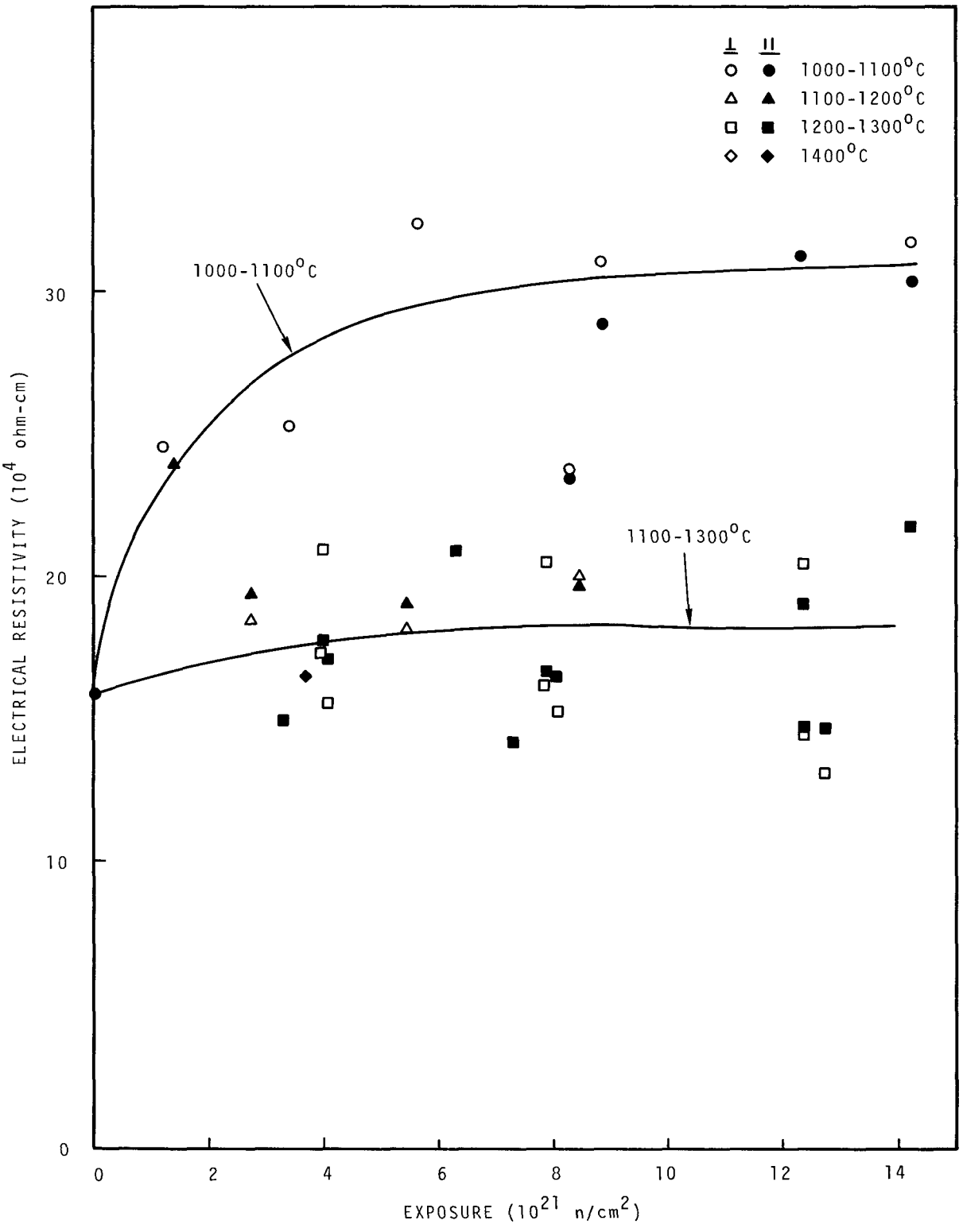

FIGURE 61. Electrical Resistivity of AXF-8Q1.

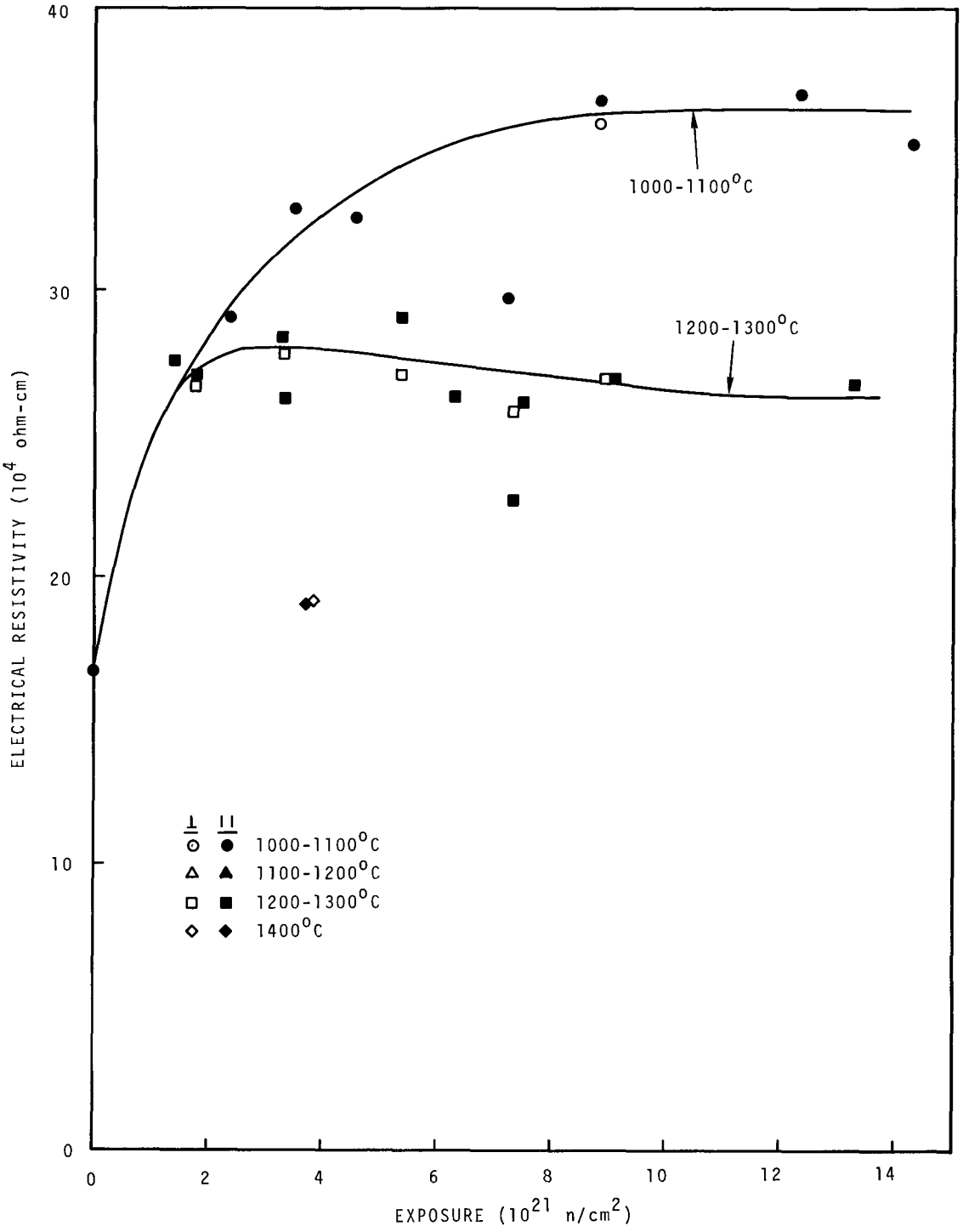

FIGURE 62. Electrical Resistivity of AXZ-5Q1.

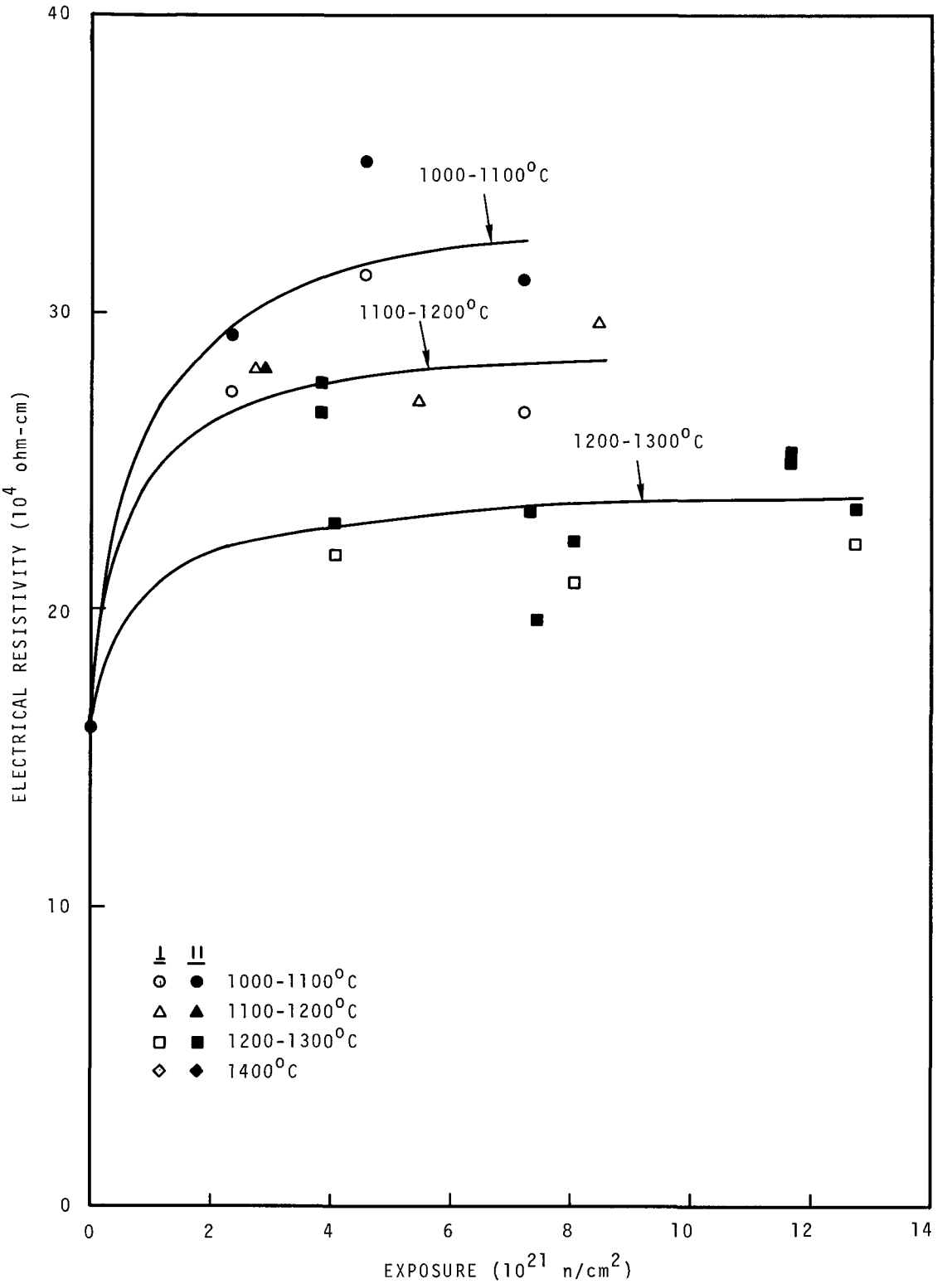

FIGURE 63. Electrical Resistivity of AXZ-8Q1.

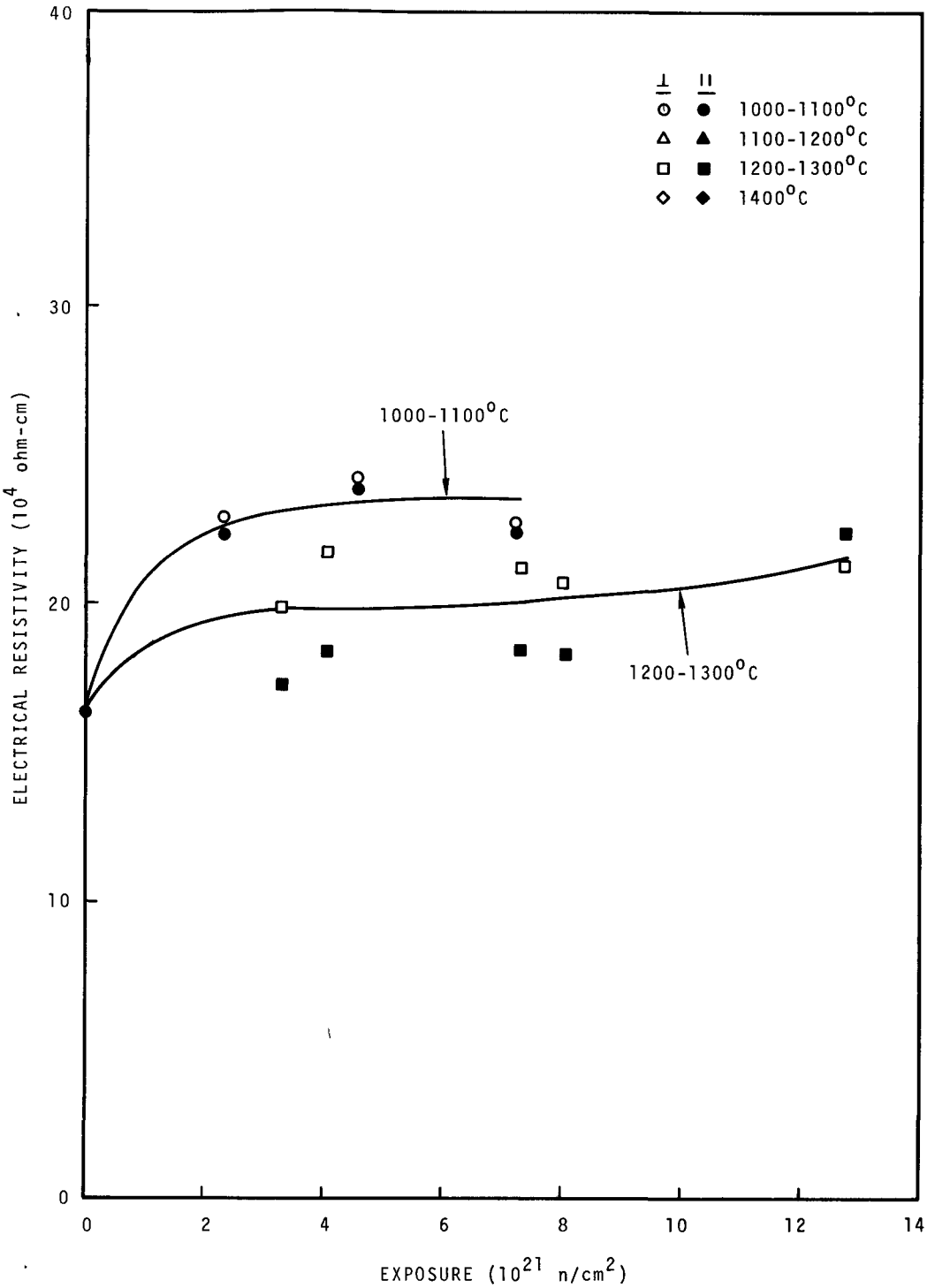

FIGURE 64. Electrical Resistivity of AXF-5QBG1.

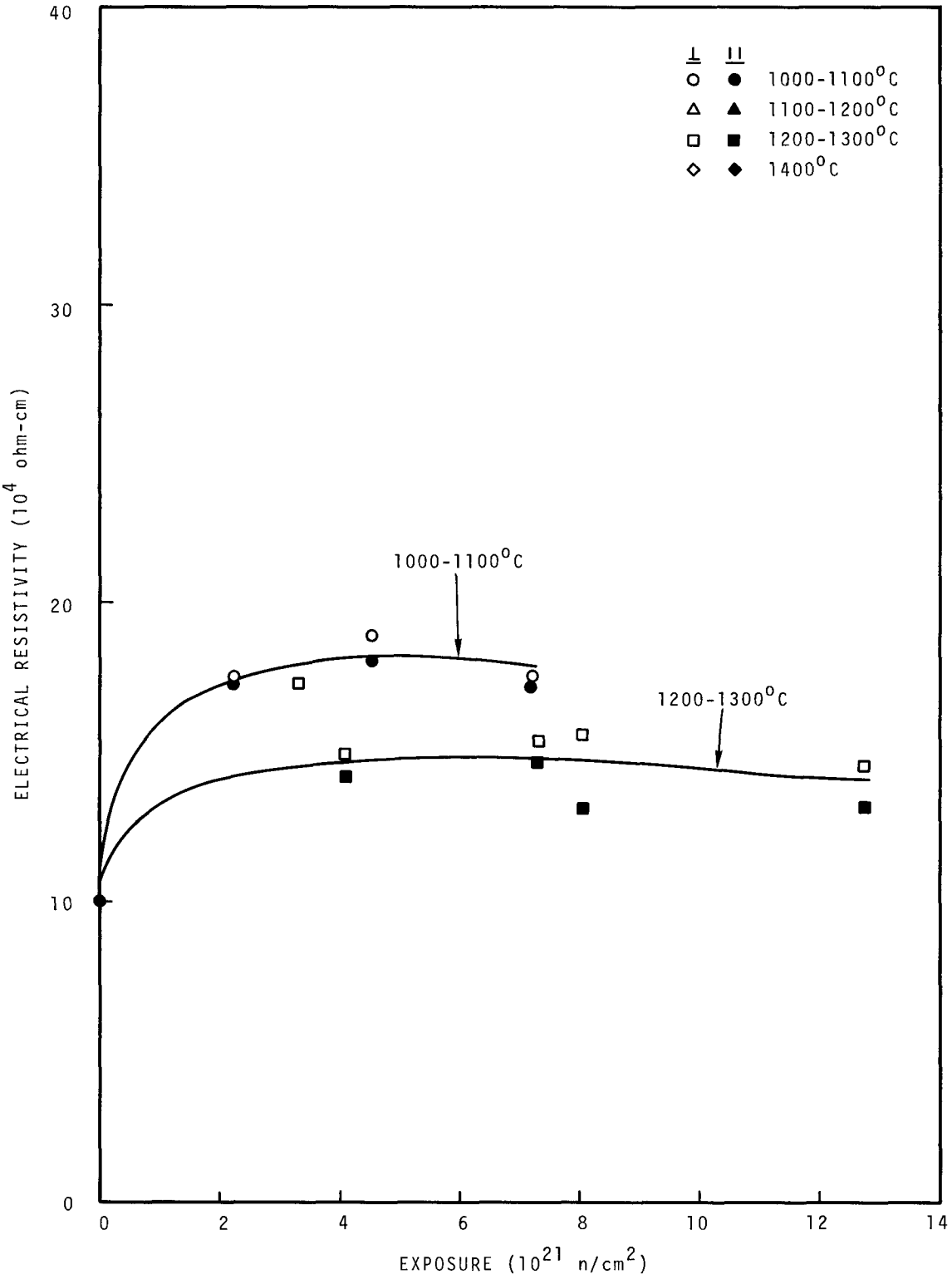

FIGURE 65. Electrical Resistivity of AXF-8QBG1.

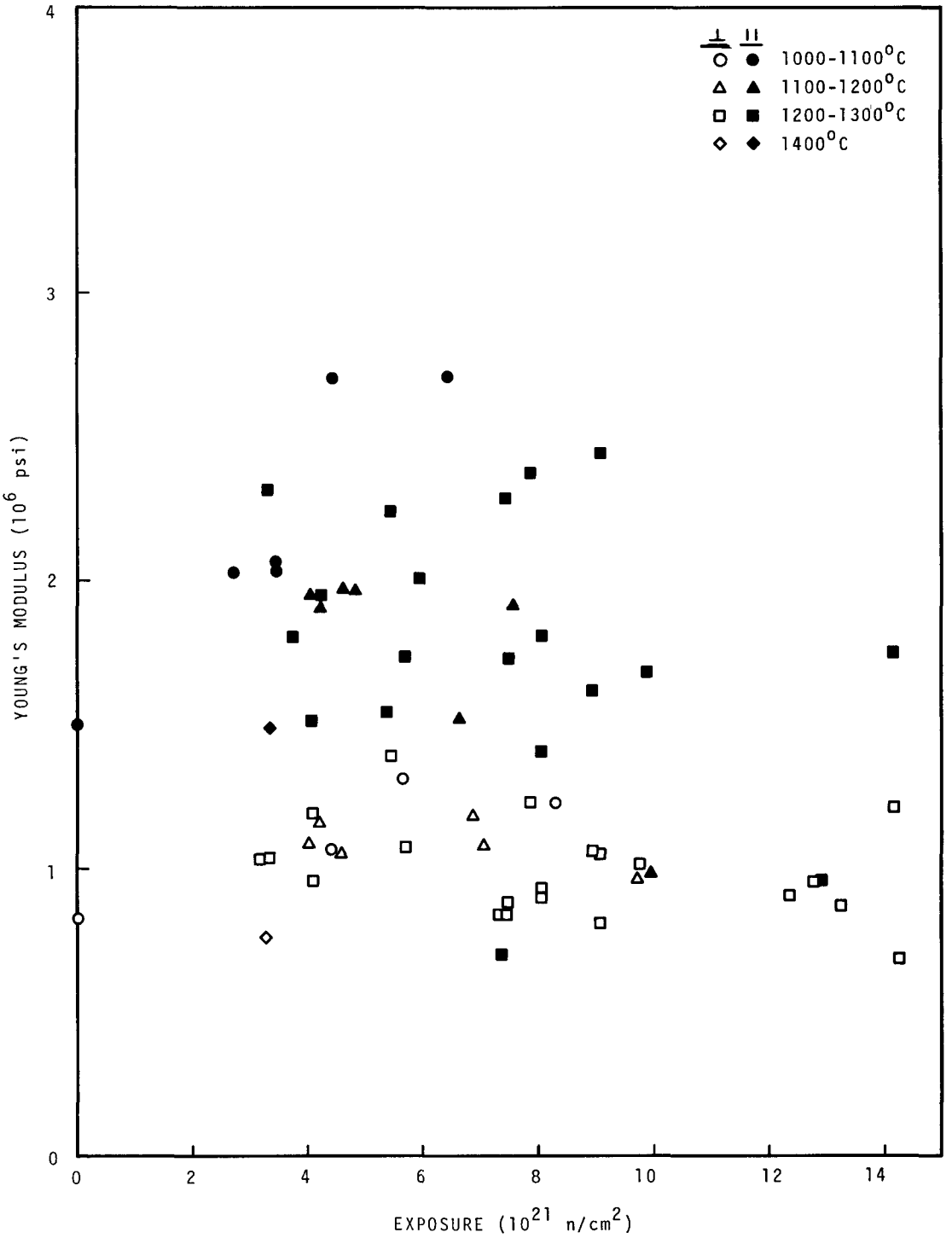

FIGURE 66. Young's Modulus of EGCR.

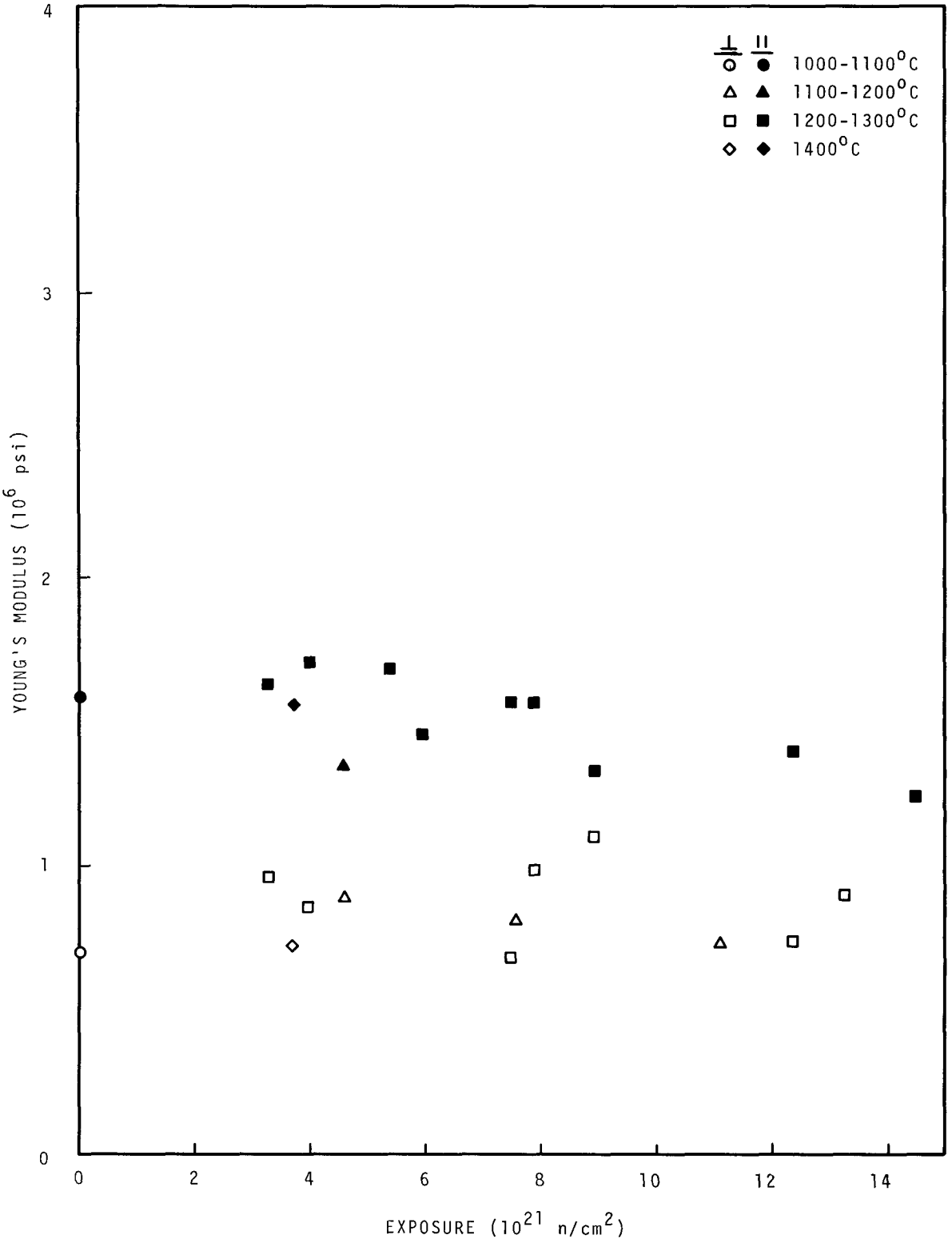

FIGURE 67. Young's Modulus of CSF.

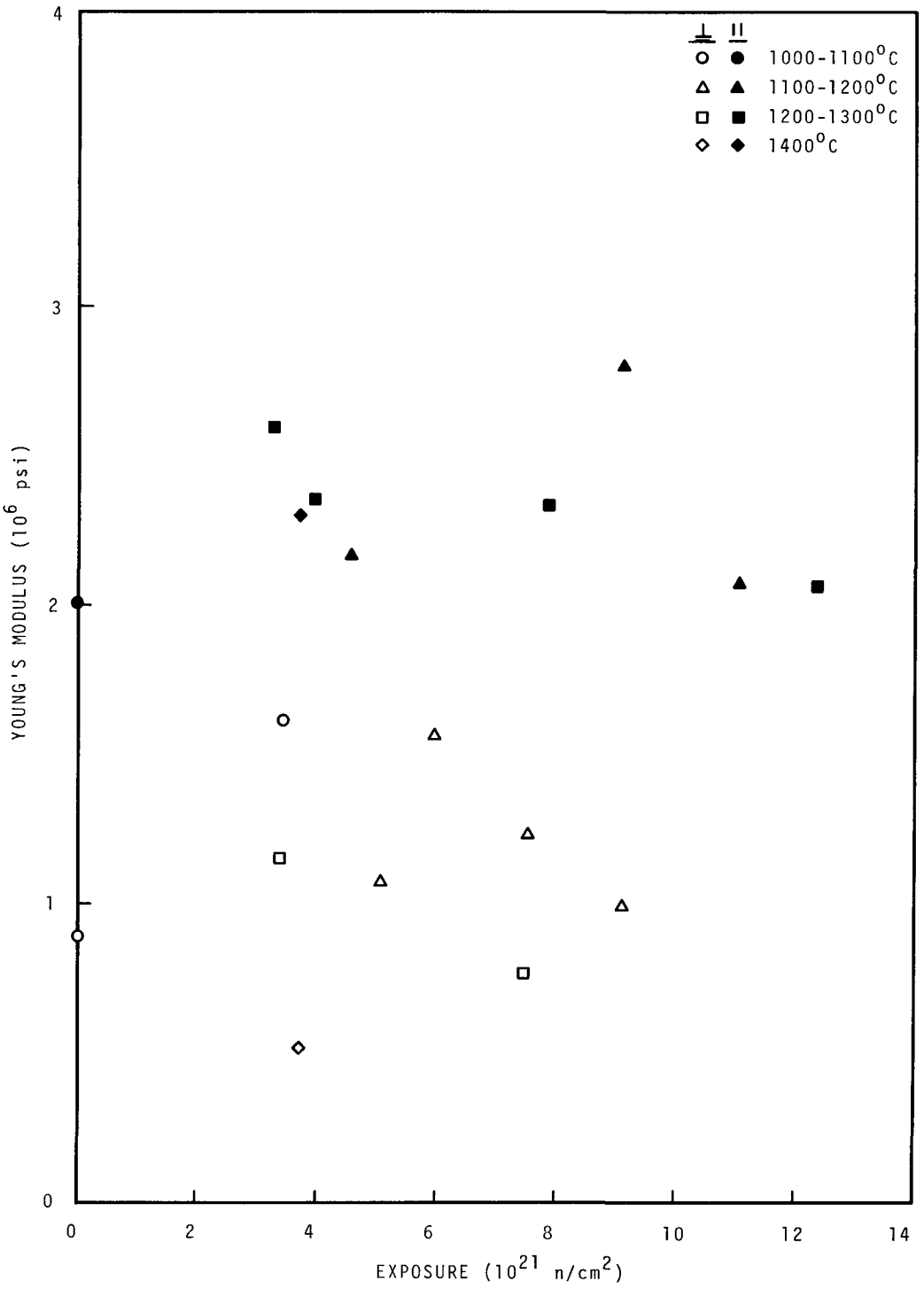

FIGURE 68. Young's Modulus of TSX.

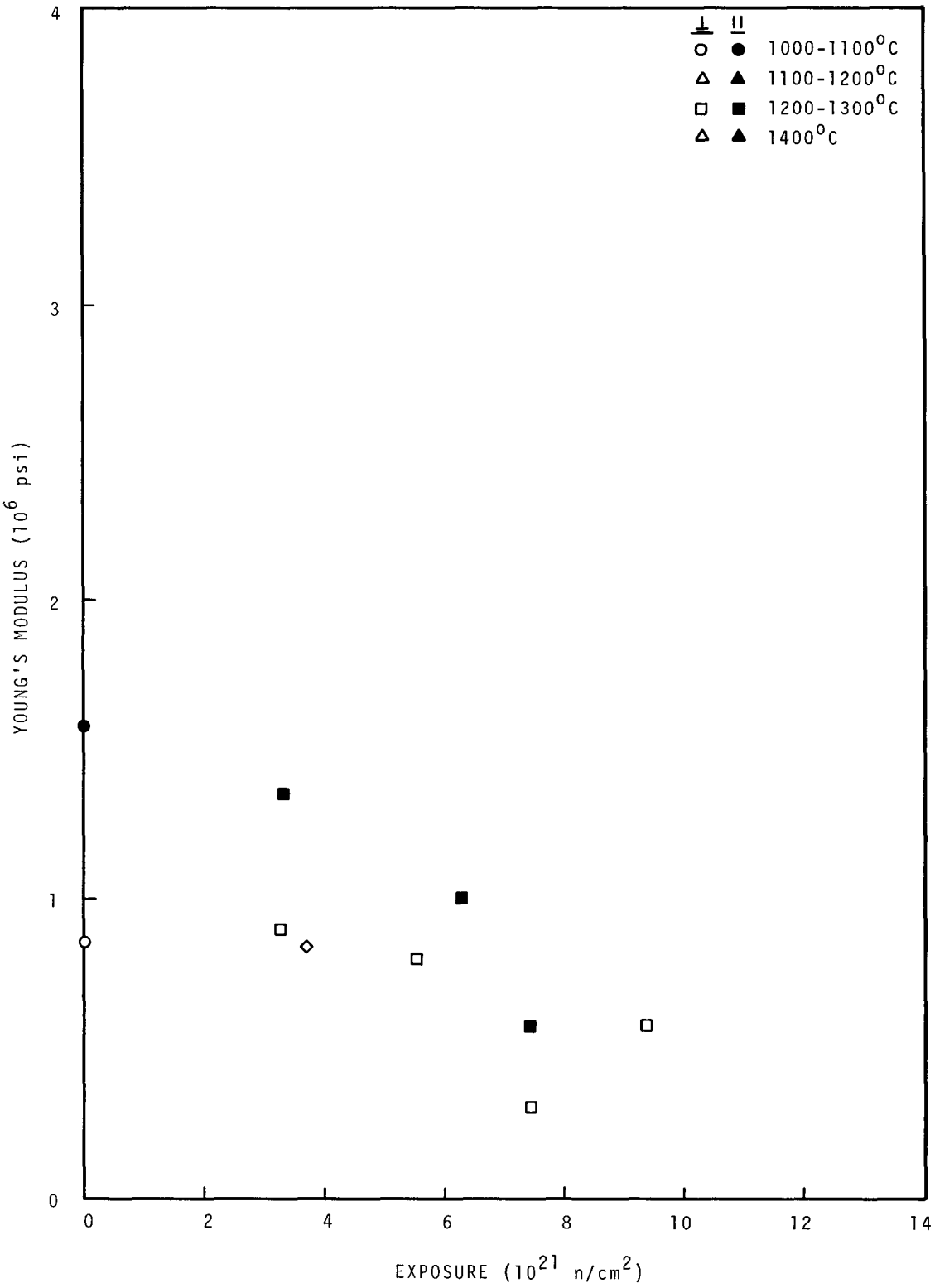

FIGURE 69. Young's Modulus of TSGBF.

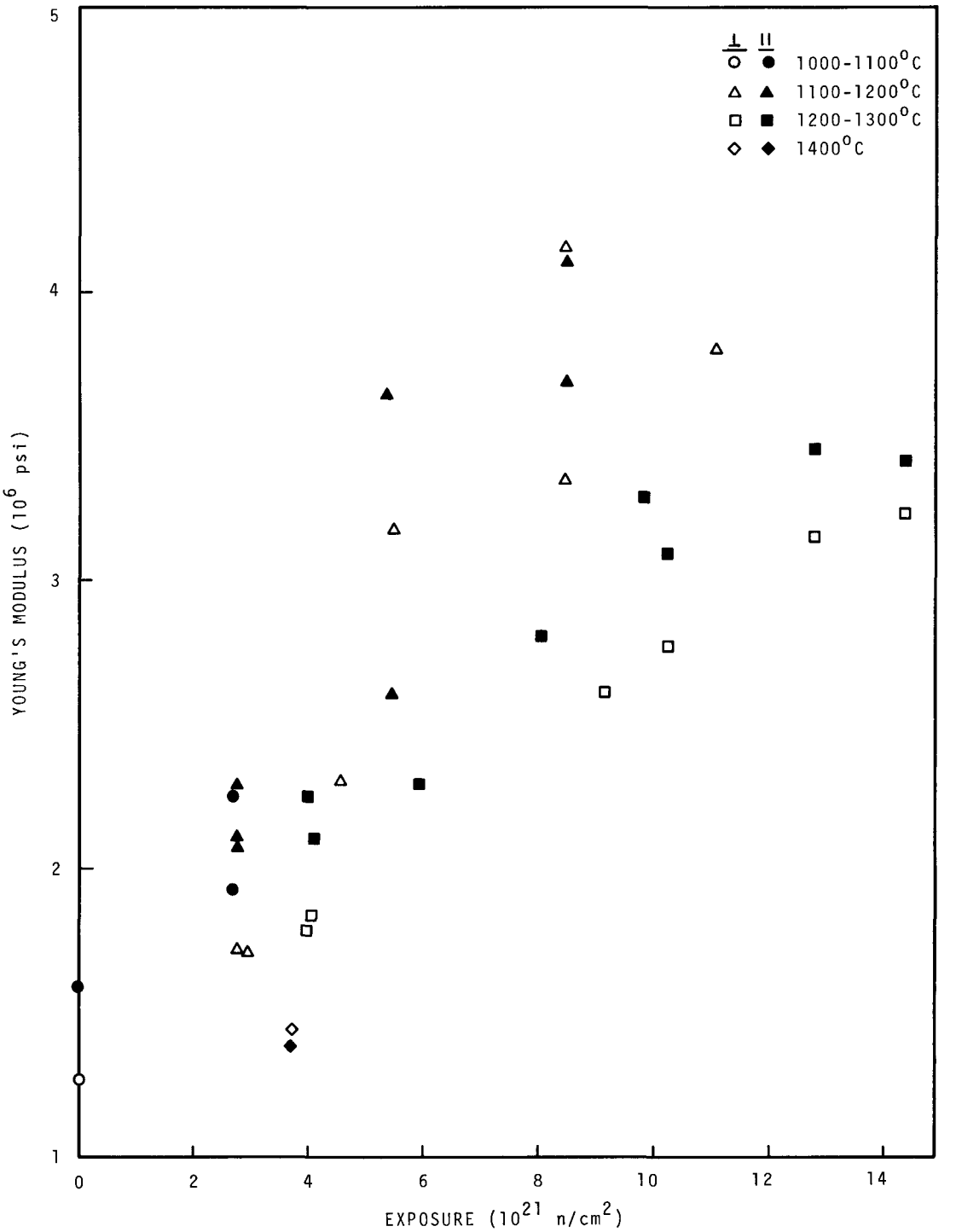

FIGURE 70. Young's Modulus of RP4.

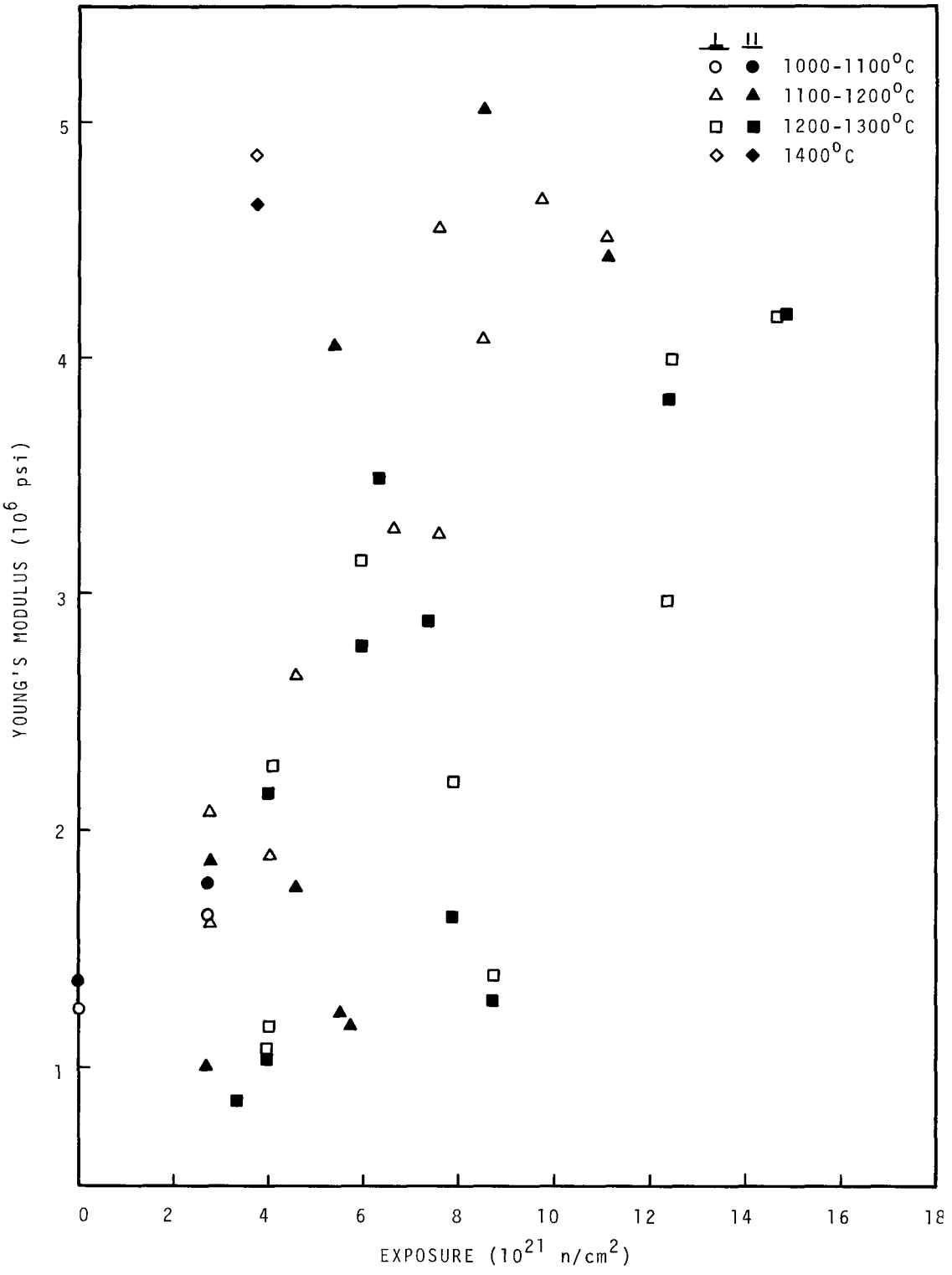

FIGURE 71. Young's Modulus of RC5.

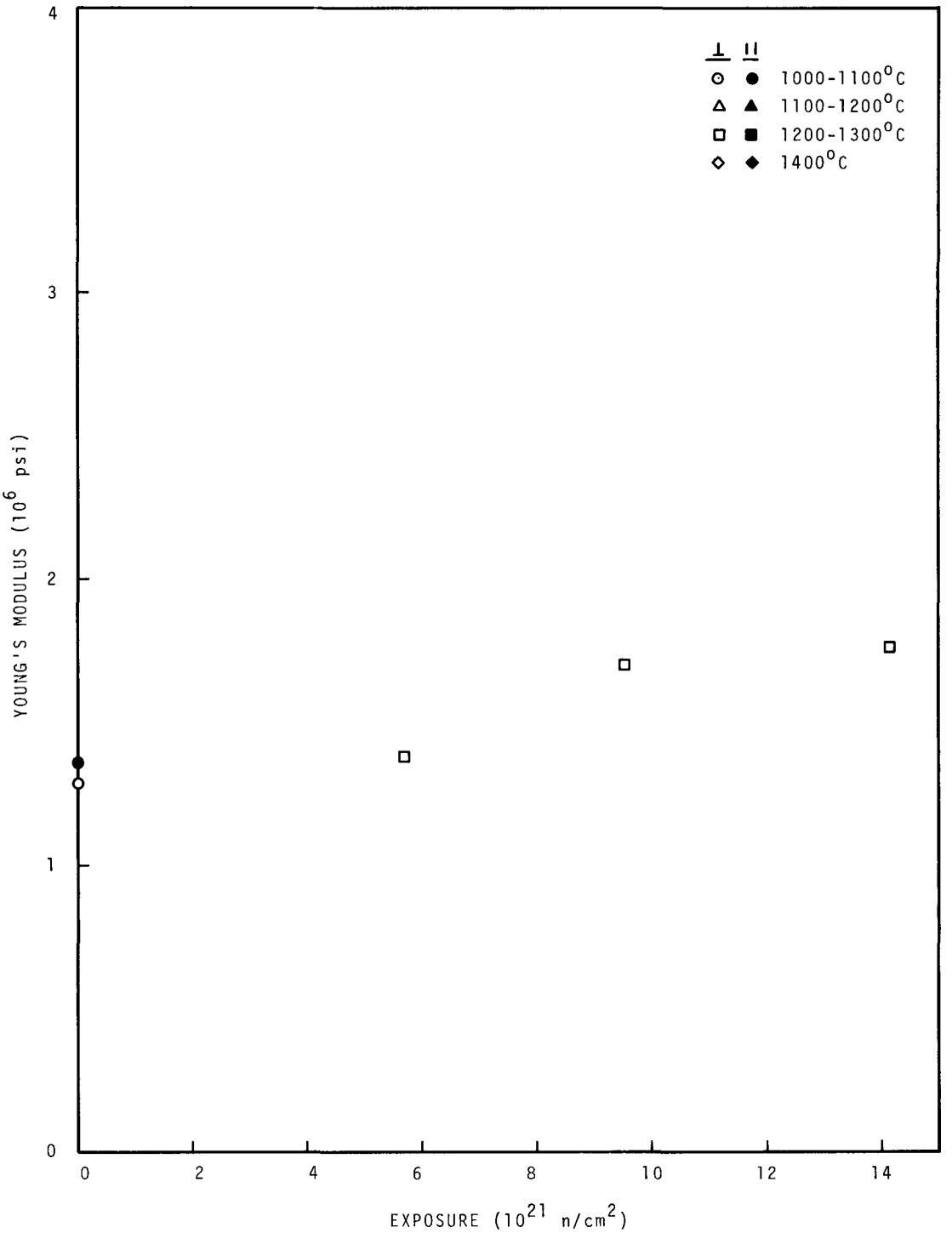

FIGURE 72. Young's Modulus of JOZ.

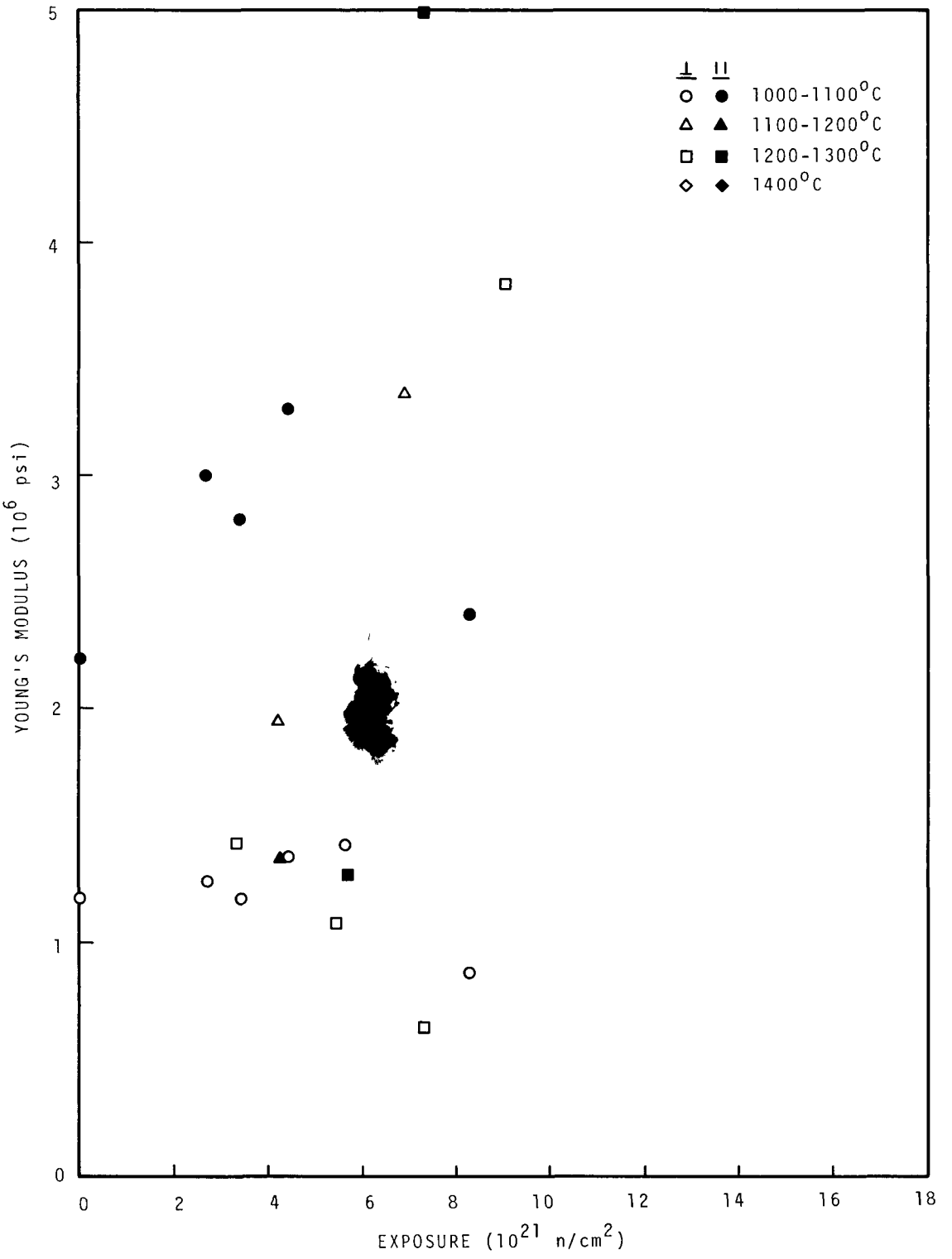

FIGURE 73. Young's Modulus of H327.

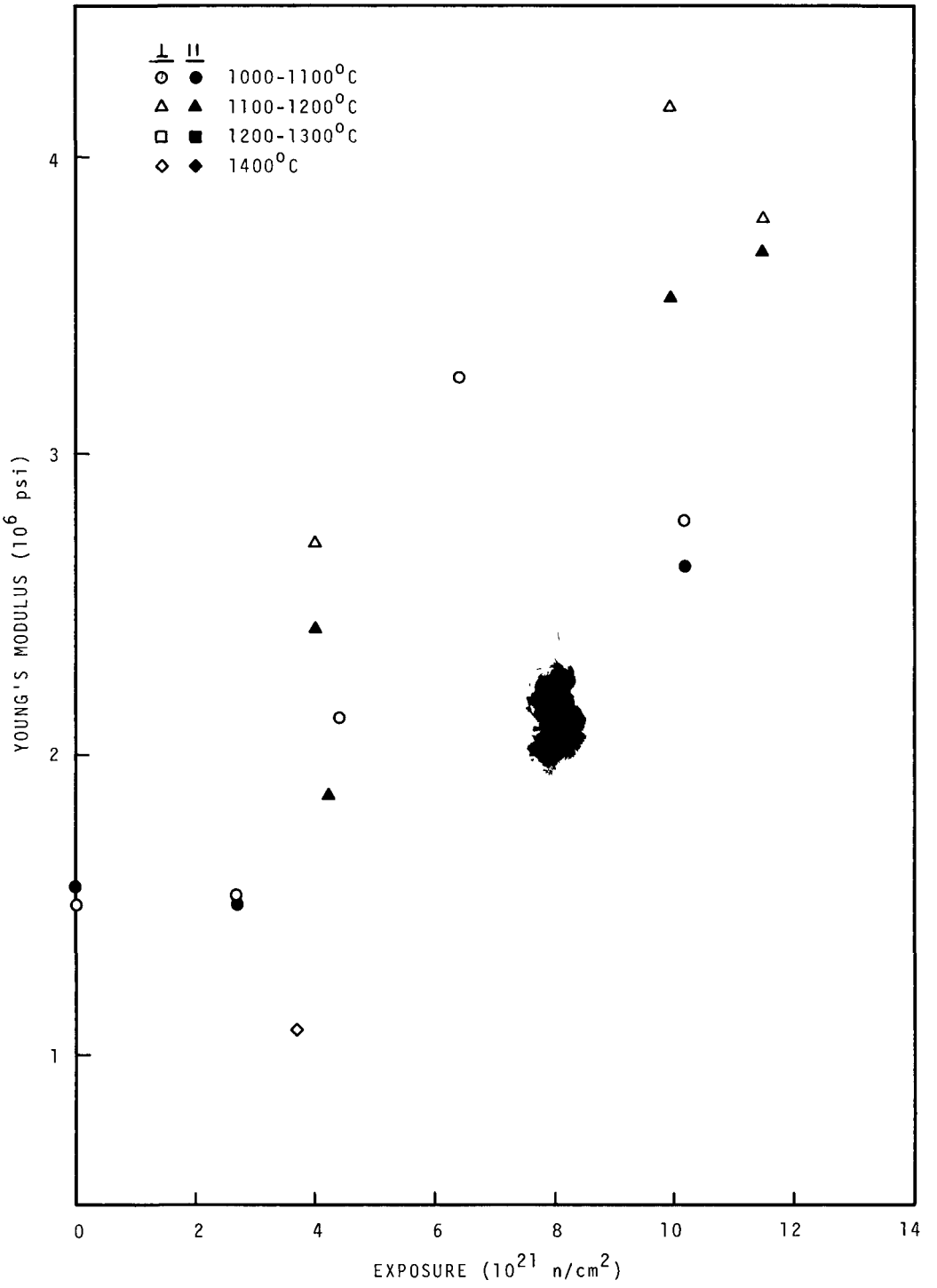

FIGURE 74. Young's Modulus of H328.

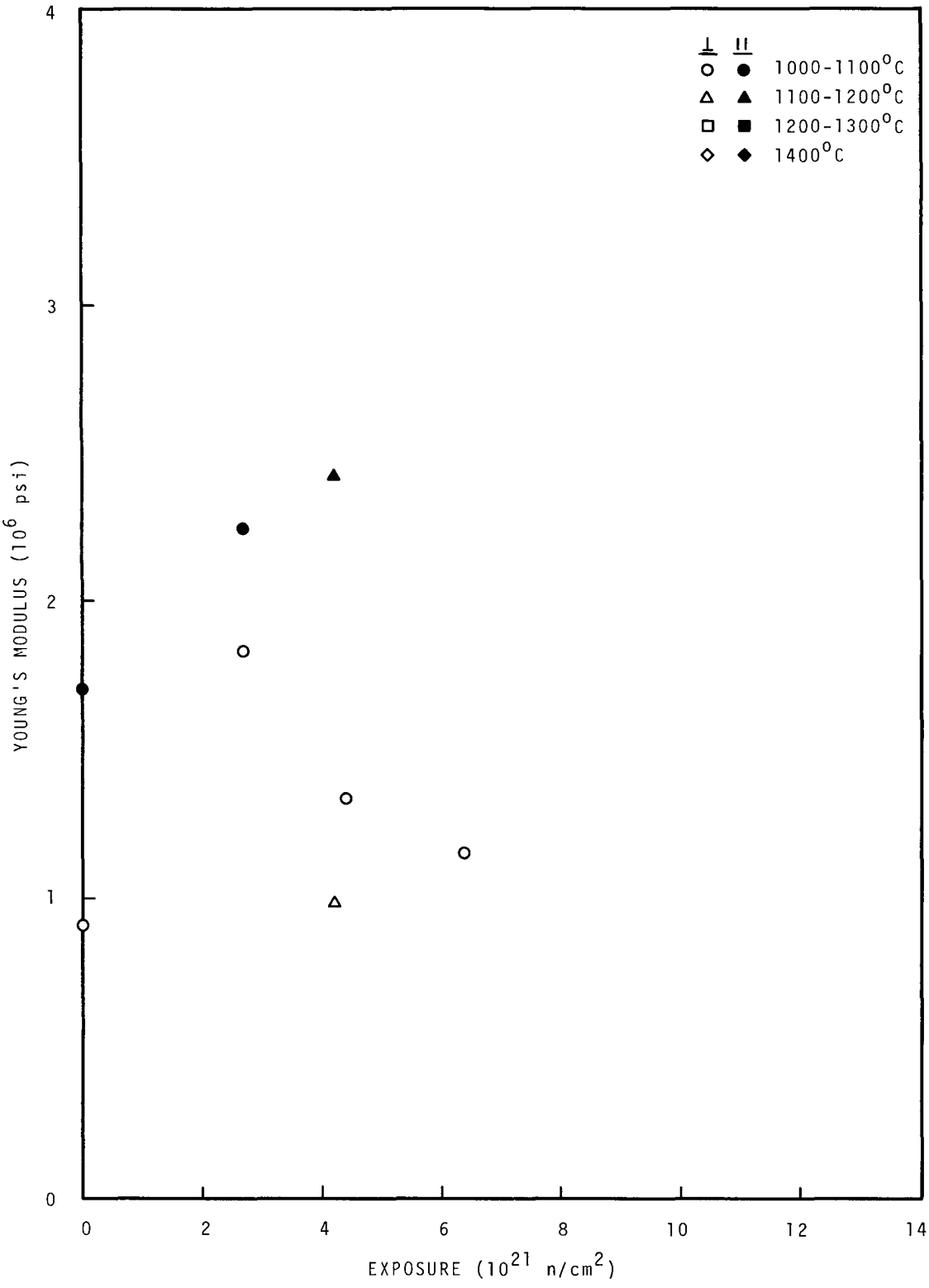

FIGURE 75. Young's Modulus of 9567.

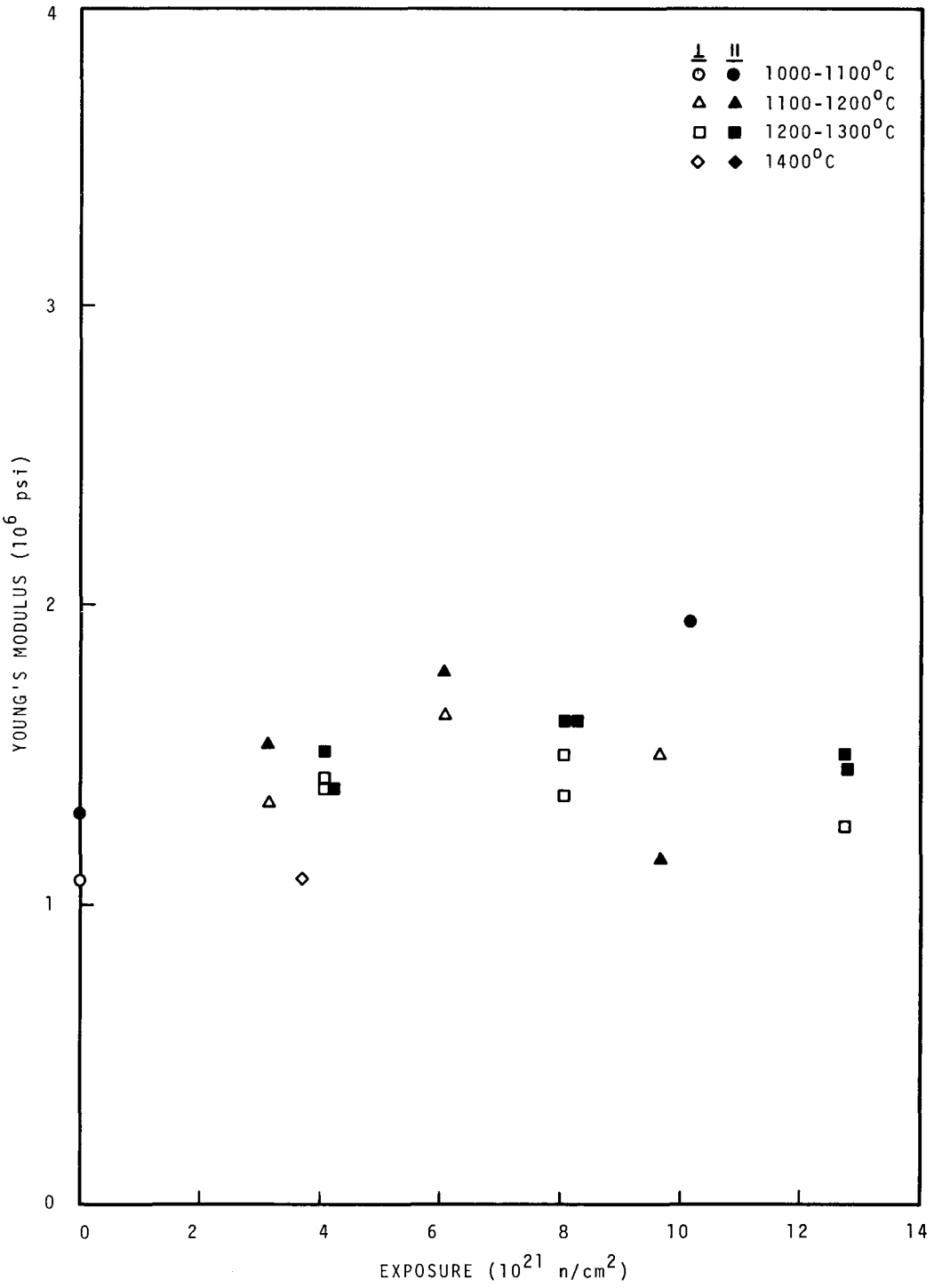

FIGURE 76. Young's Modulus of 9640.

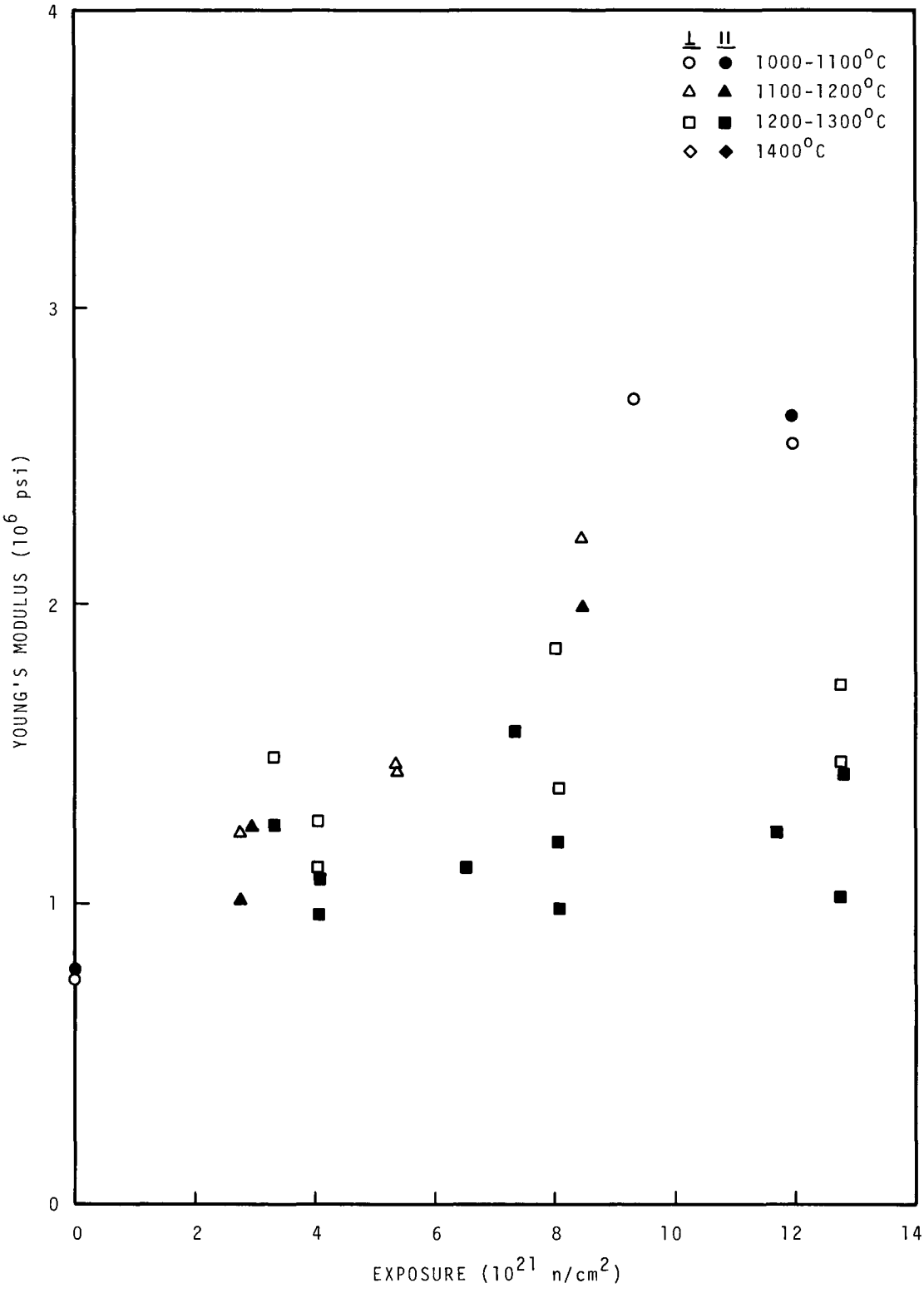

FIGURE 77. Young's Modulus of 9650.

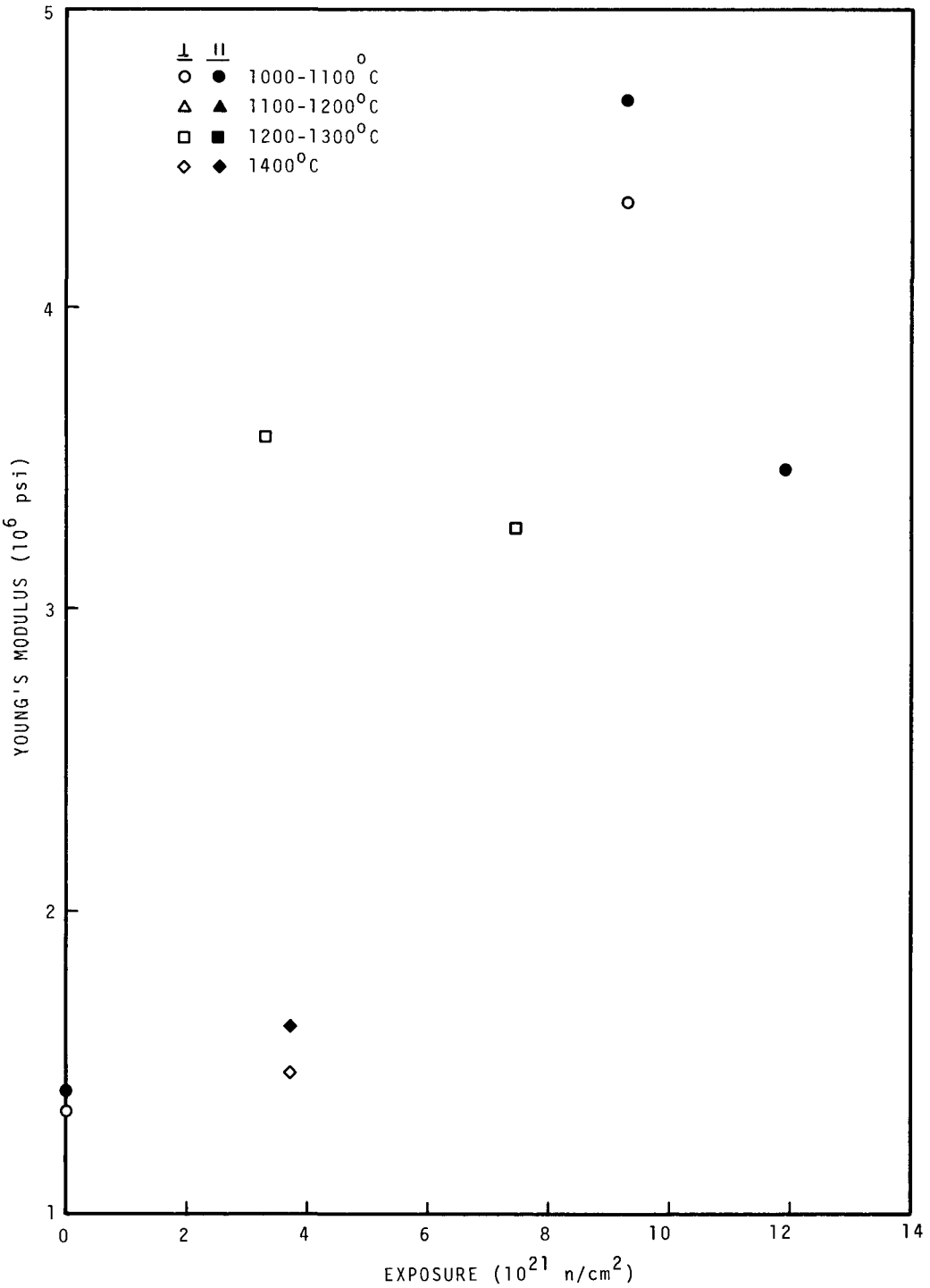

FIGURE 78. Young's Modulus of 9751.

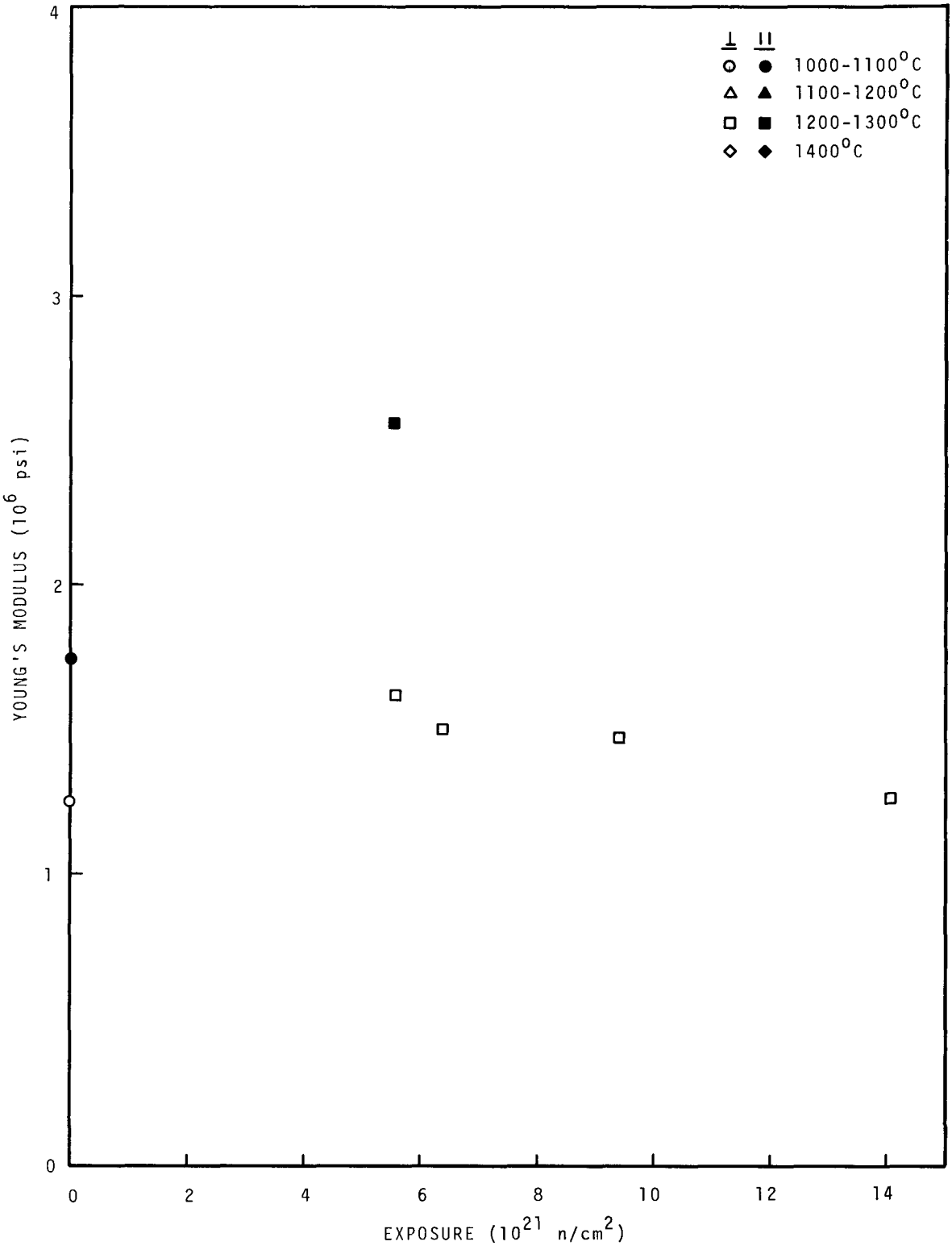

FIGURE 79. Young's Moudlus of GN.

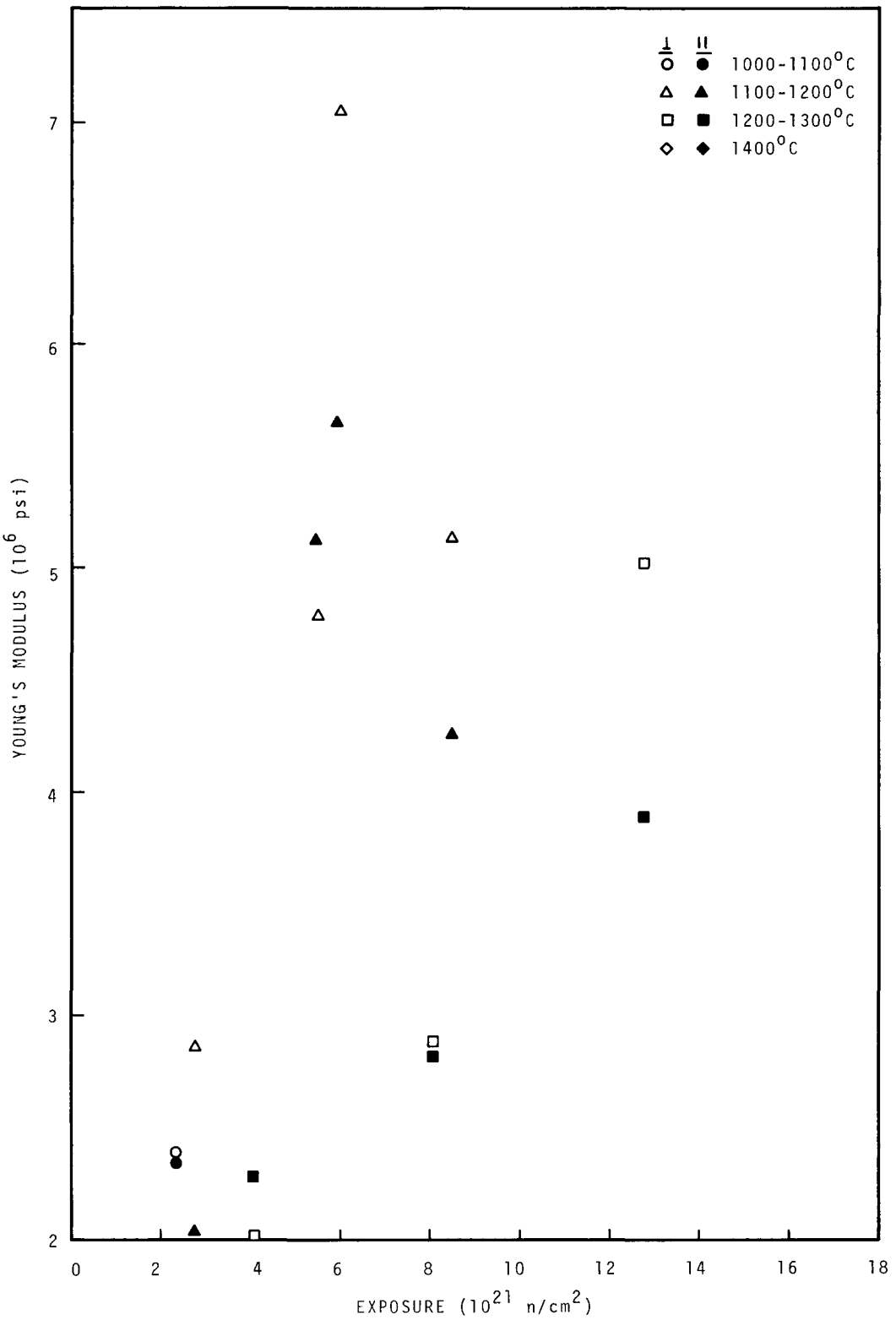

FIGURE 80. Young's Modulus of AXF-Q1.

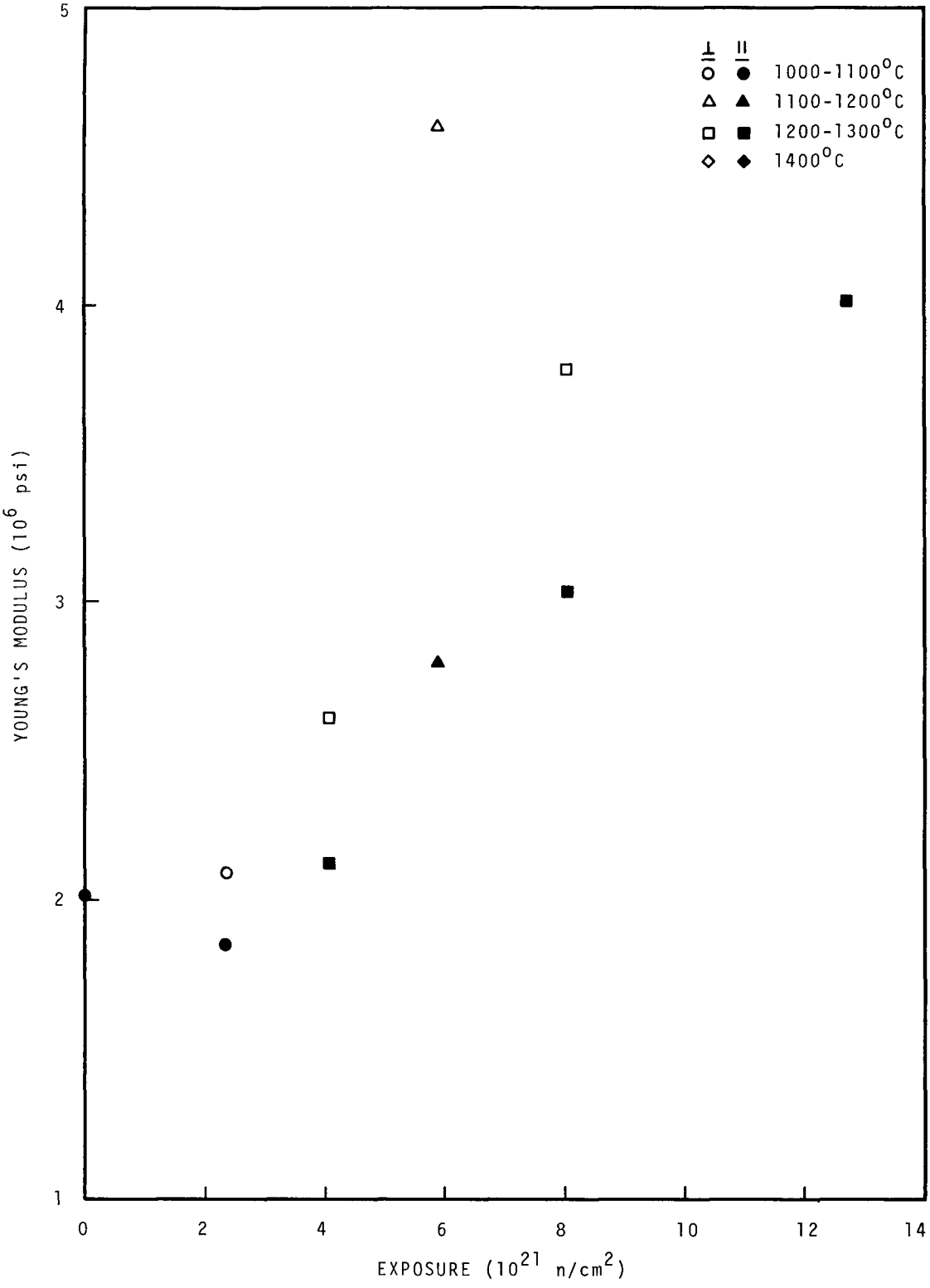

FIGURE 81. Young's Modulus of AXF-5Q1.

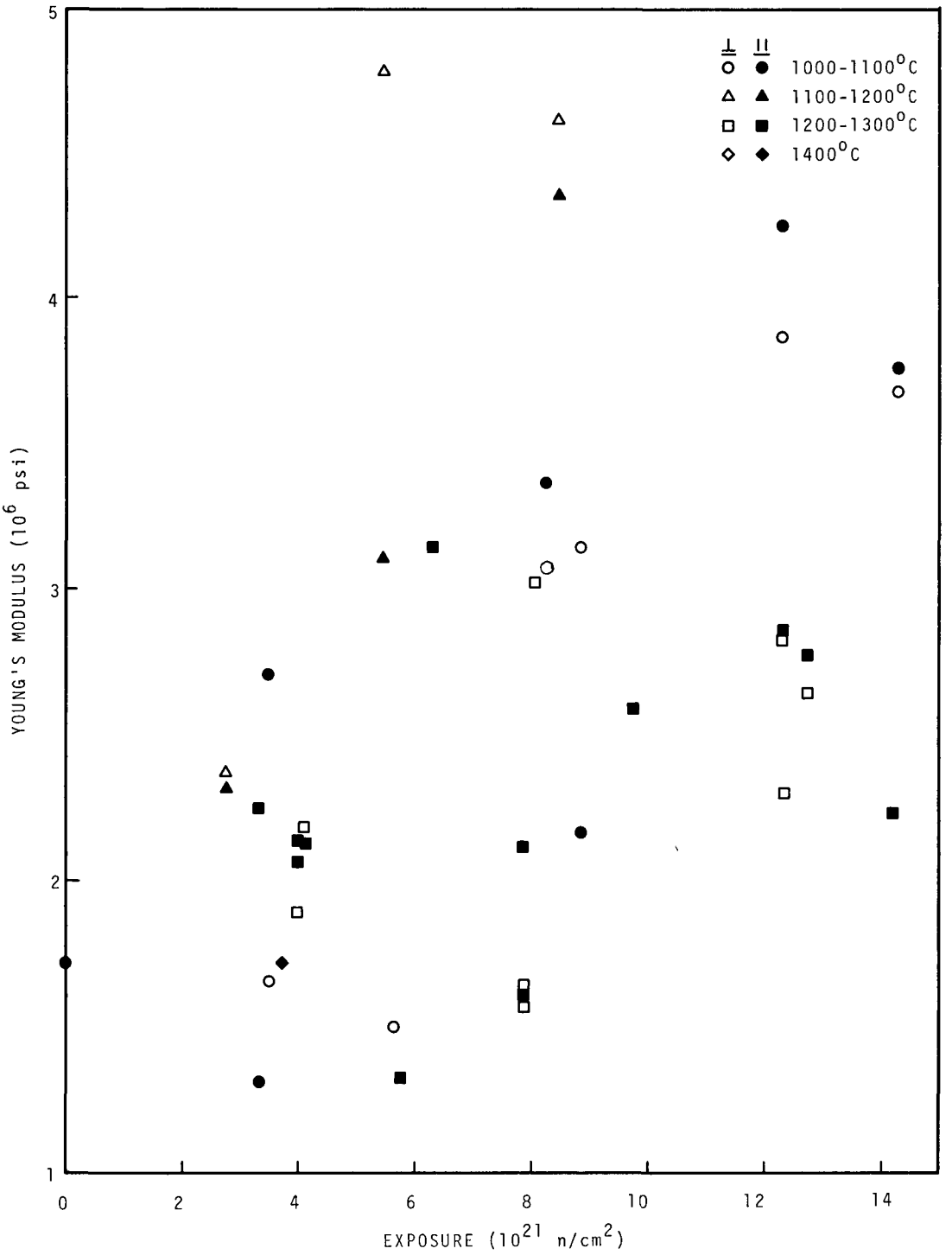

FIGURE 82. Young's Modulus of AXF-8Q1.

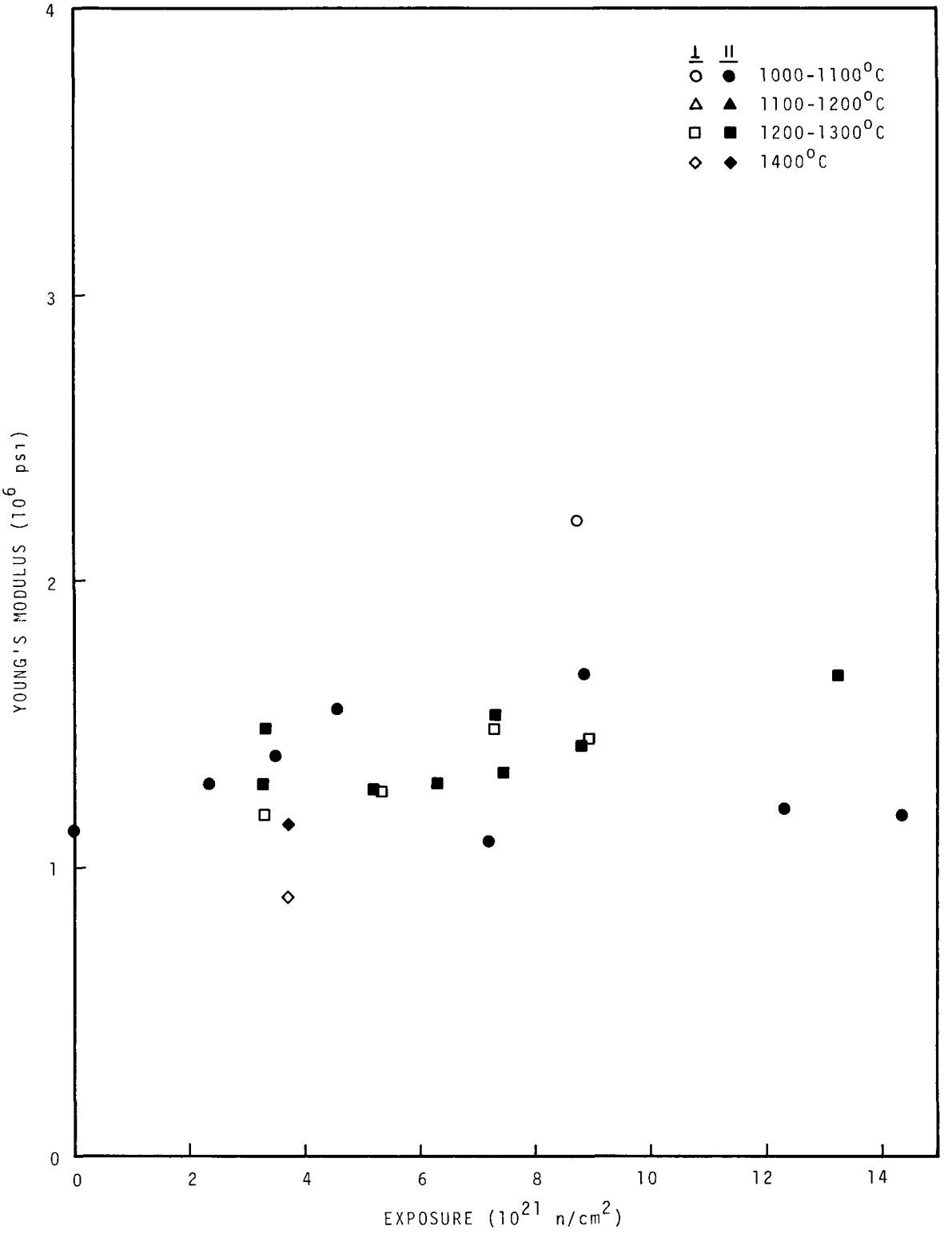

FIGURE 83. Young's Modulus of AXZ-5Q1.

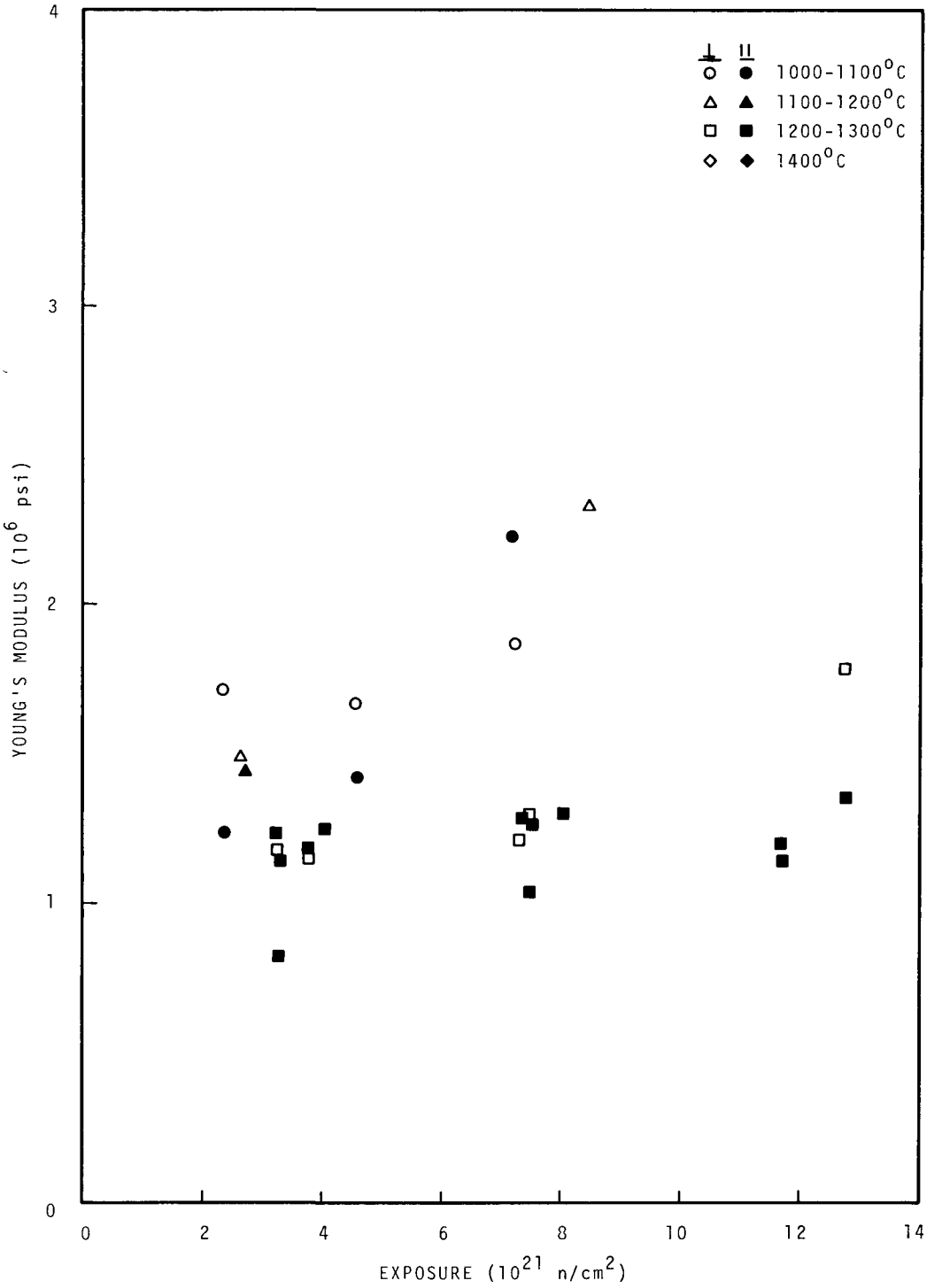

FIGURE 84. Young's Modulus of AXZ-8Q1.

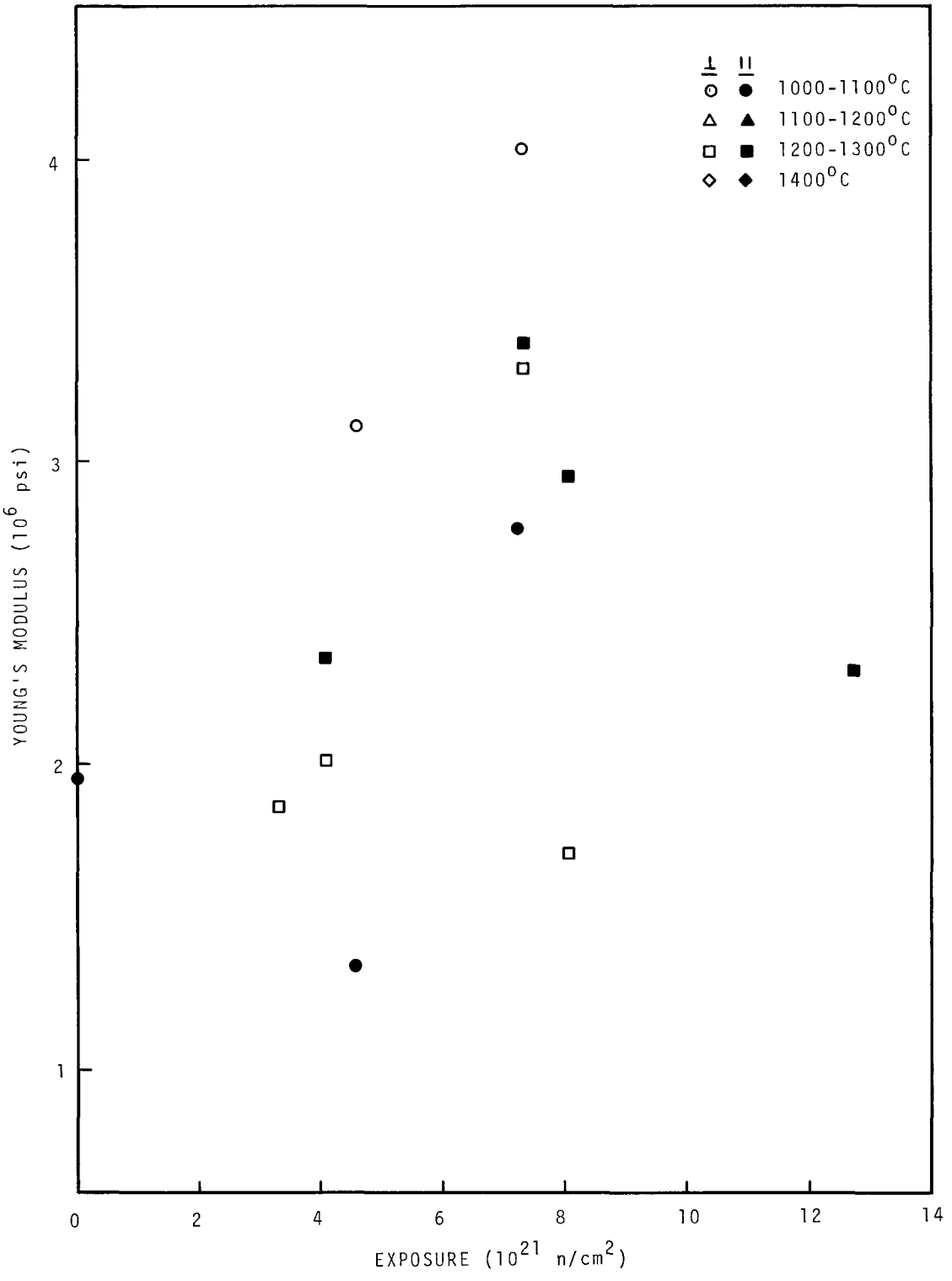

FIGURE 85. Young's Modulus of AXF-5QBG1.

DISTRIBUTION

No. of copies

OFFSITE

1 AEC Chicago Patent Group
G. H. Lee

4 AEC Division of Reactor Development and Technology
J. E. Fox(2)
R. E. Pahler
J. M. Simmons

1 AEC Division of Research
D. K. Stevens

3 AEC, Director, Division of Reactor Licensing

3 AEC, Director, Division of Reactor Standards

210 AEC Division of Technical Information Extension

3 Air Force Materials Laboratory
G. L. Denman
M. L. Minges
C. A. Pratt

2 Atomic Energy Establishment - Dragon
M. R. Everett
L. W. Graham

2 Atomic Energy of Canada, Limited
Fuels and Materials Division
Fuels Materials Branch
Chalk River, Ontario, CANADA
J. R. MacEwan
J. A. L. Robertson

1 Berkeley Nuclear Lab.
Berkeley, Glos., ENGLAND
P. P. Jennings

1 Brookhaven National Laboratory
D. H. Gurinsky

3 Centre d' Etudes Nucleaires de Saclay
Boite Postale No. 2
Gif-sur-Vvette (seine-et-Oise), FRANCE
P. Leveque
J. Rappeneau (2)

3 Culcheth Laboratories
Reactor Materials Laboratory
UKAEA
Wigshaw Lane
Warrington, Lancashire, ENGLAND
B. T. Kelly (2)
P. T. Nettley

1 Euratom C.C.R.
Petten, Netherlands
V. Lungagnani

1 General Electric Company
Pleasanton, California
G. E. Robinson

1 General Electric Company, Ltd.
Hirst Research Centre
Wembley, Middlesex, ENGLAND
Dr. H. H. W. Losty

4 Great Lakes Carbon Corporation
Research and Development Department
P. O. Box 637
Niagara Falls, New York
B. L. Bailey
L. H. Juel (3)

4 Gulf General Atomic
R. F. Turner
T. R. Moffett
T. Golden
G. B. Engle

1 Idaho Nuclear Corporation
E. Fast

1 Los Alamos Scientific Laboratory
M. C. Smith

3 Oak Ridge National Laboratory
W. P. Eatherly
R. R. Kasten
M. W. Rosenthal

1 Pennsylvania State University
P. L. Walker

2 POCO Graphite, Inc.
Garland, Texas
R. K. Carlson

2 Pure Carbon Company
St. Marys, Pennsylvania
R. R. Paxton

1 Reactor Centrum Nederland
Petten, Netherlands
R. Blackstone

1 Rice University
Houston, Texas
J. L. Margrave

2 Speer Carbon Products
Research & Development Laboratories
Packard Road & 47th Street
Niagara Falls, New york
W. E. Parker

2 Speer Carbon Products
Development Department
St. Marys, Pennsylvania
W. A. Bauer
M. B. Redmount

1 United Kingdom Atomic Energy Authority
Atomic Energy Research Establishment - Harwell
Didcot, Berkshire, ENGLAND
J. H. W. Simmons

1 University of Washington
D. G. Fischbach

ONSITE-HANFORD

1 AEC Chicago Patent Group (Richland)
R. M. Poteat

2 AEC RDT Director for Pacific Northwest Programs

1 AEC Richland Operations Office
C. L. Robinson

3 Battelle Memorial Institute

3 Douglas United Nuclear, Inc.
P. C. Carlson
D. H. Curtiss
A. Russell

15 Battelle-Northwest
J. M. Batch
P. L. Farnsworth (2)
J. W. Finnigan
W. J. Gray
W. C. Morgan
R. E. Nightingale
G. L. Tingey (2)
Technical Info Files (5)
Technical Publications

20 WADCO
A. L. Pitner